Understanding the interactions between crescentic bars, human interventions and coastline dynamics at the East coast of South Korea

P.Athanasiou

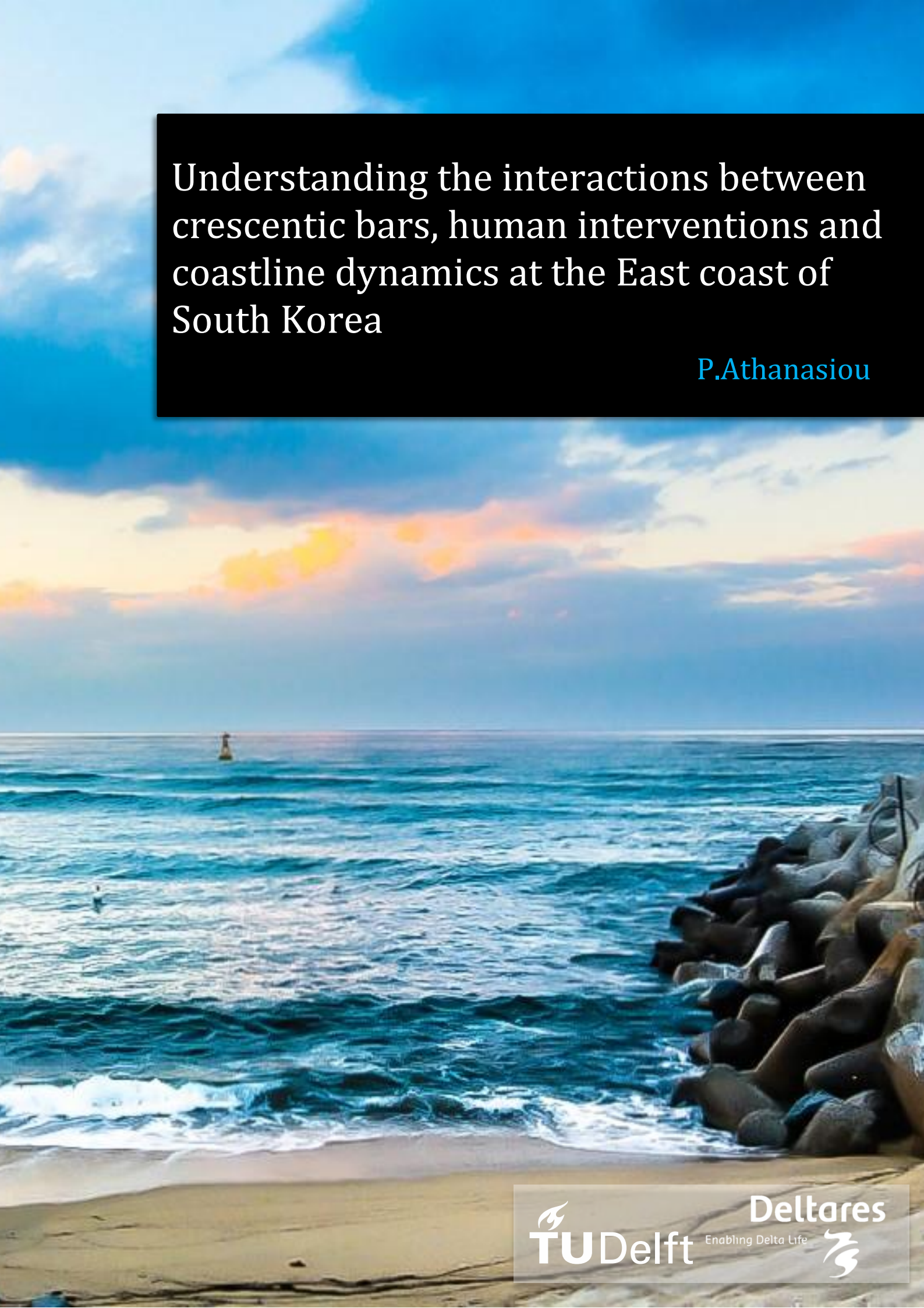

Understanding the interactions between crescentic bars, human interventions and coastline dynamics at the East coast of South Korea

by

Panagiotis Athanasiou

in partial fulfilment of the requirements for the degree of

Master of Science
in Civil Engineering

at the Delft University of Technology,
to be defended publicly on Tuesday September 19, 2017 at 09:00 AM.

Supervisor:	Prof. Dr. ir. A.J.H.M. Reniers,	TU Delft
Thesis committee:	Prof. Dr. R. Ranasinghe,	IHE Delft/University of Twente/ Deltares
	Dr.ir. M.A. de Schipper,	TU Delft
	Dr.ir. S. de Vries,	TU Delft
	Ir. P.K. Tonnon,	Deltares
	Ir. W. P. de Boer,	Deltares/TU Delft

An electronic version of this thesis is available at http://repository.tudelft.nl/.

TU Delft Delft University of Technology

Deltares Enabling Delta Life

Front cover: Photo of Anmok beach, at the point where the harbour's breakwater starts.
Downloaded from http://chulsa.kr

Preface

The present thesis concludes my Master of Science in Hydraulic Engineering at the Faculty of Civil Engineering and Geosciences of TU Delft in Netherlands. The study has been carried out at Deltares, in collaboration with TU Delft from January 2016 to August 2017.

First of all, I want to thank Wiebe de Boer for giving me the opportunity to get involved in the CoMIDAS project and for his continuous support, guidance and feedback during this period. Furthermore, I want to thank my chairman Ad Reniers, whose experience and insightful comments were always valuable for the progress of my work. Additionally, I would like to thank Rosh Ranasinghe, who provided insightful comments on my work and advised me on the approaches that were followed. Moreover, I would like to thank Pieter Koen Tonnon for being my daily supervisor and helping through the way, especially with his knowledge on Delft3D. I would like to thank Matthieu de Schipper for always having a critical approach on my results and ideas, laying the ground for in depth discussions. Last but not least, I would like to thank Sierd de Vries, for his comments, feedback and advices that improved this work.

Apart from my committee members, I would like to thank Nathaniel Plant, who in a brief meeting managed to enlighten me on the empirical models of sandbar dynamics and continued to give feedback even when he was back in USA.

Special thanks to all the people I met in Deltares this one year I spent there, who helped me have a great time and forget about work even for a bit. I am also really glad for all the people I met during these last two years in Netherlands and all the amazing times we had together.

I could not forget to thank both of my parents for supporting me in my decision to start an MSc abroad and their advices during this period.

Finally, I would like to thank Onassis Foundation for providing the scholarship that realized this master degree. Special thanks to Katerina Magkel, for her help and immediate response in any matter that came up.

P.Athanasiou

Delft, September 2017

Abstract

Crescentic sandbars are a commonly observed nearshore feature in coastal zones that strongly influence the surfzone circulations and are connected with the occurrence of rip currents. Furthermore, their spatial characteristics have been associated with the shoreline position in the form of shoreline perturbations, indicating morphological coupling between them and in turn affecting the beach width. As changes in the beach width affect coastal infrastructure and user functions such as recreation, understanding the bar dynamics is crucial for coastal zone management. The present work intends to improve this understanding by means of a case study at Anmok beach located at the South Korean East coast. Data analysis is used to estimate the long-term changes of the sandbar characteristics in time, under the influence of the ambient environmental conditions and human interventions. Additionally, this study investigates how to account for these features in modelling frameworks.

Available in-situ bathymetric surveys and high resolution aerial photographs are complemented with freely available satellite images in order to extract an estimate of the horizontal position of the sandbar crest line at Anmok beach. The introduction of satellite imagery observations dramatically increases both temporal coverage and frequency of the dataset resulting in 27 years of bar observations. Analysing this dataset shows that the sandbar maintains its crescentic features (no reset event), during the study period, which most of the time have a symmetrical shape.

The sandbar characteristics (mean cross-shore position and alongshore variability) are found to change mainly in response to high wave energy events, while the initial sandbar position seems to be an important factor e.g. the closer the sandbar to the shore the more prone to changes it is. Furthermore, the results indicate that the alongshore migration of the sandbar features and the alongshore component of the wave energy flux show an agreement between their long-term (5-10 years) trends. This highlights the potential of the alongshore wave generated current to migrate the sandbar patterns in the alongshore direction.

Moreover, the magnitude of the crescentic length and amplitude in an area 600-700m away from the port decreased after its construction. This can be connected with the sheltered zone created at the lee side of the port's breakwater and the reduction of the hydrodynamic circulations in this area. Additionally, the construction of a submerged breakwater is found to make the sandbar slowly disappear at the offshore side of the structure.

The use of coastline models that assume alongshore uniform bathymetry can be questioned in cases of pronounced alongshore morphological variability. To this end, the impact of the alongshore variability of the sandbar on net annual sediment transports is investigated with the process based morel Delft3D for a selection of schematized bathymetries, created based on the natural variability of the sandbar at Anmok. It appears that for the symmetrical shaped crescentic sandbars, which are mostly present at Anmok beach, the influence of the alongshore variability on the net sediment transports is not large (~10%).

The shoreline response to different sandbar configurations is investigated by computing alongshore incoming and outgoing sand volumes in cells specified close to the shoreline.

It is found that the cross-shore distance between the sandbar and the shoreline is critical for the intensity of the erosion and accretion patterns formed at the coastline. Moreover, according to the predominant direction of the wave climate the alongshore location of these shoreline patterns can vary.

After highlighting the importance of the sandbar location for the beach width, an attempt to model the sandbar mean cross-shore location in response to the wave forcing is realized in pursuit of predictive capability for future changing wave conditions. As process based numerical models have shown limitations in producing any predictive skill, two empirical models selected from literature are used. The calibration and validation of the models is unsatisfactory, possibly connected with the spatial accuracy and varying temporal resolution of the dataset or the simplification of the models themselves.

From the present work, the use of satellite imagery for studying of long-terms sandbar dynamics and the derivation of its characteristics is proven to be quite promising. It allowed us to increase the number of observations and hence, study the sandbar dynamics beyond the time-frame of in-situ surveys and aerial photography. Therefore, we could study the effects of human intervention on the long-term sandbar characteristics. This technique is believed to be useful for other sites with crescentic sandbars around the world.

Furthermore, the results of the sensitivity analysis of the sandbar variability on the net sediment transport rates indicate that the use of coastline models in the presence of a crescentic sandbar with symmetric characteristics is expected to be valid for the computation of the large scale reorientation of the coastline. Predictions of the coastline position though, should take into account the smaller scale shoreline perturbations related to the presence of a crescentic sandbar, by adding a bandwidth to the average coastline position. This bandwidth can be derived from data analysis of shoreline position observations.

Table of Contents

List of Figures

List of Tables

List of Symbols

Symbol	Unit	Description
H_s	m	Significant wave height
T_p	s	Peak wave period
T_{mean}	s	Mean wave period
L	m	Length scale of individual crescent measured from observations
A	m	Amplitude of individual crescent measured from observations
S	-	Asymmetry of individual crescent
λ	m	length scale of the rhythmic sandbar patterns computed from spectral analysis
α	m	Crescentic scale amplitude computed from spectral analysis
x_b	m	Cross-shore distance of sandbar crestline from reference line
$\overline{x}_b$	m	Alongshore mean cross-shore distance of sandbar crestline from reference line
x_{eq}	m	Equilibrium cross-shore location of the sandbar
Dir	^{o}N	Mean wave direction
θ_{mean}	^{o}	Angle of incidence relative to the shore normal
P_y	kW/m	Alongshore component of the wave energy flux
ρ	kg/m^3	Water density
g	m/s^2	Gravitational acceleration
x_s	m	Cross-shore distance of shoreline from reference line
E	m^2	Variance density spectrum of sandbar cross-shore location
x_{b5}	m	Cross-shore perturbation of the sandbar
r	-	Pearson correlation coefficient
s_{x_b}	m	Standard deviation of the cross-shore distance of sandbar crestline from reference line
s_{x_s}	m	Standard deviation of the cross-shore distance of shoreline from reference line
D_{50}	μm	Mean grain size
z_{sb}	m	Profile of bed level
A_b	m	Height of sandbar

R_b	m	cross-shore length scale of sandbar
q_s	$m^3/s/m$	Alongshore sediment transport rate
Q_s	m^3/s	Cross-shore integrated alongshore sediment transport
$Q_{s,AVG}$	m^3/s	Beach state averaged alongshore sediment transport
V	$m^3/year$	Yearly accretion volume in a cell

List of Acronyms

Acronym	Description
KIOST	Korean Institute of Ocean Science and Technology
CoMIDAS	Coastal Modelling, Intelligent Defence and Adaptation based on Scientific understanding
D3D	Delft3D
GLM	Generalized Lagrangian Mean
SBW	Submerged breakwater
RBB	Rhythmic bar and beach state
TBR	Transverse bar and rip state
ORB	Offshore rhythmic bar
ARB	Attached rhythmic bar
ECMWF	European Centre for Medium-Range Weather Forecasts
MSL	Mean Sea Level
RMSE	Root Mean Square Error
1DH	One Dimensional Horizontal
2DH	Two Dimensional Horizontal
3D	Three Dimensional

1. Introduction

1.1. Background

The nearshore area of sandy beaches is the most dynamic part of the coast, mainly due to the combined action of ocean waves, currents and consequent sediment transports they introduce. The temporal and spatial variation of these processes results in a great variability of the morphological patterns that can be found in the surf zone, both in time and space. A quite common feature that appears in most of the dissipative sandy beaches is sandbars, which can be described as shallow anomalies in an otherwise monotonic beach profile. They can be present either as a single feature or a multiple sandbar system, consisting of two or even more shore parallel sandbars (Price et al., 2014). These nearshore morphological patterns frequently exhibit an alongshore variability in their crest line depth and cross-shore position, which has a (quasi-)rhythmic character. When this periodic variability in the alongshore direction has developed, these sandbars are called crescentic (from their shape which resembles a half-moon). They can be described as a sequence of shoals that are called horns and (cross-shore) troughs that are called bays, which alternate shoreward and seaward from a line parallel to the coastline (van Enckevort et al., 2004). Rhythmic features are observed at the shoreline as well, in the form of seaward perturbations that are called shoreline horns and landward perturbations, called shoreline embayments (Orzech et al., 2011). An example of these sandbar and shoreline features is presented in Figure 1.1 for the case of Anmok beach in South Korea.

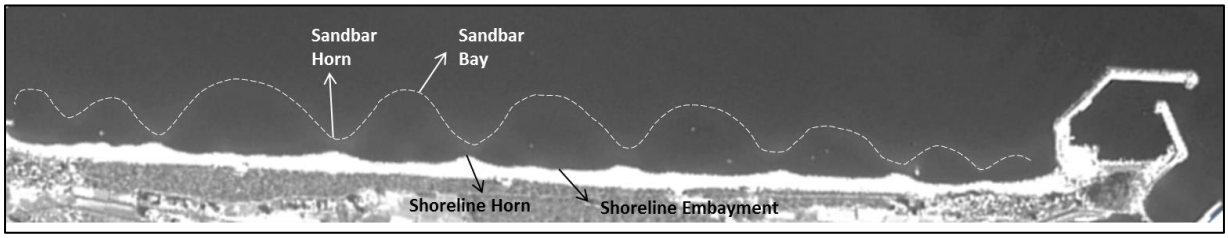

Figure 1.1: Definition of sandbar horns/ bays and shoreline horns/embayments on a satellite image taken from Arirang 2 satellite on 23/11/2008 showing Anmok beach at the East coast of South Korea. Dashed white line represents the sandbar crest line.

Crescentic sandbar systems are a nearshore feature that is quite often encountered in coastal areas across the globe, including beaches in Denmark, France, Algeria, Japan, USA, Canada, Ireland, Australia, Israel, Netherlands, Egypt, Spain, South Korea and more.

(Castelle & Bonneton, 2006; Ribas et al., 2007; Arifin & Kennedy, 2011; van de Lageweg et al., 2013). The characteristics of these rhythmic features though, seem to differ both spatially and temporally according to location and the accompanied climate and geological conditions.

Three-dimensional (3D) morphology severely influences the wave transformation in the nearshore and subsequently the hydrodynamics near the coastline. The circulations patterns that are formed in the surfzone can create localized accretion or erosion in the form of local perturbations of the shoreline around its average position (shoreline horns and embayments-Figure 1.1). Therefore, it is important to know their magnitude and their connection with the sandbar position, as they can be of relevance for coastal zone management and local infrastructure in coastal areas. Furthermore, the sandbar patterns are connected with occurrence of rip currents, which are of importance for recreational safety.

1.2 Problem Definition and Field Case

The South Korean East coast is a complex and dynamic system both due to its morphological and environmental conditions, as well as due to the numerous human interventions that are present along the coastline. The East Coast suffers from coastal erosion, leading to significant impacts for the local infrastructure, while the processes driving this erosion are not well understood. One of the factors that appears to affect the local width of the beach is the sandbar alongshore location (Figure 1.1).

The East Coast is characterized by a rocky coastline, often interrupted by sandy beaches. Rhythmic sandbar features are encountered at the nearshore area of these beaches (Figure 1.2) and seem to be quite persistent through time, in contrast with observations at other sites across the globe where the beaches seem to pass through several stages through the year (Wright & Short, 1984; van Enckevort et al., 2004) . Additionally, along the East Coast, one can find human interventions at relatively small intervals, sometimes in the order of one kilometre. These interventions vary quite a lot in type and dimensions. They mainly include fishing ports or larger ports, submerged breakwaters, groins and sea walls.

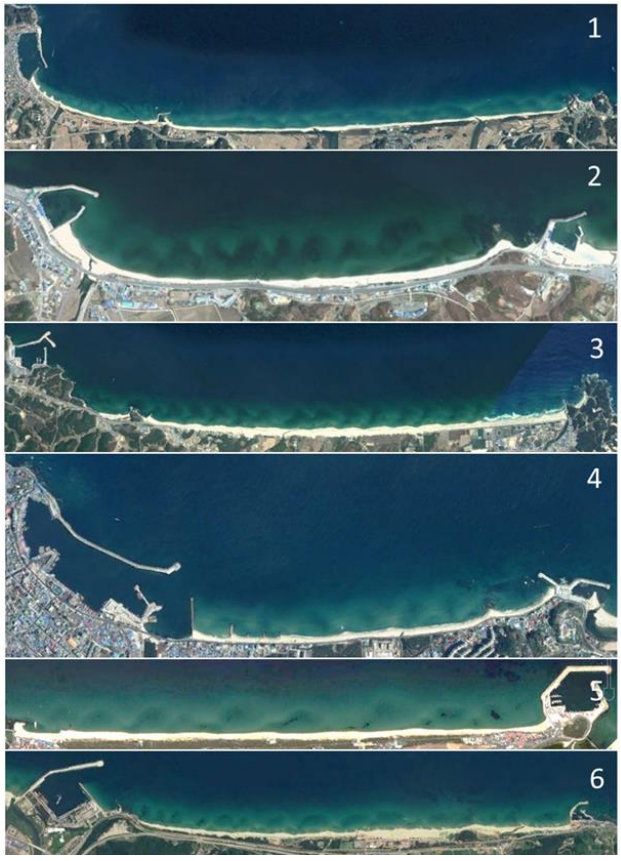

Figure 1.2: Satellite images (with different scale) of various beaches along the South-Korean East coast obtained from Google Earth. The order of the images follows the north to south direction along the coast: 1) Goseong beach, 2) Jung-Am beach, 3) Dong-Ho beach, 4) Ju Mun Jin beach, 5) Anmok beach (Study case), 6) Mangsang beach.

In order to effectively and efficiently deal with coastal erosion problems that have arisen at the South-Korean East coast, a 3-year research cooperation between Deltares and the Korean Institute of Ocean Science and Technology (KIOST) which is part of a larger project called CoMIDAS (Coastal Modelling, Intelligent Defence and Adaptation based on Scientific understanding), was launched by the government of South Korea. The overall objective of the cooperation is the development of a coastal modelling framework for coastal erosion studies and the transfer of knowledge to improve the Korean competency in this matter. In the first year of the project a demand-driven model development was followed for the study case of Anmok beach, which is a representative case for the East coast of South Korea (Figure 1.2-5).

Anmok Beach is located in the city of Gangneung, Gangwon Province, and forms the southern end of the 9.5-km long beach between Sacheon and Gangneung fishing ports (Figure 1.3). It is a straight wave-dominated beach facing NE. In the middle of the beach a small stream discharges from Gyeongpo Lake (Deltares 2016). During the past decades, there has been significant human activity in the coastal area around Gangneung. The main human interventions that have taken place in the Anmok beach area are:

- Northern Breakwater of Gangneung Port (finished end 2002) (Figure 1.4-1)
- Submerged Breakwater at southern end of the beach(finished mid 2014) (Figure 1.4-2)
- Beach Nourishment at the southern end of the beach (finished end 2014) (Figure 1.4-3)

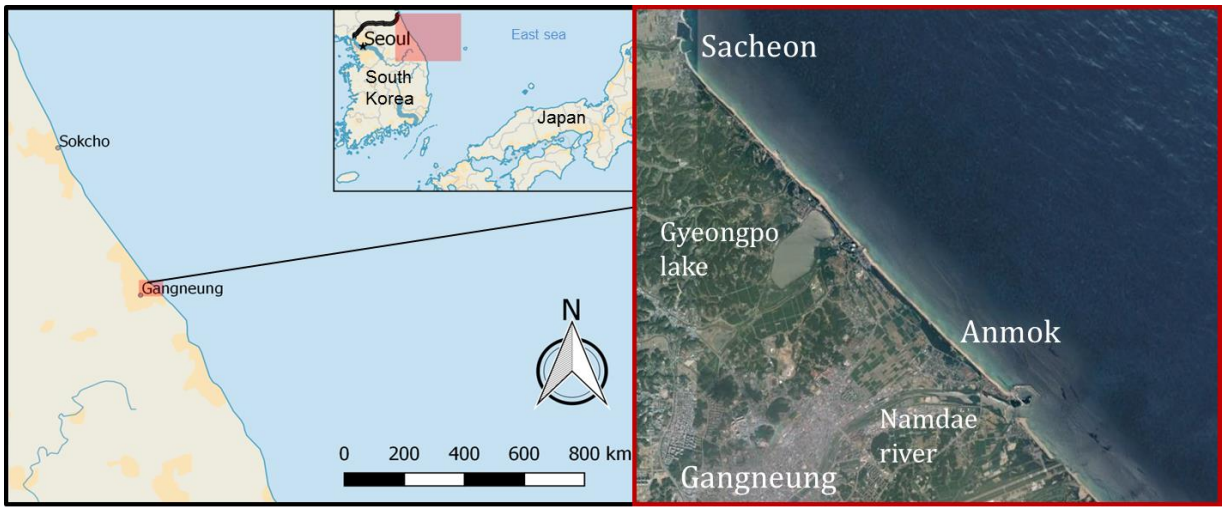

Figure 1.3: Study case of Anmok beach located in north-eastern South Korea, at the city of Gangneung in Gangwon Province.

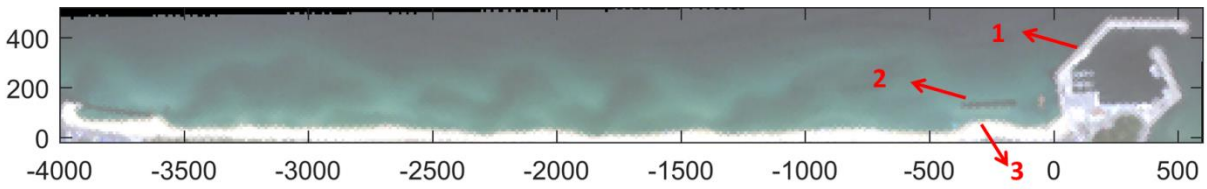

Figure 1.4: Sentinel 2 satellite image presenting Anmok beach on 25/04/2016 with the human interventions presented labeled as 1: Northern Breakwater of Gangneung Port, 2: Submerged Breakwater and 3: Beach Nourishment.

The East coast of South Korea is a micro-tidal environment, with a tidal range of a few decimetres. The average sediment grain size of the beach is roughly 400 μm. The wave climate can be characterized as relatively mild for most part of the year. However, extreme offshore significant wave heights of over 8 m and peak wave periods of more than 15 s have been observed as well, related to typhoons and winter storm events (Deltares, 2016).

At the end of the first year of the CoMIDAS project, different knowledge gaps were identified (Deltares, 2016), which demanded additional research. One of the main knowledge gaps determined was the understanding of the rhythmic sandbar dynamics and how they influence the local hydro–morphodynamics and subsequently the shoreline position and beach width. The sandbar alongshore variability is expected to introduce local gradients in the alongshore sediment transports that can lead to localized sedimentations and erosion patterns. For this reason, the interrelation between the sandbar horizontal patterns and the expected coastline position is a really crucial step in order to predict to some extent the beach width and effectively manage the coastal zone. Furthermore, sandbars form a natural defence mechanism against high energy ocean events (storms), as they dissipate the wave energy before reaching the shore. These storm events can introduce great threats both to valuable infrastructure and human life, located at the coast.

Besides the rhythmic sandbars, human made coastal structures are another feature encountered commonly at the East coast of South Korea (Figure 1.2). To this end, the interactions between these human interventions and the sandbar system need further studying and understanding.

In order to assess the long term coastline evolution, a common approach is the use of coastline models like Unibest-CL+, developed by Deltares. In these large scale approaches, alongshore gradients in sediment transports rates are the driving mechanism of coastline changes. These sediment transport rates though, are calculated at specific locations along the coastline (1D bed level profiles). This approach does not take into account 2D circulation effects that can develop in the presence of alongshore variable bathymetries. On study areas where the alongshore variability of the bathymetry is not that high, this approach might be valid, but an arising question is what happens when the alongshore variability is pronounced, like in the case of crescentic sandbars.

1.3 Research Objective and Research Questions

The aim of the present study is to gain insight in the complex dynamics between the crescentic sandbars, the shoreline and the adjacent human interventions at Anmok beach and their potential effects on sediment transports. As described in Section 1.2, this understanding can contribute to improve the coastal zone management at the South Korean East coast.

Following the problem definition and objectives, the following research question and sub-questions are formulated:

What are the interactions between the sandbar, human interventions and shoreline dynamics at Anmok beach?

1. What are the characteristics of the sandbar patterns at Anmok beach over the last decades?
2. What is the correlation between the position of the sandbar and the local wave conditions at Anmok beach?
3. What are the observed effects of the harbour and breakwater construction on the sandbar position?
4. Is it possible to predict the sandbar's horizontal position based on the local wave conditions?
5. What is the importance of the sandbar alongshore variability for the alongshore sediment transport rates?
6. What is the expected shoreline response to different sandbar horizontal patterns and wave conditions?

1.4 Methodology

The approach that is followed in order to answer the research questions above consists of data analysis, empirical modelling and numerical modelling. It is decided to use different approaches, due to the lack of each individual method to incorporate all of the sandbar dynamics and answer the research questions. Data analysis can provide insight and understanding on the system and can quantify the shoreline perturbations, but misses the relevant processes. Studies focused on numerical process based models were so far able to reproduce the growth of 2DH morphology but fail to have long-term predictive skill (Reniers et al., 2004; Smit et al., 2010). On the other hand, empirical models might be able to produce fair predictive skill, but their capabilities include simplifications and parameterizations, both concerning the inputs and the results.

This study can be divided into four main phases, which are briefly described below:

Phase 1- Literature study and dataset collection

Literature study is essential in order to identify the state of knowledge on the topic of crescentic sandbar dynamics, identify possible gaps, familiarize with previous works and get an idea on the kind of data needed.

The most critical part of this starting phase though is the dataset completion. An extended dataset, including surveys, shoreline measurements, hydrodynamic measurements, wave hindcasts, satellite and aerial images is available for Anmok beach.

The sandbar positions of the last decades are extracted manually from satellite images or surveys (when available). Furthermore, the nearshore long-term wave time series are computed using an offshore wave hindcast and previous wave transformation numerical model results.

This phase provides the background information and data in order to deal with the next steps.

Phase 2- Data analysis

This stage is mainly devoted to gain a general understanding of the beach dynamics at the study site.

Various parameters of the sandbar (e.g. alongshore mean cross-shore location, crescentic amplitude and length) are calculated for all the available observations. Additionally, the sandbar's cross-shore and alongshore migration and its connection with the local wave conditions are investigated. Furthermore, for the concurrent sandbar-shoreline observations, correlations are calculated in order to identify the coupling magnitude. To gain some insight on the effects of human interventions, sandbar characteristics are compared for pre and post construction periods. This contributes to the answers of the 1st, 2nd and 3rd research questions. The results are used as guide for the specifications of the modelling phases to follow.

Phase 3- Empirical model development

The importance of the sandbar position on the shoreline response has already been highlighted in Section 1.2. For this purpose, a tool to predict the horizontal position of the sandbar can be quite useful for future wave climate scenarios. This led to the formulation of the 4th research question.

The results of the 2nd phase are used for the realization of a behavioural/empirical model able to predict the horizontal position (average cross-shore position and magnitude of variability) of the sandbar in response to the local wave conditions. The models that are tested in this study are the ones presented by Plant et al. (1999) and Plant et al. (2006). In order to calibrate these models for the Anmok beach case, linear regression analysis is performed on the available observations. The model's predictive skill is validated based on the available sandbar position observations.

Phase 4 - Numerical modelling

In order to investigate the processes and characteristics governing the sandbar and shoreline interactions in more detail, numerical modelling with a process based model is necessary. This way, the alongshore sediment transports are computed and the coastline response is estimated. This phase focuses on the 5th and 6th research questions.

To this end, a Delft3D model that has been set-up in previous phases of the CoMIDAS project is used to understand the hydrodynamic processes at Anmok beach. Furthermore, a new Deflt3D model is created, to study the influence of the sandbar configuration on the alongshore sediment transports and the shoreline response. This is realized through schematized bathymetries and a yearly wave climate. The schematized bathymetries are created according to statistical analysis of the sandbar observations at Anmok beach, during Phase 2. Finally, scenarios concerning the port construction are investigated.

The general outline of the approach and targets of this study can be seen in the flow chart of Figure 1.5.

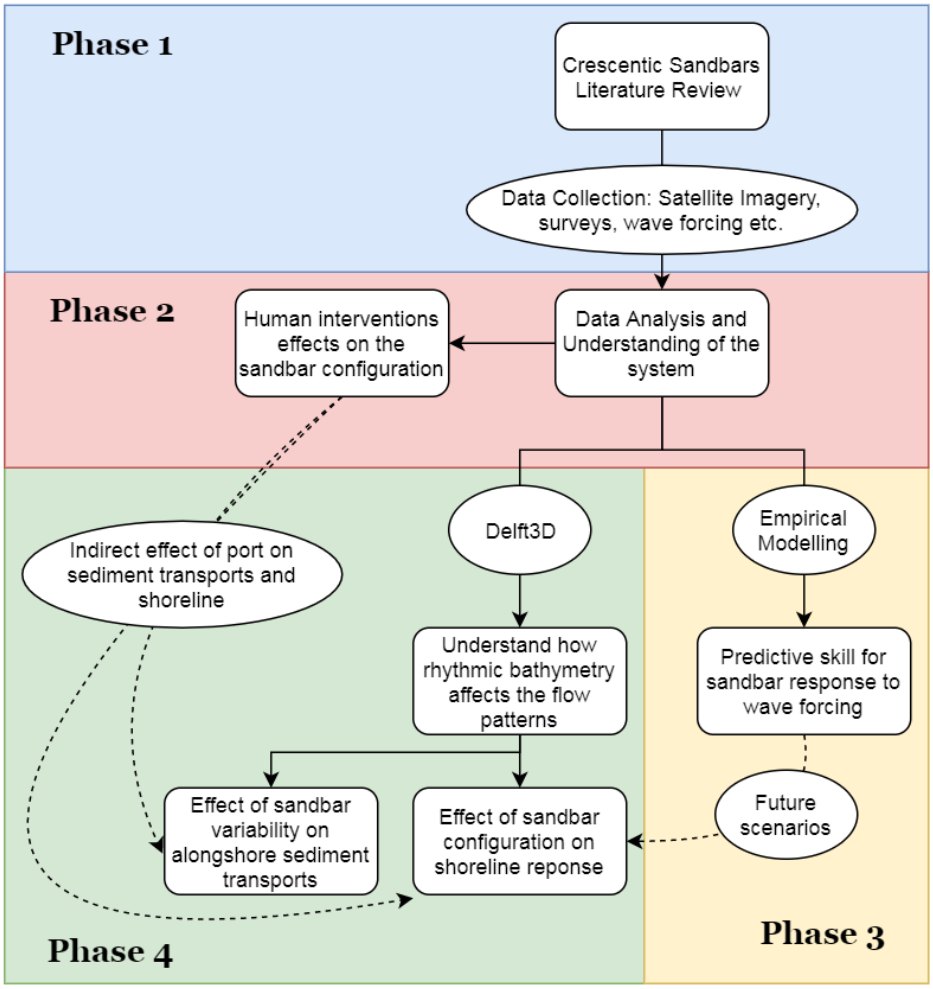

Figure 1.5: Flow chart of the approach and targets of this study.

1.5 Reader

In Chapter 2 the literature study can be found, after which the data analysis part follows in Chapter 3. There the field case is discussed and the available observations are analysed. Following, in Chapter 4, the calibration and validation of the empirical model is presented. Chapter 5 is devoted for the numerical modelling approach where the effects of the crescentic sandbar on the sediment transports and the shoreline are investigated. Finally, in Chapter 6 a discussion concerning the decisions and assumptions of the present work are presented and in Chapter 7 the general conclusions of this study and various recommendations for the ones to follow are discussed.

Appendix A concerns the extraction technique that is used for acquiring the sandbar horizontal location for the study period. Additionally, in Appendix B, one can find the approach followed to compute a hindcast of the wave time series near the shore. In Appendix C various graphs mainly from the numerical modelling phase can be found.

As this study consisted of different phases and methods in each chapter there is a conclusion as the last section, where the main results are described and any possible input for the other phases is defined.

2. Literature Review

2.1 Introduction

In this chapter a general overview of the available research on the rhythmic nearshore morphology and shoreline response is presented. More specifically, we start with an outline of the available beach state classifications, followed by an explanation of the proposed mechanisms behind crescentic sandbar formation. Then, attempts of modelling the alongshore variability and cross-shore position of sandbars are discussed. Furthermore, available analysis and modelling concerning the sandbar-shoreline coupling and interactions is presented.

2.2 Beach states

The variability of the observed nearshore morphology can be classified in the so called beach states. In the classification of beach states proposed by Wright and Short (1984), two alongshore uniform beach states were identified: one with a reflective and one with a dissipative character. In between, four other intermediate states are described which are characterized by a three-dimensional structure of the morphology. Crescentic sandbars belong to the intermediate beach states and more specifically, the clear crescentic shape is described by the rhythmic bar and beach (RBB) state, while the accretional phase where the crescent horns are moving to the shore and finally weld to it, is called transverse bar and rip (TBR) (Figure 2.1). The transition from the RBB state to the TBR state is part of a down-state evolution of the beach which is governed by accretive wave conditions. The mean current flow is directed onshore over the horns of the crescents and offshore at the location of the bays, where rip currents are formed. During high energy (storm) events, the sandbar can lose its longshore variability and migrate offshore, transforming in an alongshore uniform bar, a so called reset event.

In an alternative beach classification proposed by Lippmann and Holman (1990), which mainly described the bar type per class, crescentic sandbars can be associated with two classes again: the offshore rhythmic bar (ORB) and the attached rhythmic bar (ARB). Both of them are characterized by an alongshore rhythmicity but differ in the continuity of the trough, which is discontinuous for the latter case. For their classification they used time exposure images of wave breaking at sandy beaches to identify bar morphology.

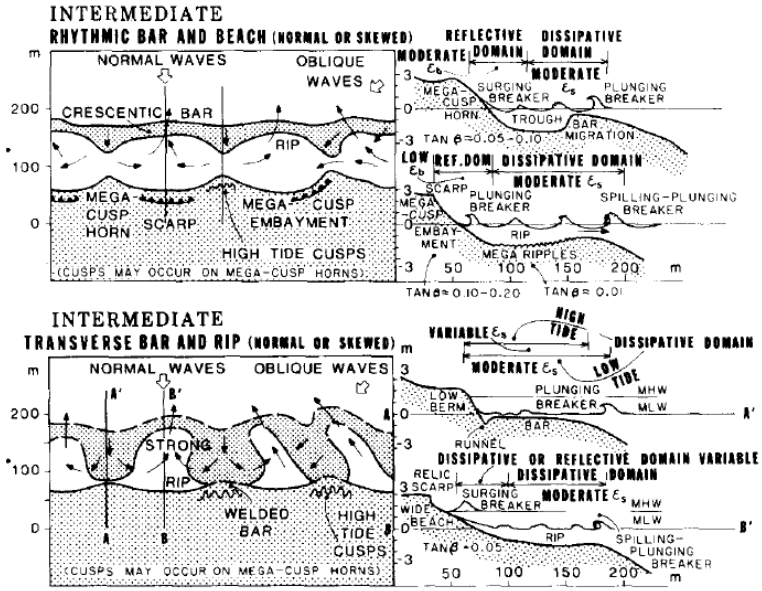

Figure 2.1: Plan and profile features of two intermediate beach states that are connected with crescentic sandbars as taken from Wright and Short (1984).

Crescentic sandbars can be found in embayed or straight sandy beaches with slopes of the barred part of the profile less than 1:20-1:30 in non or micro tidal marine environments (van Enckevort et al., 2004). Furthermore in the study of van Enckevort et al. (2004), various field observations concerning the appearance of crescentic bars were presented and the length scale characteristics of individual crescents were defined (Figure 2.2). This study showed that the length scale of the sandbar's rhythmicity presents a great variability from site to site, even reaching differences of two orders of magnitude, while even for the same site the alongshore length scales of the perturbations might vary quite intensely. This variability in the length scales of the patterns that develop in the alongshore direction led to the use of the "quasi-rhythmic" description for the crescentic sandbars.

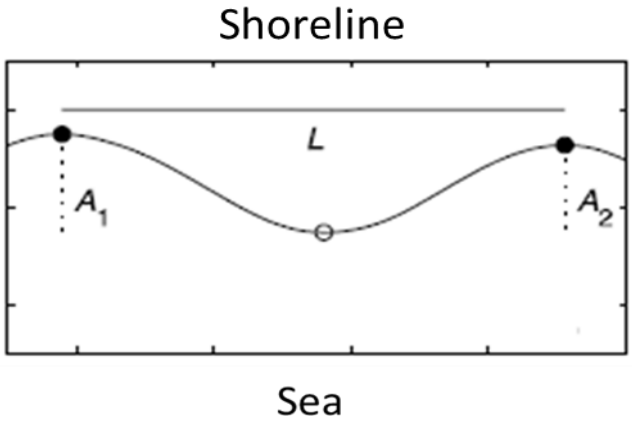

Figure 2.2: Sketch of an individual crescent with length (L) and amplitude ($A = \frac{0.5(A1 + A2)}{2}$) definition, as adapted from (van Enckevort et al. 2004). The full circles represent the sandbar horns while the open one the sandbar bay.

2.3 Formation mechanisms of sandbar alongshore variability

The observed rhythmic features of the sandbars have initiated a lot of different attempts to understand their formation mechanisms and explain the observed length scales. The different approaches that have been introduced through the years can be divided into two general groups: the template and the self-organization models (forced vs. free behaviour).

Originally, it has been assumed that the crescentic spatial patterns originate from a template in the hydrodynamics, which forces the three-dimensional pattern in the morphology. This means that there is a direct correlation between the length scale of the forcing and the length scale of the sandbar rhythmicity. Bowen and Inman (1971), found a satisfactory explanation to this in edge waves, claiming that the crescents alongshore length is half of the edge waves length. Edge waves are infragravity waves trapped against a shoaling beach as a result of refraction near the shore, with their amplitude varying sinusoidally along the beach and diminishing in the seaward direction (Bosboom & Stive, 2012). Video observations from different sites around the world showed that crescentic sandbars form in the periods after storms where the edge wave energy is expected to be lower (van Enckevort et al., 2004). Furthermore, their length scales changed with merging and splitting phenomena that cannot be explained by forcing template mechanisms (Coco & Murray, 2007).

On the contrary, according to the self-organization approach, the morphological patterns do not directly mirror the pattern of the hydrodynamic forcing, but develop as a response to small, initial perturbations of the seabed, which evolve due to positive feedback mechanisms between the sediment motions and the morphology. A description of the processes is found in Falqués et al. (2000): At locations where the water depth is smaller than average, wave breaking is enhanced resulting in an onshore flow, which subsequently leads to the development of offshore flow between points with lower depth. Furthermore, assuming that suspended sediment concentrations decrease from the breaking point to the shoreline, where water depth is smaller than average and the flow is on-shore directed; sediment transport decreases in the flow direction. This leads to sediment deposition and a further decrease of the water depth. Where the water depth is locally larger than average and the flow is offshore directed, sediment transport increases in the flow direction, leading to sediment erosion and a further increase of the depth. These sediment transport convergences and divergences create sequential erosion deposition patterns and thus the crescentic shape of the sandbar. The self-organization mechanism has been verified using process-based non-linear models (Caballeria et al., 2002; Reniers et al., 2004; Smit et al., 2010) or linear stability models (Falqués et al., 2000; Tiessen et al., 2010). Furthermore, concerning the sandbar response Smit et al. (2010) observed that local hydrodynamics and existing morphological patterns variability play an important role. In their study they describe that with low initial variability, hydrodynamic conditions play a critical role in the formation and development of the crescentic patterns, while for an increased initial variability, the hydrodynamic forcing will affect the existing patterns only in case of high hydrodynamic energy (storm), resulting in a reset event.

Overall, the self-organization mechanism appears to be more consistent in explaining the appearance of rhythmic features in the nearshore, as it focuses on the flow-sediment interactions and feedbacks, without requiring the presence of organized flow structures. Common ground for the two approaches can be found with the quasi-forced approach (de Schipper et al., 2011), in which the forcing mechanism can initiate perturbations that result in instabilities, which are then enchanted by feedback mechanisms and develop the final crescentic shapes (Coco & Murray, 2007).

2.4 Empirical modelling attempts of sandbar response to wave forcing

Parametric models offer a simplified perspective of the complex processes at the nearshore area. Furthermore they enable the better understanding of the relationships between forcing mechanisms and system characteristics in a more straightforward approach. The basic assumption governing their implementation is that the morphology can be represented by using a discrete set of parameters (e.g. sandbar position) whose variation in time can be modelled without explicitly accounting for sediment transport variations (Splinter et al., 2011).

Plant et al. (1999) proposed a simple empirical model, assuming alongshore uniform bar behaviour, for the interannual cross-shore migration of the sandbar. The cross-shore sandbar migration rate was specified as the difference between the mean cross-shore sandbar location $\overline{x}_b$ and the equilibrium location x_{eq} at time t, times the inverse of the response time τ:

$$\frac{d\overline{x}_b(t)}{dt} = \frac{1}{\tau}\left(x_{eq}(t) - \overline{x}_b(\mathrm{t})\right) \tag{2.1}$$

The model explained up to 80% of the sandbar observed position at Duck, North Carolina.

Plant et al. (2006) developed a simple empirical model in order to predict the sandbar response, including its two dimensional effects, to a storm wave forcing. In this model the sandbar morphology was represented by the alongshore mean cross-shore position of the crest-line ($\overline{x}_b$) and the alongshore variability about that mean value (α). Alongshore variability α was defined as the alongshore standard deviation of bar position for the length scales between 200 and 1000 m. The difference between this parameter (α) and the crescentic amplitude A presented in Figure 2.2, is that α represents the alongshore sandbar variability for all its length, while A indicates the amplitude of an individual crescent. Moreover, the wave forcing (F) was described by a function of the offshore root mean square height. The model consisted of two coupled linear differential equations, as following:

$$\begin{bmatrix} \frac{d\overline{x}_b}{dt} \\ \frac{d\alpha}{dt} \end{bmatrix} = A\begin{bmatrix} \overline{x}_b \\ \alpha \end{bmatrix} + B\begin{bmatrix} 1 \\ F \end{bmatrix} \tag{2.2}$$

While the behaviour of a bar system is expected to be non-linear as mentioned before, this model admitted both stable and unstable dynamics. These dynamics are determined by the model coefficients (A and B), which were obtained by fitting to observations. In their study, Plant et al. (2006) observed that the slow response of the bar characteristics in comparison to the fast wave forcing changes, does not allow the system to reach equilibrium. They found out that the sandbar cross-shore position and alongshore variability depend on each other, making a link to self-organized behaviour. The model predictive skill was tested for the two months period of August and September 1998 at Duck, N.C., USA during Hurricane Bonnie. The model's skill for the test period was quantified by R^2, with a 0.9 value and was significant at the 95% confidence level. The linearized formulation of this model assumed that it describes small perturbations about a mean state and was applied for a small period (e.g. 2 months).

Splinter et al. (2011) extended the work of Plant et al. (2006) in order to study the non-linear feedbacks between 3D morphology and sandbar position. They used a set of dynamically coupled equations based on sediment transport derived from energetics-based formulations under the assumption of roughly constant bar forms. The model investigated the influence of the 3D morphology of the sandbar on the shore-averaged sandbar position. This model considered sediment transport as nonlinearly dependent on wave breaking over the bar and explicitly included the influence of the 2DH processes on the cross-shore bar migration rates. The coefficients of the equation system were determined by weighted nonlinear least squares method, to estimate best fit based on 566 days of data from Palm Beach, New South Wales, Australia. The model was able to explain 49% and 41% of the variance in measured mean cross-shore bar crest position and alongshore variability respectively.

2.5 Alongshore sediment transports and beach states

The impacts of different beach states on the alongshore sediment transports have been investigated for single representative wave conditions at the Sand Engine in Netherlands (Huisman et al., 2017). This influence was approximated by using the difference between beach state averaged alongshore sediment transports and their alongshore uniform case as a proxy. They found that the net sediment transports are considerably influenced for a beach state with pronounced transverse bar rip configuration, while the influence was much smaller for bathymetries with smaller alongshore variability. These effects were related to the obliqueness of the rip channels and the diffusive wave breaking patterns that are expected in a spatially variable bathymetry. It was specified though, that bathymetries will adapt according to the prevailing wave conditions, which means that the impact on the net alongshore transports may be variable over time.

2.6 Sandbar-Shoreline interactions

The interrelation of the rhythmic patterns of the sandbar with observed rhythmicity in the shoreline has been presented in Wright and Short (1984), where, as can be seen in Figure 2.1, the crescentic sandbar horns are faced by megacusp horns in the shoreline.

The sandbar-shoreline coupling for an embayed beach in New Zealand was studied from video observations and found to be strongly related with the reduced separation between the sandbar and the shoreline (van de Lageweg et al., 2013). The results quantified the coupling between the sandbar and the shoreline by performing cross-correlation analysis between the two patterns and calculating the phase of the observed coupling. Out of phase coupling represents the beach state when the sandbar horns are faced by shoreline horns (Figure 1.1), while when they are faced by shoreline embayments it is defined as in-phase coupling. Additionally, for their case study of an embayed beach they used the alongshore component of the wave energy flux (P_y) to study the correlation with the rotation of the sandbar and shoreline:

$$P_y = \frac{\rho g^2}{32\pi} H_s^2 T_{mean} \sin(\theta_{mean}) \cos(\theta_{mean}) \tag{2.3}$$

where $\rho = 1025\ kg\ m^{-3}$ is the water density and $g = 9.81 m\ s^{-2}$ is the gravitational acceleration.

Based on video observations and wave data at the southern Monterey Bay, California, a profound connection between the location of beach megacusps and rip channels was found (Orzech et al., 2011). The observations indicated megacusps forming shoreward of rip channels when larger waves were arriving at the beach. Furthermore, their morphodynamic modelling attempt suggested that the existence of an embayment shoreward of a rip channel or shoal is connected with the mean daily water level and the pre-existing beach bathymetry.

Except the single sandbar systems that were mainly discussed previously, there are systems with two or multiple sandbars present. As the waves transform while approaching to the shoreline, they are first affected by the outer bar, which introduces spatial gradients in the wave height and direction that affect the sediment transports rates at the inner bar. This implies a coupling between the positions of the two sandbars. The case of morphological coupling between an inner and outer subtidal sandbar has been studied using video observations, numerical modelling and data-model integration (Price et al., 2014). They found that coupling is connected with the water-depth variability of the outer bar crest, the wave height and the wave angle of incidence. This forced behaviour of the outer bar pattern to the inner bar morphology can be connected to a similar forced behaviour of a single sandbar or the inner bar to the shoreline position.

2.7 Conclusion

As presented in this chapter, research concerning beach rhythmic morphology is abundant. Topics that have been studied include formation mechanisms, behavioural analysis and coupling mechanisms. The approaches followed vary from observations analysis, empirical models and numerical process based models.

Although the South Korean East coast is a coast that is governed by the appearance of crescentic sandbars, so far there is no comprehensive study on its nearshore morphology and how it changes in respect to the wave climate.

Furthermore, even though connections between the sandbar position and shoreline position have been identified (Orzech et al., 2011; van de Lageweg et al., 2013), there is no extensive analysis on the system controls that are governing the shoreline response to the sandbar's position. The study of Price et al. (2014) investigated the influence of the wave forcing and outer-bar depth variability but for the case of an inner-outer bar system.

This study focuses in studying the sandbar evolution at the South Korean East coast and identifying the connections between the sandbar and shoreline position. As highlighted by the approaches presented in this Chapter, the targets, advantages and drawbacks behind each method vary. To this end, due to the diverse research questions that are specified in the present study, different approaches are used. This way, one can complement the other, while when integrating their results a better understanding of the system dynamics can be achieved.

3. Observations at Anmok beach

3.1 Introduction

This chapter mainly focus on gaining a general understanding and insight of the beach dynamics at the study site of Anmok beach. First, the available data concerning local wave conditions, sandbar position, shoreline position and bathymetric surveys are presented. This dataset forms the foundation for any data analysis and modelling attempts to follow. Then, the sandbar characteristics (e.g. cross-shore location, crescentic amplitude and length) are calculated for all the available observations. Additionally, the sandbar's cross-shore and alongshore migration and its connection with the local wave conditions are investigated. Furthermore, for the concurrent sandbar-shoreline observations, correlations are calculated in order to identify the coupling magnitude. In order to gain some insight on the effects of human interventions, sandbar characteristics are compared for pre and post construction periods. This chapter forms the basis for the calibration and validation of the empirical model attempt (Chapter 4) and the formulation of the schematic bathymetries for the numerical modelling phase (Chapter 5).

3.2 Available data

3.2.1 **Local wave conditions**

As highlighted in Chapter 1, the waves that arrive at Anmok beach form the main forcing mechanism for any change in nearshore morphology, as the tidal range is quite small. The local wave time series are computed at point W1 located roughly 800m from the shore at a water depth of about 17m (Figure 3.1). For the computations, hindcasted offshore wave data obtained from ECMWF are used. The transformation from the offshore location to the nearshore is performed using relations obtained from previous numerical modelling phases of the CoMIDAS project. The transformation is validated and corrected using wave measurements at W1 available from a measuring campaign of KIOST at 2015. Further information on the method used and the validation of the results can be found in Appendix B.

Figure 3.1: W1 location (Image obtained from Google Earth)

The local wave data are available at 6-hour interval and included significant wave height H_s (m), mean wave period T_{mean} (s) and mean wave direction Dir (°N) estimations. For further analysis the wave mean angle of incidence relative to the shore θ_{mean} (°) is calculated. Moreover , in order to check the effect of the alongshore wave current on the alongshore migration of morphology features, the alongshore component of the wave energy flux is calculated following Lageweg et al. (2013) as described in equation 2.3.

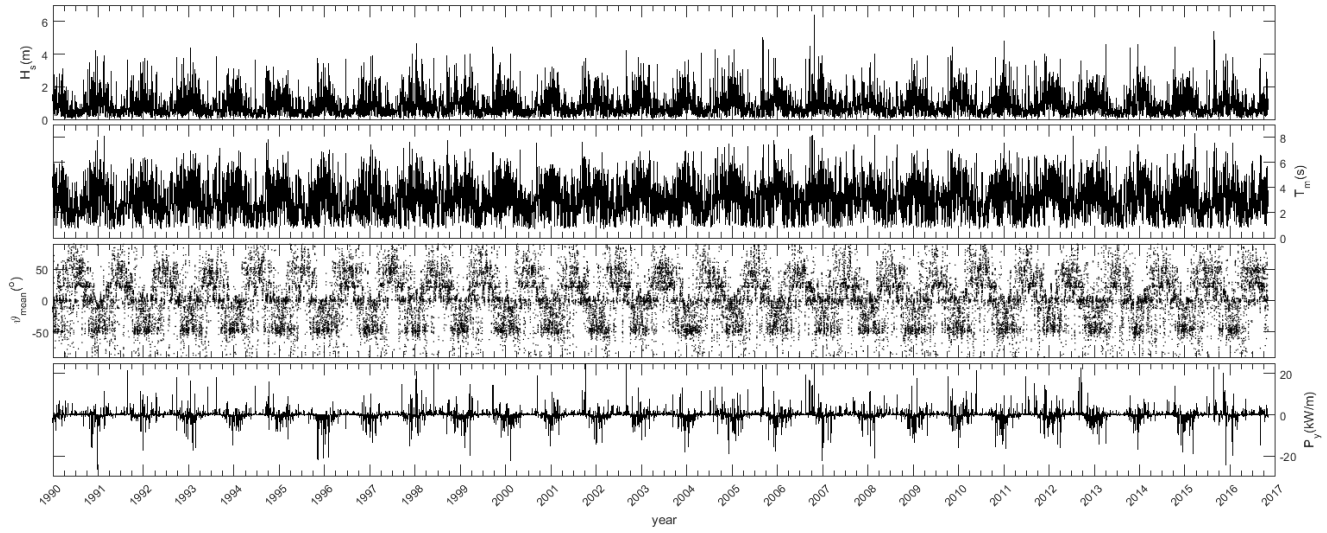

Figure 3.2: Time series of (from top to bottom): significant wave height H_s (m), mean wave period T_{mean} (s), wave mean angle of incidence θ_{mean} (°) and alongshore component of the wave energy flux P_y (kW/m) (Equation 2.3). A positive P_y indicates an alongshore current directed to the Northwest while a negative one indicates a southeast direction.

The wave climate seems to follow a seasonal character (Figure 3.2), with the highest waves appearing in the winter period. Some events of high wave energy are present during the summer as well, which are related to typhoons. The wave direction follows a seasonal character as well, with the predominant direction coming from the North during winter time and from the East during summer. This gives rise to a wave energy alongshore component which is on average directed to the Southeast (to the port) of Anmok beach (Figure 3.2).

3.2.2 **Sandbar position**

The sandbars horizontal position through the study period is used as a proxy of the nearshore morphology. The sandbar position for the study period of 1990-2017 is extracted manually from a collection of satellite/ aerial images and available surveys. Each of them is graded according to the quality of the source used for the extraction from 1 (best quality) to 4 (worst quality). This results in a dataset of 201 sandbar cross-shore positions $x_b(y)$ (Figure 3.3) over the study period with a temporal interval ranging from one day to almost a year and an average value of 1.5 months. In case the worst quality images (grade=4) are taken out of the dataset, the total number of available observations is reduced to 164 and the average temporal interval is almost two months. From now on, the first dataset will be referred to, as MG4 (Max Grade 4) and the second dataset as MG3 respectively. More information on the extraction technique and accuracy can be found in Appendix A.

An overview of the sandbar position over the study period can be seen in the timestack image of Figure 3.4. Over the whole period of study, the sandbar at Anmok beach maintains a crescentic shape, as has been previously observed in Chapter 1. This can be identified from the continuous alongshore alternation of colors in the timestack image. The response time of the sandbar seems to be quite high as the sandbar maintains its main characteristics for periods of even years. It is assumed that the sometimes high temporal interval between the data does not mask any other behavior. There are periods where the sandbar is located relatively shoreward (bluish colors) while other periods when it is positioned further seaward (reddish colors). Furthermore, during the study period even though the sandbar features seem to migrate in the alongshore direction they have more or less the same patterns, but from the end of 2015 onwards the patterns shape changes abruptly.

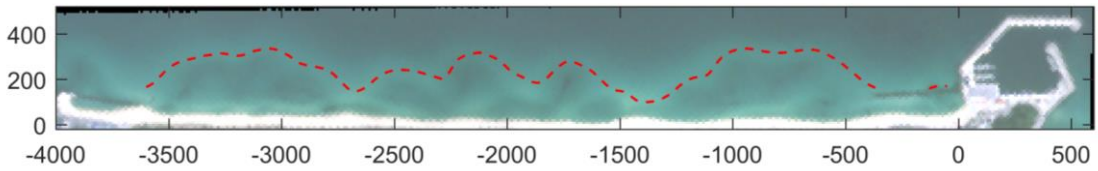

Figure 3.3: Sandbar crest's distance $x_b(y)$ at 15/10/2016 presented with dashed red line on the satellite image from Landsat 2.

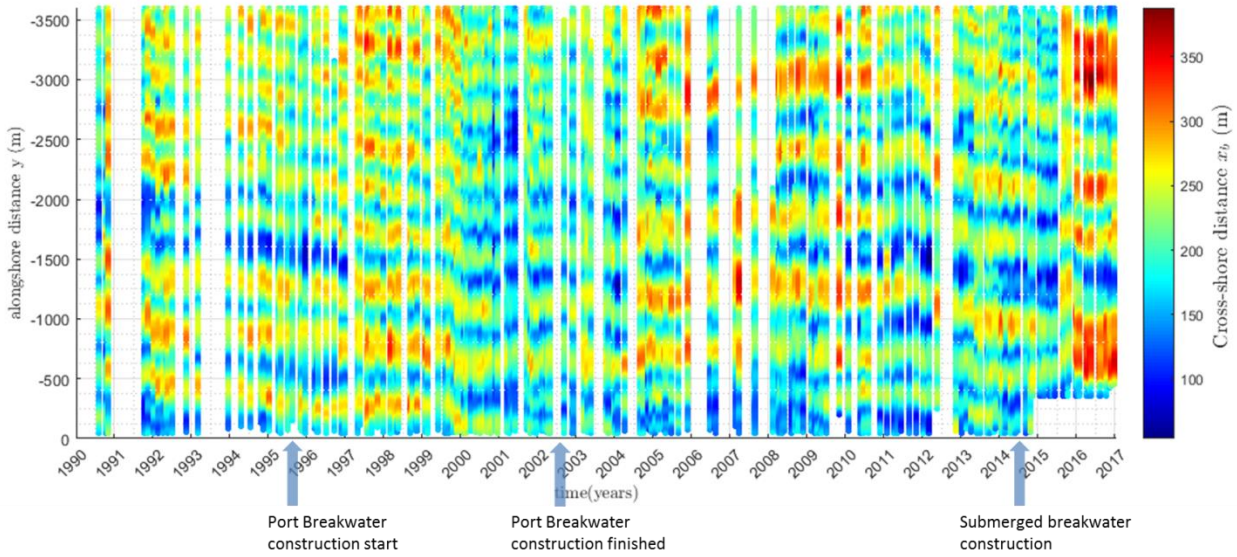

Figure 3.4: Time stacks showing $x_b\ (y,t)$ of the MG4 dataset. The blue colour indicates a part of the sandbar that is located closer to the shore while the red colour indicates a part of the sandbar that is located more seaward. Furthermore the times when human interventions took place are indicated by arrows.

3.2.3 **Shoreline position**

Shoreline position can be used to identify underlying correlations with the sandbar patterns and quantify the shoreline's localized erosion or accretion hotspots. About 30 shoreline measurements at Anmok beach are provided by KIOST for the period of 2008-2015 with almost monthly intervals at the first two years and the frequency dropping to 3-4 measurements per year in the end. Moreover, shoreline positions are manually extracted from the satellite and aerial imagery. This is the case only for the aerial, Arirang and Sentinel imagery available due to the smaller scale perturbations of the shoreline compared to the sandbar, which are visible only from the high resolutions images. As mentioned before the tidal range and expected storm surge are both quite low for the study area, so it is assumed that the detection provided the shoreline at the MSL water level, as the images used are always described by calm wave conditions and no wave run-up.

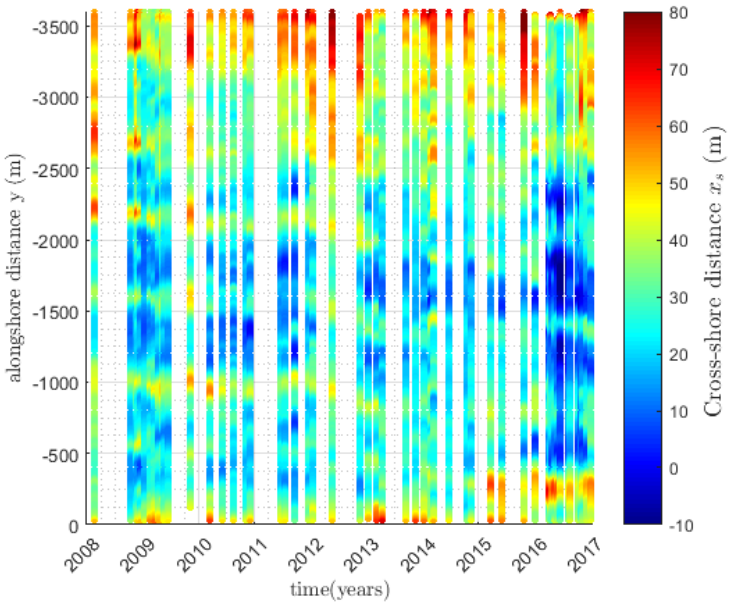

Figure 3.5: Time stacks showing$x_s\ (y,t)$. The blue colour indicates a shoreline position closer to the land while the red colour indicates a shoreline position more seaward.

Following the same method as explained for the sandbar in Appendix A, a dataset of 63 shoreline positions $x_s(y)$ is obtained for the study period. As prior to 2008 the main source of data is Landsat imagery, which has too coarse resolution to identify shoreline perturbations, the shoreline available data mainly describe the period of 2008 onwards. For this reason, regarding the shoreline analysis and the sandbar-shoreline relation analysis the study period is defined as 2008-2017.

An overview of the shoreline locations can be seen in Figure 3.5. The change of color scale in the alongshore direction indicates that rhythmicity is present at the shoreline as well. As observed for the sandbar, the events at end of 2015 until the start of 2016 seem to have a big influence on the position of the shoreline.

3.2.4 **Bathymetric data**

Survey data from field measuring campaigns at Anmok beach are available. Their spatial resolution is roughly 5x50m (cross-shore x alongshore), and they were conducted mainly at two periods: 2007-2008 and 2013-2016. In total there are 14 surveys available. Some of the surveys cover the entire stretch of the beach while some of them cover only the first 2km from the port. The survey measurements are interpolated using a triangulation-based linear interpolation in a grid a 5m x 10m resolution (cross-shore x alongshore). An overview of the interpolated bathymetric data can be seen in Figure 3.6.

As previously mentioned the morphology is quite dynamic with the sandbar location being variable through the surveys period. This includes both the sandbar crest location and depth. During the period of 2007-2008 the sandbar becomes shallower and there are crescentic shapes formed at the y=-500m to y=0m area. Furthermore the horns (locations y=600m, 1000m, 1700m and 2100m) migrate shoreward. After five years, in 2013 the sandbar patterns have changed profoundly. Until June of 2015 the patterns of the sandbar seem more stable, with the exception of the south part where the submerged breakwater was constructed and at the north part where the crescents of the sandbar have split into smaller scale ones. Moreover, the crescent that was located at y=-1300m migrated onshore and lost its crescentic shape. From June to August 2015 the sandbar patterns changed abruptly and migrate offshore due to a typhoon hitting the South Korean East coast, while until January 2016 the sandbar moved even more seaward at some locations due to a big sequence of storms attacking the coast. These events are going to be further discussed at Chapter 3.3.3.

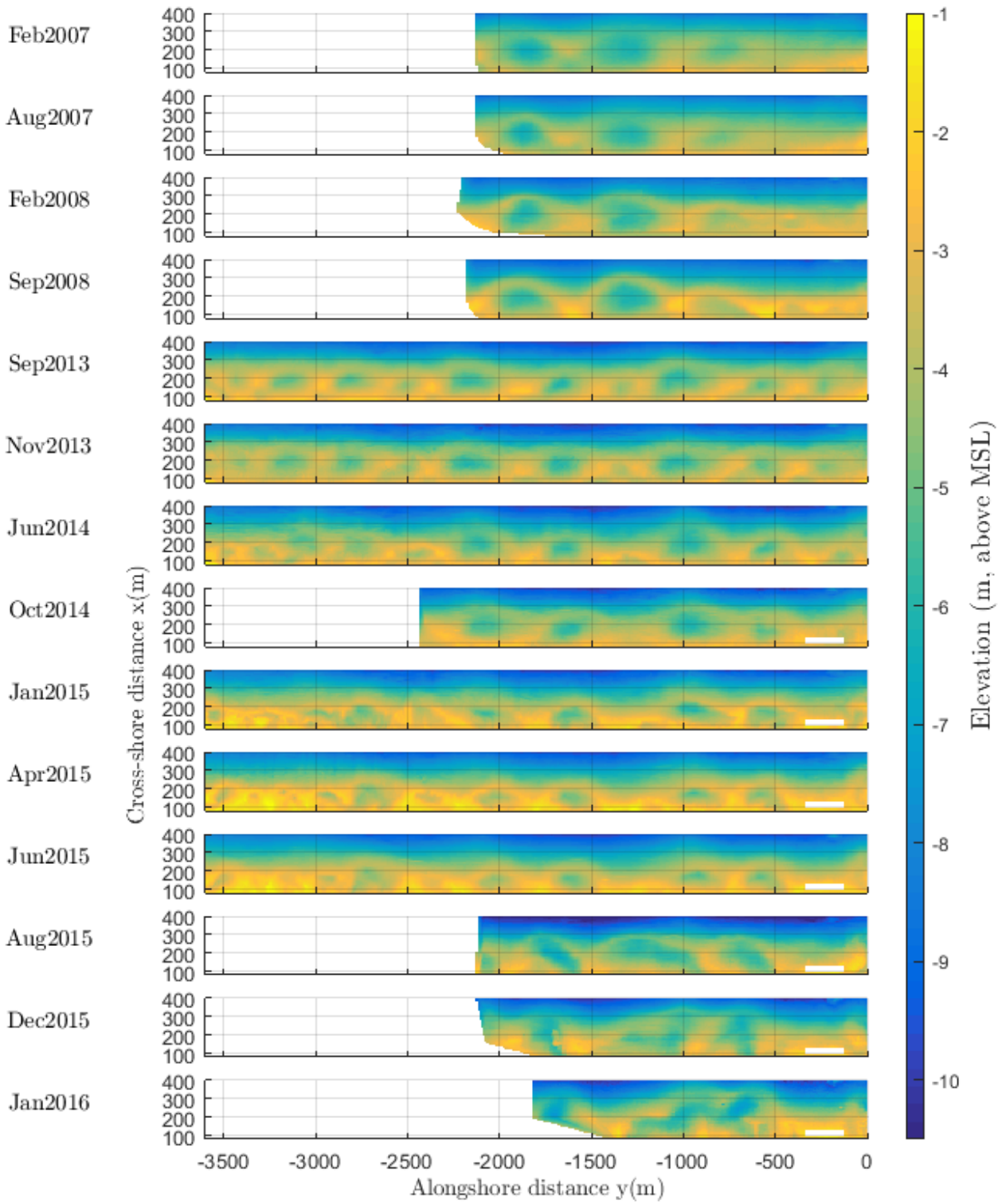

Figure 3.6: Bathymetric data of Anmok beach, showing the elevation of the bottom with respect to the mean sea level. At the left side the month and year of the survey is visible.

3.3 Sandbar characteristics

In order to understand how the sandbar changes over the study period, a set of different parameters describing the sandbar's shape and location needs to be calculated. These parameters can indicate the length scales of rhythmicity, the magnitude of alongshore variability, the mean cross-shore position of the sandbar etc. Furthermore, in order to model the response of the sandbar to the wave forcing (Chapter 4), these parameters are used as proxy to describe the nearshore morphology. Additionally these parameters are used for the creation of schematized bathymetries and a sensitivity analysis (Chapter 5).

3.3.1 Length, amplitude and asymmetry of crescents

As defined by Van Enckevort et al. (2004) an individual crescent can be described by its amplitude A and length L (Figure 3.7 and Figure 2.2). The length is defined as the alongshore distance between two consecutive horns while the amplitude is calculated as half the cross-shore distance between a bay and two adjacent horns. First the horns and bays locations are detected for each sandbar crest observation $x_b(y)$ available (Figure 3.8).

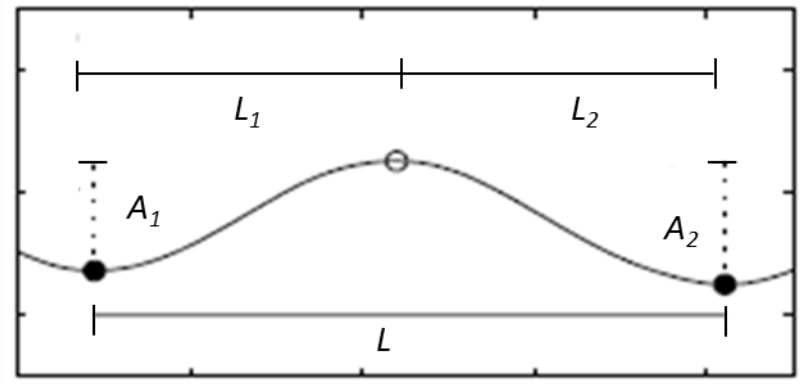

Figure 3.7: Schematisation of individual crescents parameters. Sandbar horns are represented with filled circles while sandbar bays with open. The shoreline is located at the bottom end of the figure.

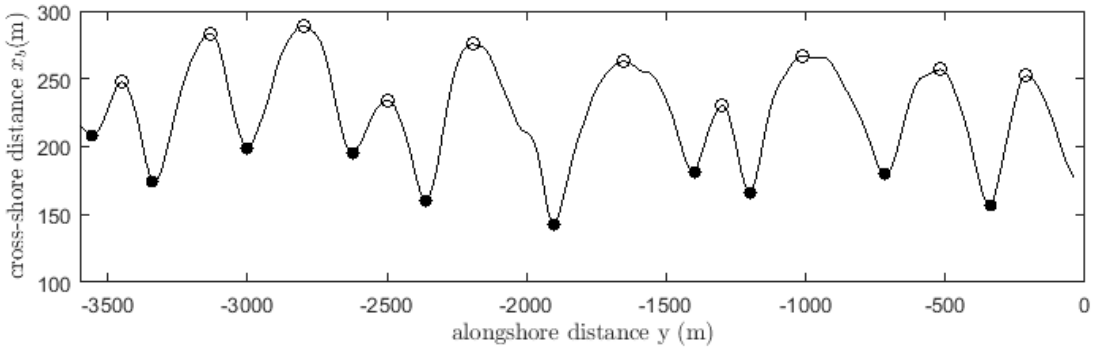

Figure 3.8: Example of determination of horns (filled circles) and bays (open circles) for the sandbar crest at 12/11/2013.

In Figure 3.9 the changes of the crescentic characteristics over the study period can be seen. From the span of minimum and maximum values it is clear that the characteristics vary in the alongshore direction a well. Moreover, there seems to be a correlation between the two characteristics.

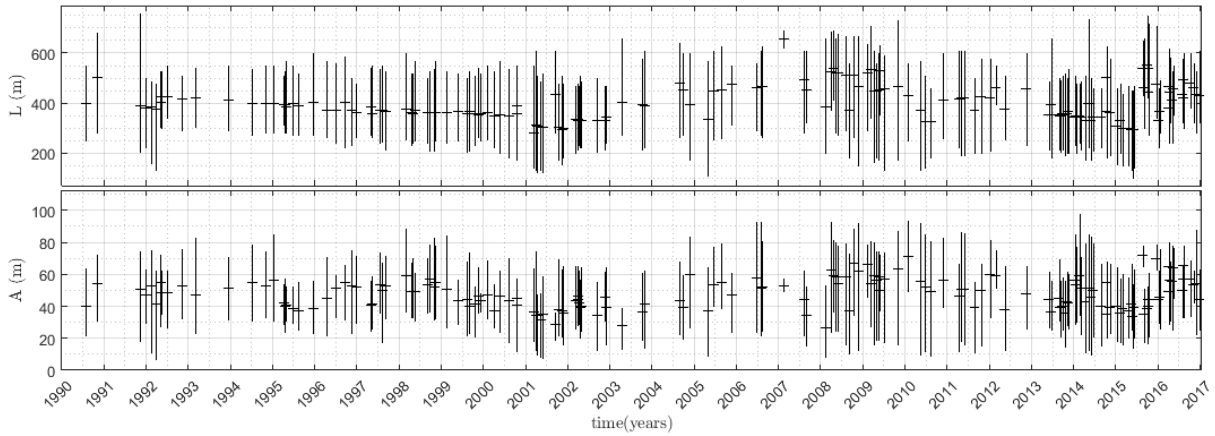

Figure 3.9: Length and amplitude timeline of the crescents for the MG3 dataset. The horizontal line represent the average alongshore value while the vertical line spans the minimum and maximum values.

This is more clearly observed in the scatter plot of Figure 3.10. Smaller wavelength is most of the times accompanied by smaller amplitude and vice versa. The correlation coefficient between the two parameters is r=0.76, showing a high linear relation between them. In general, for the study period the larger crescentic features appear in the area of y= -1800m to y=-600m, while at the north-western stretch the crescentic features are on average a lot smaller (Figure 3.20).

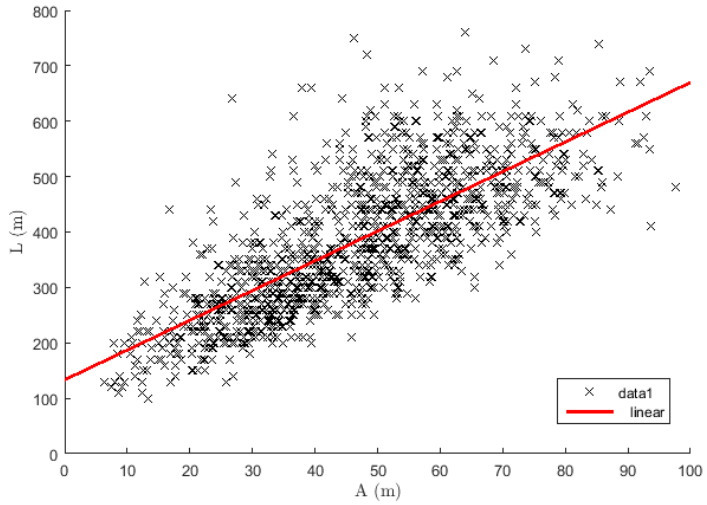

Figure 3.10: Scatter plot of amplitude vs. wavelength for all individual crescents detected in the study period for the MG3 dataset. The red line is the best linear fit of the data.

Additionally, in order to calculate the magnitude of the crescent's asymmetry (relative to the point defined as the middle between two consecutive horns) a new non-dimensional parameter S is defined as:

$$S = \frac{|L_1 - L_2|}{L} \tag{3.1}$$

Where L_1 is the distance from the one horn to the bay location and L_2 the distance from the other horn to the bay location (Figure 3.8). A low value of asymmetry S (close to zero) indicates a symmetric crescent (bay relatively in the middle of the horns) while

values close to 1 represent an intense obliqueness of the crescent. The mean alongshore values of the crescents asymmetry $\bar{S}$ is calculated for each of the available sandbar observations $x_b(y)$ and can be seen in Figure 3.11. The values of the crescent asymmetry keep quite low values for most of the study period (0.05-0.2), while only in the year 2016 they present a moderate increase, but never going above the value of 0.4. This result indicates that the shape of the crescents at Anmok beach can be characterized as symmetrical for the study period.

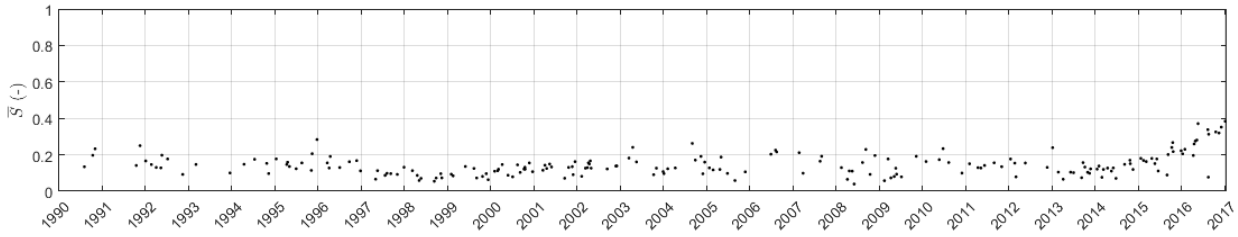

Figure 3.11: Alongshore mean value of asymmetry $\bar{S}$ for each of the available sandbar observations.

3.3.2 **Spectral analysis of sandbar location**

The alongshore sandbar crest position for each observation can be transformed using discrete Fourier decomposition in a variance density spectrum (Figure 3.12). From the variance density spectrum two pieces of information can be extracted. First of all, the length scales λ of the rhythmic patterns can be identified from the peaks in the spectrum. Furthermore, the crescentic-scale amplitude of the sandbar α can be defined, following Plant et al. (2006) as the root mean variance in the band $200\ m < \lambda < 800\ m$:

$$\alpha = \sqrt{\int_{800^{-1}}^{200^{-1}} E(\lambda^{-1}) d\lambda^{-1}} \quad \text{(m)} \tag{3.2}$$

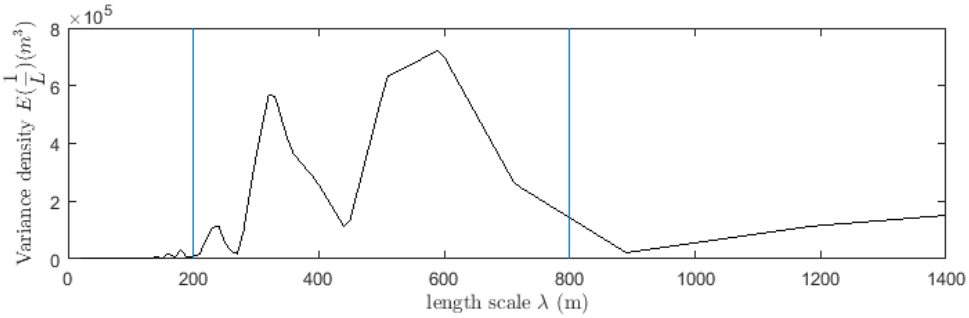

Figure 3.12: Variance density spectrum $E(\lambda^{-1})$ resulted from the Fourier decomposition of the sandbar crest line $x_b(y)$ at 12/11/2013. The two blue vertical lines define the bands between which the integration takes place to calculate α.

This band is defined according to the crescents length L range presented in Figure 3.9 and shows the length scales over which it is assumed that the 2DH processes are of importance at Anmok beach. Parameter α indicates the intensity of variability presented in the previously specified length scale band and is used in Chapter 4, in the empirical model formulation. The difference with the previously defined amplitude A is that α describes the whole sandbar and its variability in a specific length scale range, while A describes the amplitude of a specific crescent.

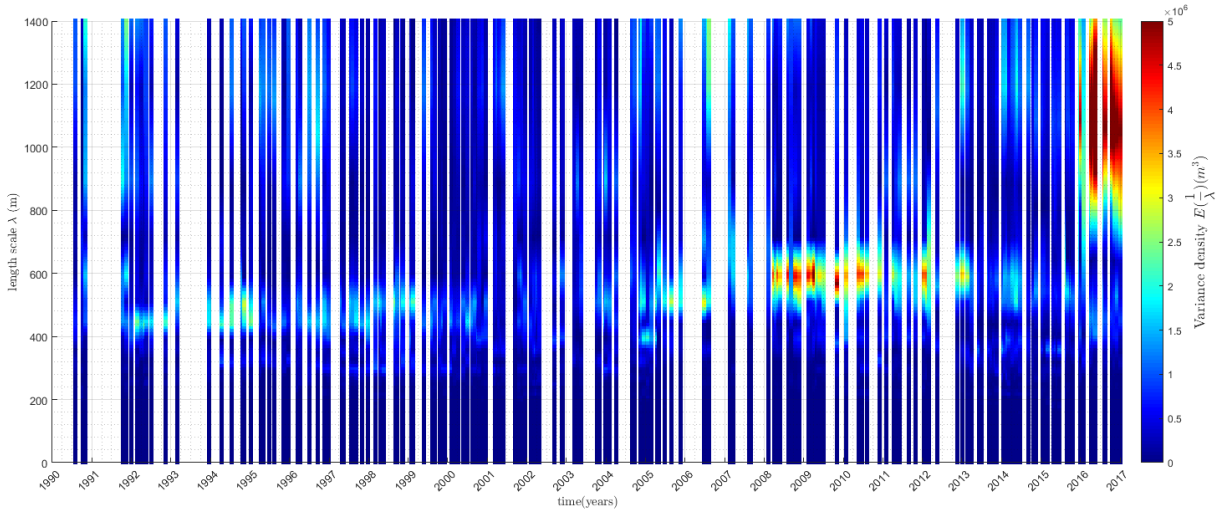

Figure 3.13: Time stacks showing the variance density $E(\lambda^{-1})$ of the MG3 dataset. Warm colours show higher intensity.

In Figure 3.13, it can be observed that until late 2015 the length scale of the rhythmicity present in the sandbar crest line is mainly concentrated in the length scales of the range 400-600m, agreeing with the wavelength L calculated in the previous chapter. But after, 2016 there is a high variance density in the length scales in the range of 1km. This greater scale rhythmicity can be seen as well at the satellite images in Figure 3.14, where there are crescents (length scale 100-300m) appearing on three larger crescents with a length scale of about 1 km. It is the only time that the sandbar has developed a shape like that during the study period. This unusual response can be connected to the uncommon sequence of wave forcing during that period. High wave energy events occurred in a sequence during November and December 2015, while they succeeded a typhoon hitting the coast during end of August.

3.3.3 **Second half of 2015 events**

Taking a closer look to the sequence of the events of the second half of 2015 (Figure 3.14), it can be observed that prior to April 2015 the sandbar was located close to the shore and had a distinct crescentic shape. After Typhoon's Goni attack on Anmok beach at the end of August 2015, generating a high alongshore wave energy component to the NW direction the sandbar migrated seawards while the alongshore variability of the crest location dropped significantly. Furthermore, it is important to notice that there is an observable difference in the response of the NW and SE parts of Anmok beach to the typhoon. While at the north-western part the bar lost most of its rhythmicity and almost got an alongshore uniform shape, at the south-eastern part the crescentic patterns are still present. This is speculated to be connected with two processes. First, that the port's breakwater is blocking the alongshore wave originated current, which develops further away from the port. Secondly, the sandbar is located closer to the shore at the northwest part as can be seen in the satellite image from June 2015 in Figure 3.14, which means that it is easier for the hydrodynamic forcing to reset it to an alongshore uniform state or something close to that. This does not hold for the south eastern part where the sandbar is on average located more offshore. This agrees with observations from Smit et al. (2010) and Lageweg et al. (2013) on the importance of the initial morphology on the response of the morphology to the hydrodynamic forcing. Furthermore, in the evolution of the morphology from June 2015 to September 2015 merging phenomena seem to take

place while during the period October 2015 to January 2016 splitting phenomena are noticeable (van Enckevort et al., 2004).

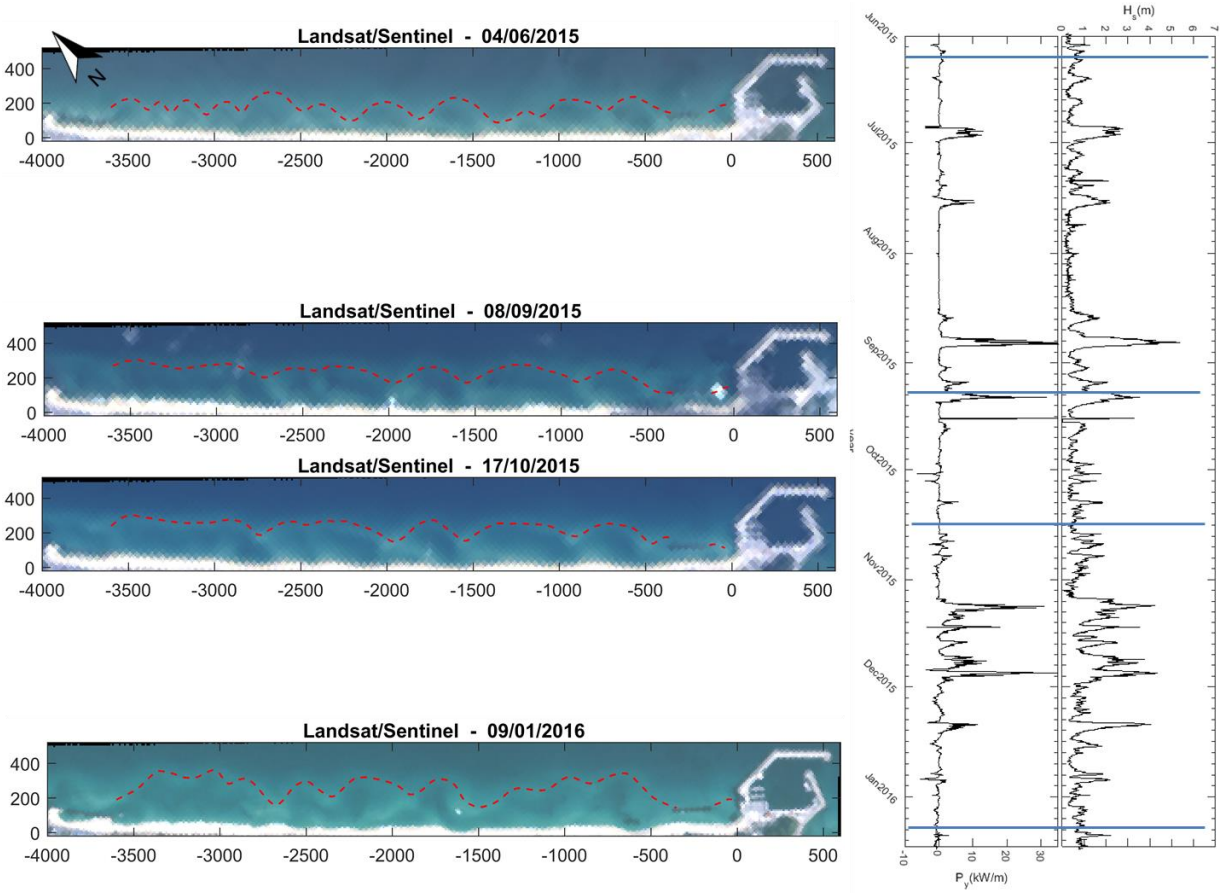

Figure 3.14: (Left) Satellite images with the sandbar crest line presented with a dashed red line for the period Jun2015-Jan2016. (Right) Measured wave data at location W1 for the same period. From right to left: H_s *and* P_y (spikes in the P_y diagram that point to the right describe an alongshore direction to the NW (away from the port).

3.3.4 **Sandbar system parameterization**

Following Plant et al. (2006) the sandbar state for each of the available observations can be described in a simple way with two parameters. The first one is the alongshore mean cross-shore bar position $\overline{x_b}$ (where the overbar denotes averaging in the alongshore), while the other one is the crescentic scale amplitude α as defined previously (Section 3.3.2). Both of these parameters are calculated for each of the available observations and are plotted for the study period in Figure 3.15 with the computed squared significant wave height at W1, which acts as a description of the wave energy. These parameters are used in the sandbar empirical modelling attempt in Chapter 4.

The mean sandbar cross-shore position varies between $\overline{x_b} = 260m$ and 150m, whereas the crescentic scale amplitude varied between $\alpha = 10m$ and 28m for the study period. Moreover, the mean sandbar cross-shore position seems not to respond directly to the wave energy. The same holds for the crescentic amplitude α. For example, during periods, when the sandbar was located seawards, like 1991-1992 or 1997-2000, $\overline{x_b}$ does not change in response to the high wave energy events. However, during periods when the sandbar was located closer to the shore, like winters of 1995-1996, 2001-2002 and 2015-2016, the sandbar moves quite offshore in response to the high energy events. This

implies that the response of the sandbar is not governed by the concurrent wave energy conditions only, but by the initial sandbar position as well (Plant et al., 2006; Yates et al., 2009; Smit et al., 2010). The sandbar appears to migrate onshore quite slow (years) while when it migrates offshore its response is faster (days to month).

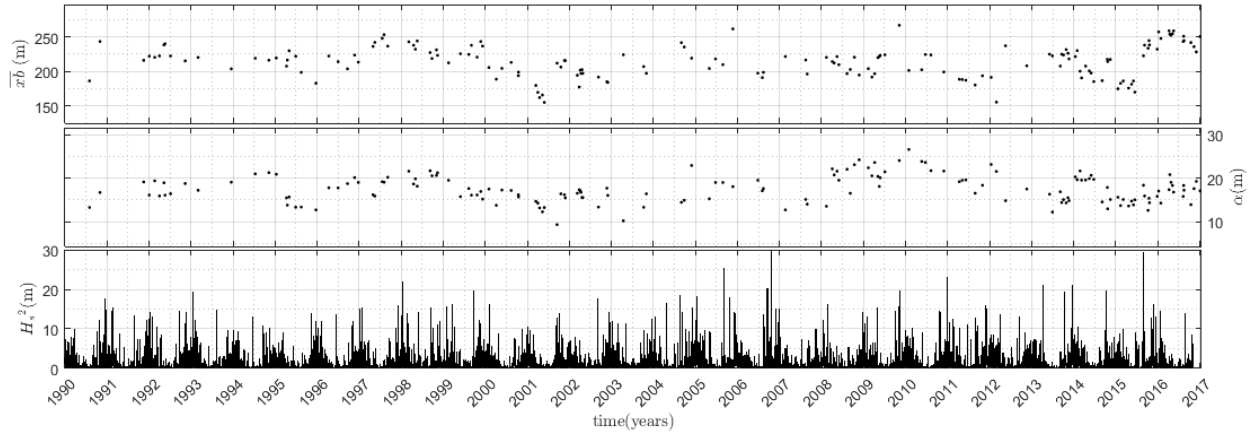

Figure 3.15: Timeline of the calculated alongshore mean cross-shore sandbar location $\overline{x}_b$ (top) , alongshore variability about that mean α (middle) and significant wave height squared computed at W1 (bottom) for all the available of observations of the MG3 data set.

Furthermore, in order to construct schematized bathymetries with crescentic sandbar features (Section 5.3) an analysis of the sandbar characteristic over the study period is performed. These characteristics are the mean cross-shore location of the sandbar $\overline{x}_b$, the amplitude A and the length L of the individual crescents. The histograms of these parameters including their mean and standard deviation values can be seen in Figure 3.16 and describe the natural variability of the sandbar at Anmok throughout the study period.

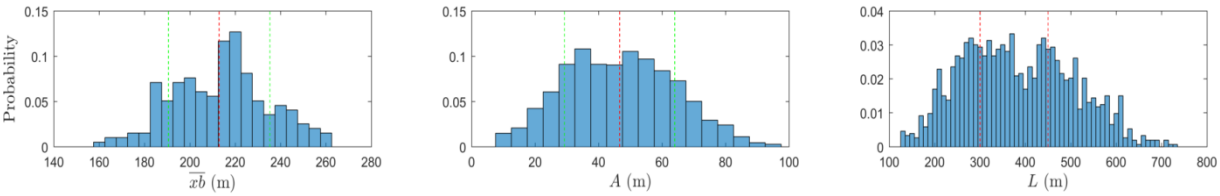

Figure 3.16: Histograms of: (Left) Mean cross-shore location of the sandbar $\overline{x}_b$, (Centre) Amplitude A of the individual crescents, (Right) Length L of the individual crescents. In the first two histograms, the red dashed lines indicate the mean value, while the green dashed lines the standard deviation. In the last histogram the red dashed lines indicate the two peaks.

3.3.5 **Alongshore migration**

The alongshore migration of the sandbar features has been connected with the wave generated alongshore current (Orzech et al., 2010; van de Lageweg et al., 2013). In order to make the sandbar features stand out more clearly, a fifth-order polynomial P_5 is fitted to the sandbar crest cross-shore position x_b for each of the available observations (Equation 3.3). The polynomial's order is chosen after testing which order can identify the perturbations better. Removing the fifth order polynomial fit from all available $x_b(y,t)$ resulted in the sandbar perturbations (Figure 3.17):

$$x_{b5}(y,t) = x_b(y,t) - P_5(y,t) \quad (3.3)$$

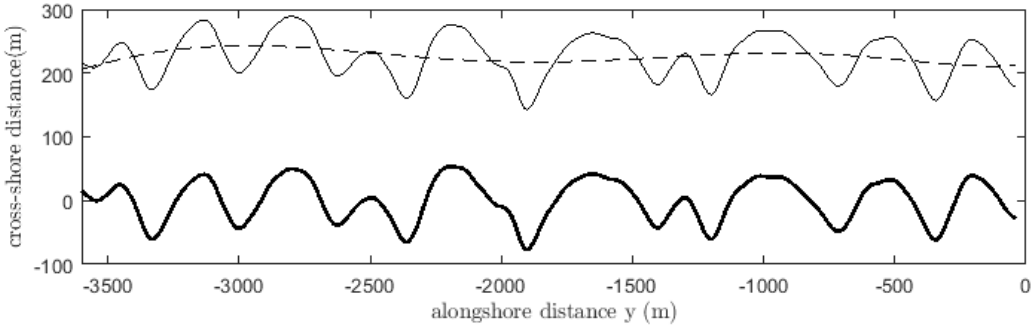

Figure 3.17: Example of sand bar crest line location x_b (thin line) with its fifth-order polynomial fit P_5(dashed line) and the resulting sandbar perturbations x_{b5} (thick line) at 12/11/2013.

The sandbar alongshore migration of its features is quite distinct in the time stack image of Figure 3.18. The features seem to have a general trend of alongshore migration that follows the net wave alongshore energy component over the same periods. For example during the periods of 1994-1997 and 2013-2015 there is a net alongshore wave energy directed to the Southeast which is accompanied by an alongshore migration of the sandbar features in the same direction. Furthermore, during the peaks of the alongshore wave energy directed to the Northwest at end of 2001 and 2nd half of 2015 the sandbar features migration direction is again in line with P_y.

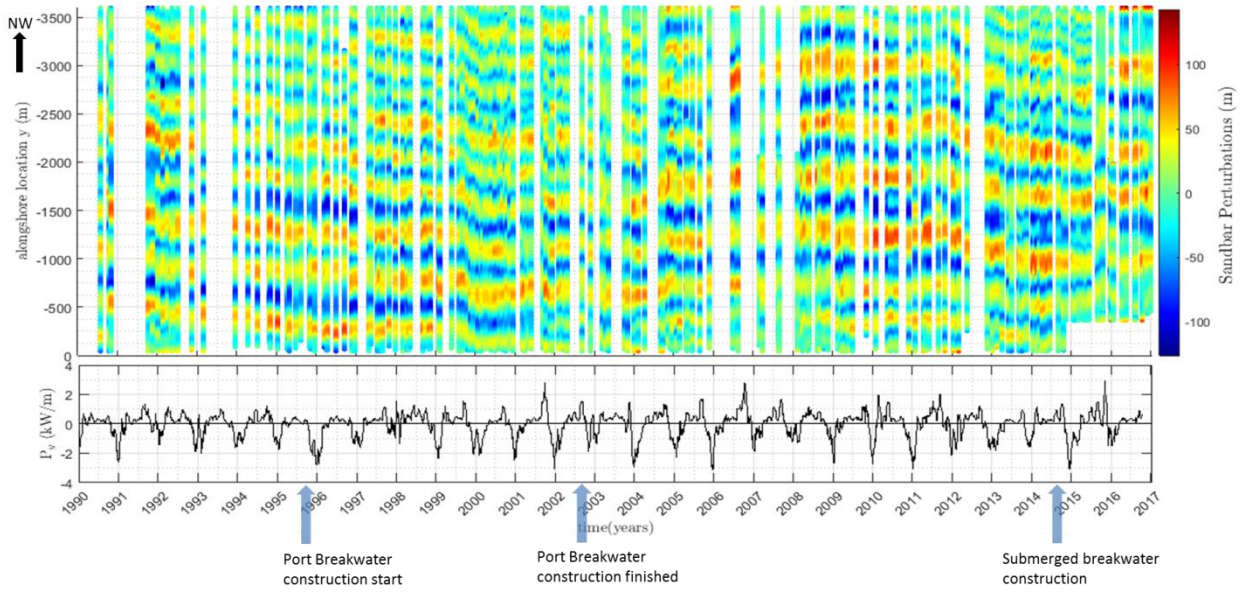

Figure 3.18: (Top) Time stacks showing x_{b5} (y,t) of the MG4 dataset. The blue colour indicates a shoreward bar perturbation (horn) while the red colour indicates a seaward bar perturbation (bay). (Bottom) Thirty-days averaged alongshore wave energy component P_y (Equation 2.3).

In order to calculate the alongshore migration of the sandbar between available observations, a cross-correlation between the sandbar crest lines of each subsequent observation is performed. The longshore migration is defined as the lag at the positive peak closest to the origin of the cross-correlogram (van Enckevort et al., 2004). The resulting alongshore migrations are compared with the integral of the wave alongshore energy component between the observations but the correlation is low. This might be

connected with the non-coherent interval of the observation and the migration noise due to the manual extraction technique.

As an alternative the cumulative plots of the two parameters are plotted (Figure 3.19), in order to identify and compare their long-term trends. In addition, the wave observations with a significant wave height smaller than 1m are excluded from the analysis, as they are assumed to create a surf zone width that does not affect the sandbar. The seasonal character of the alongshore wave energy component is quite pronounced during the study period. In both plots some general trends can be identified. First, for the period 1990-2004, there is a trend of the southeast directed wave energy flux overwhelming the one to the northwest. This is accompanied with an alongshore migration trend to the southeast. Then from 2005 until 2012, the opposite pattern occurs. For the period, 2012-2015 the south eastern directed trend appears again, while at the end of 2015, due to typhoon Goni there is an abrupt migration of the sandbar patterns to the Northwest.

The plots in Figure 3.19 give an indication of the connection between the alongshore migration of the sandbar patterns and the alongshore wave generated current. The long-term trends between the direction of migration and longshore-current direction follow the same patterns. The linear correlation between the two plotted cumulative time series reached a value of r=0.79.

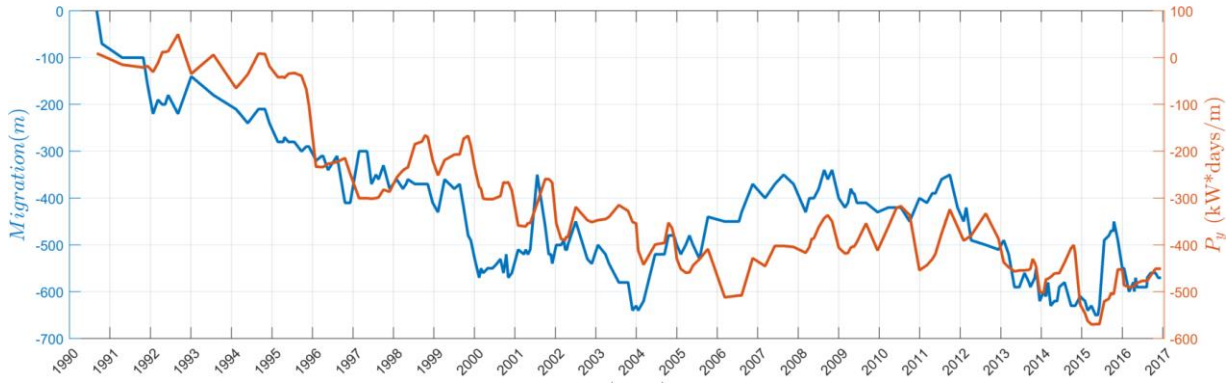

Figure 3.19: (Left axis) Cumulative alongshore migration (m) of the sandbar patterns between the available observations in the study period. (Right axis) Cumulative alongshore wave energy component P_y (Equation 2.3) integral (kW*days/m) at W1 location between the available observations. For both graphs positive values represent northwest directed migration or wave energy flux.

3.3.6 **Human interventions**

Submerged Breakwater construction

The SBW was constructed at the southern end of Anmok beach during the summer of 2014. The breakwater has a length of roughly 250 meters and a crest level up to -0.5 m MSL. After the SBW's construction the sandbar morphology offshore starts to slowly disappear (Figure 3.6). This seems to be connected with the blocking of the return current from the SBW which is expected to be the forcing mechanism that creates the sandbar.

Moreover, from January 2015 onwards the SBW seems to take the role of an "artificial" sandbar horn as the sandbar starts from the same cross-shore distance adjacent to the breakwater. The hydrodynamic cell patterns that are developed due to the presence of the breakwater are speculated to force the appearance of sandbar bays adjacent to the SBW. This is visible at the north side of the breakwater but not at the southern part,

where it is expected that the limited area due to the confinement from the port does not allow a bay to form.

Port construction

After the northern breakwater of Gangneung port has reached its most offshore point at beginning of 2000 (as derived from satellite images), the sandbar cross-shore location at the area adjacent to the port has on average moved closer to the shoreline (Figure 3.4).

Furthermore the influence of the port's construction on the sandbar characteristics can be observed to some extent in Figure 3.20, where the sandbar's crescentic characteristics are plotted versus the alongshore location. After the port construction the amplitude and wave length of the crescents present at a distance of 600-700m from the port's breakwater are reduced significantly (Figure 3.20).

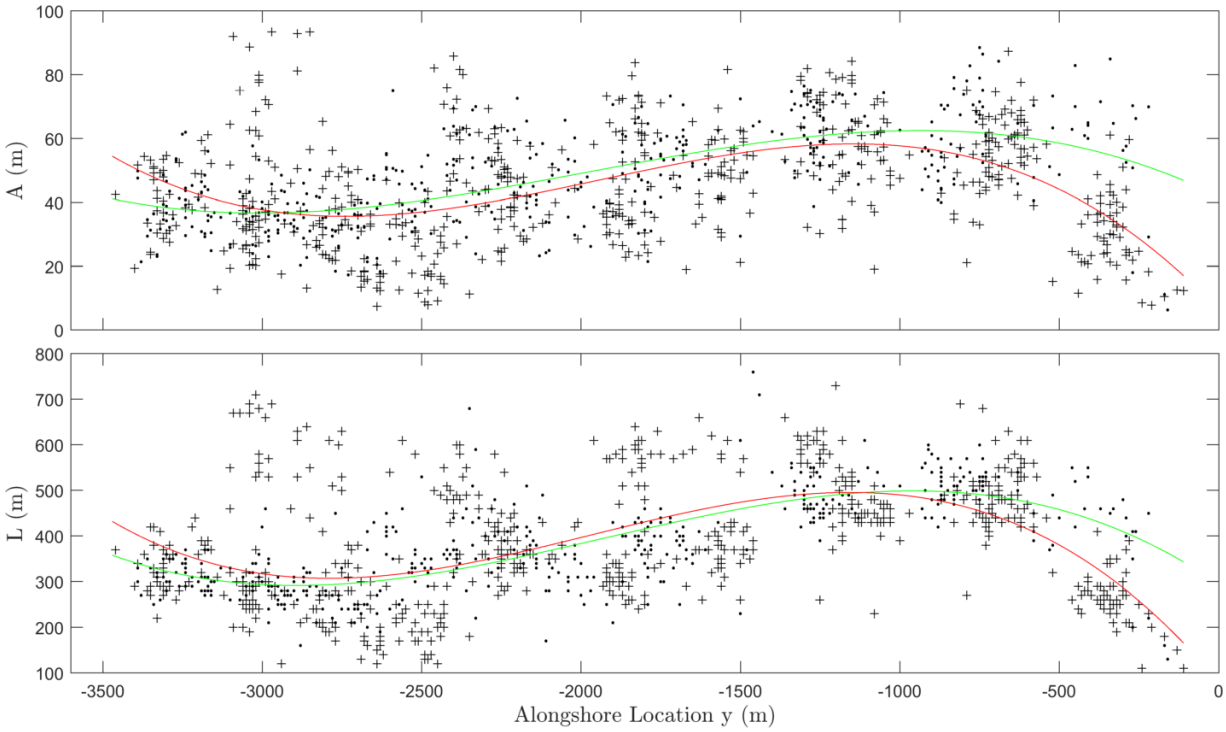

Figure 3.20: Amplitude (top panel) and wavelength (bottom panel) scatter plots of all the crescents detected in the period 1990-2000 (dots) and 2000-2010 (crosses) vs. their alongshore location (MG3 dataset). The green and red lines represent the best cubic fits for the pre-port (1990-2000) and post port (2000-2010) periods respectively.

Moreover, plotting the sandbar characteristics histograms for the two periods, before and after the port construction, separately for the area 650m from the port verifies the change of the sandbar features (Figure 3.21). The same graphs for the rest of the Anmok beach show that even though the sandbar has on average moved closer to the shore, the crescent characteristics stay the same before and after the port construction (Figure 3.).

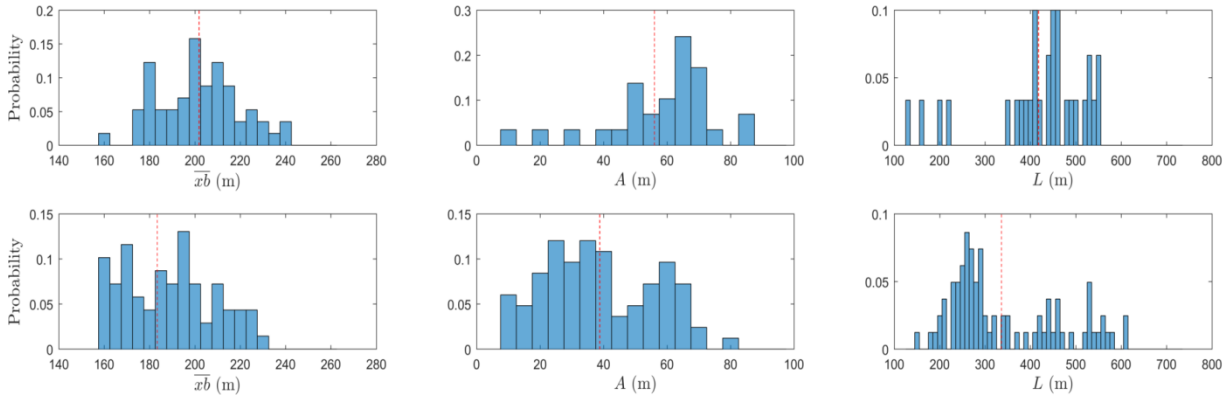

Figure 3.21: Histograms of: (Left) Mean cross-shore location of the sandbar $\overline{x}_b$, (Centre) Amplitude A of the individual crescents, (Right) Length L of the individual crescents, for the area y=-650m to y=0 m. The red dashed lines indicate the mean value. The graphs at the top describe the pre-port period (1990-2000) while the ones at the bottom the post-port period (2000-2010).

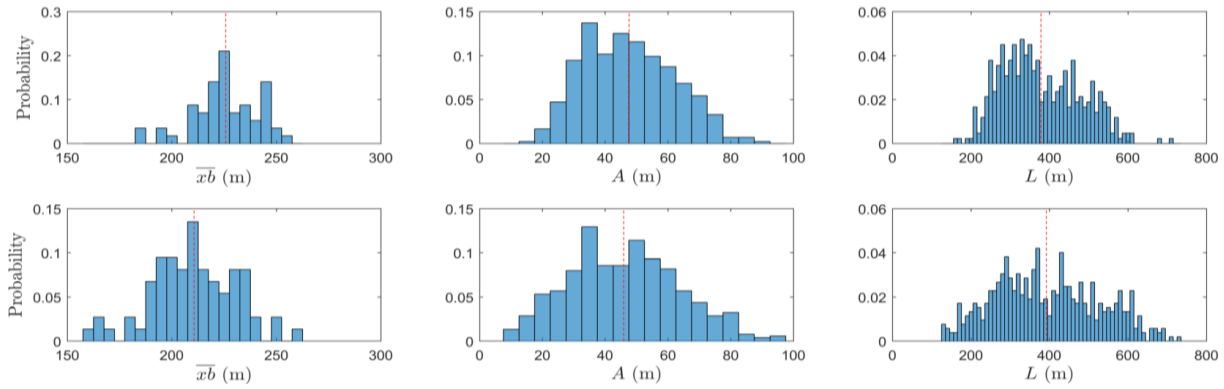

Figure 3.22: Histograms of: (Left) Mean cross-shore location of the sandbar $\overline{x}_b$, (Centre) Amplitude A of the individual crescents, (Right) Length L of the individual crescents, for the area y=-3.500m to y=-650m. The red dashed lines indicate the mean value. The graphs at the top describe the pre-port period (1990-2000) while the ones at the bottom the post-port period (2000-2010).

3.4 Shoreline characteristics

In order to get an indication of the magnitude of the shoreline perturbations, the same procedure as in Section 3.3.5 is followed. A 5th order polynomial is subtracted from the shoreline cross-shore position to get the perturbations around the mean shoreline position. This is performed for the period of 2008-2017. The area shoreward of the submerged breakwater is excluded, as it contains processes connected with the SBW dynamics and the nourishment that took place there. A timestack image of the perturbations and the alongshore maximum of the seaward and landward perturbations can be seen in Figure 3.23. What can be observed is the maximum values of the seaward perturbations (shoreline horns) are on average about 10m larger than the landward perturbations (shoreline embayments). The embayments in the study period get values of 10-20m while the horns 10-30m.

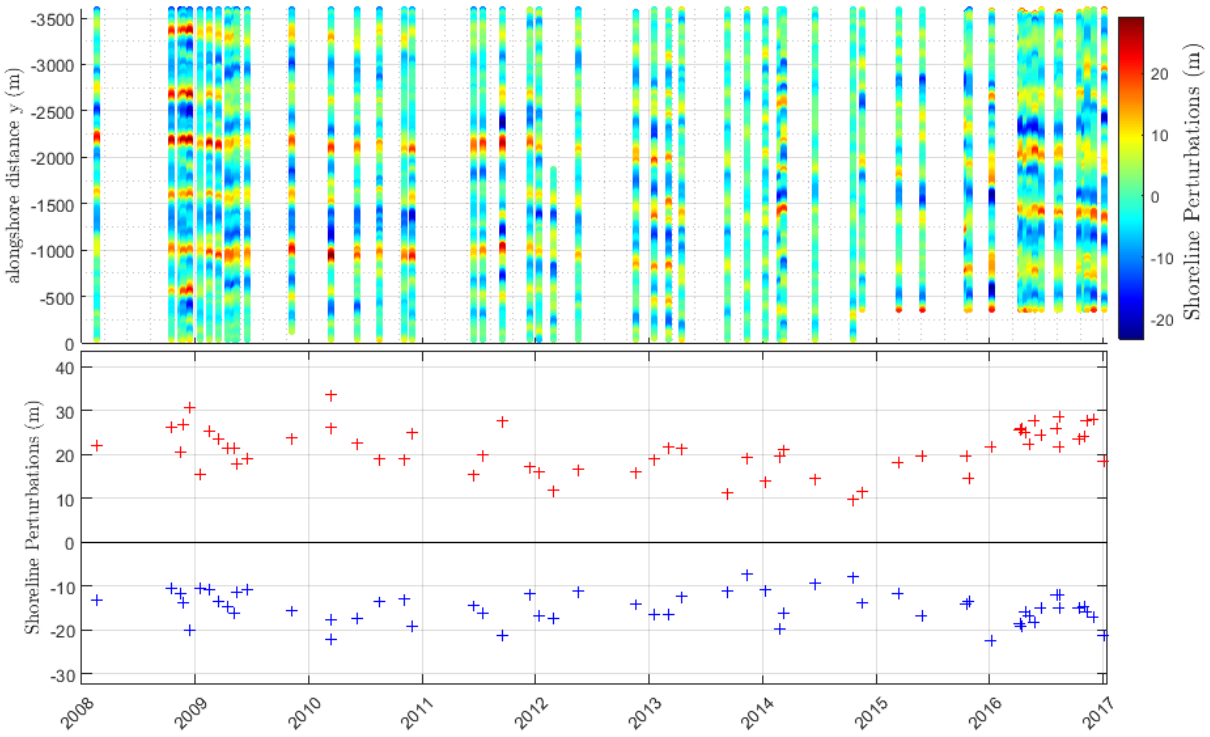

Figure 3.23: (Top) Time stacks showing $x_{s5}(y,t)$. The blue colour indicates a landward perturbation (embayment) while the red colour indicates a seaward perturbation (horn). (Bottom) Alongshore maximum values of the horn (red crosses) and the embayments (blue crosses)

3.5 Sandbar-Shoreline Interactions

3.5.1 Observations from satellite images

Studying the satellite and aerial images available, the connection between the sandbar and shoreline cross-shore locations is most of the times quite evident (Figure 1.1). In Figure 3.24-B an example of out of phase coupling between the sandbar and the shoreline is presented. This can be described by sandbar horns facing shoreline horns at the shore and sandbar bays facing shoreline embayments at the shore. On the other hand, Figure 3.24-C shows an example of a moderate in phase coupling, where the sandbar horns are face by shoreline embayments and the sandbar bays from shore horns. Furthermore, it can be observed that for the first case the mean sandbar cross-shore position is closer to the shore while the antecedent wave climate is moderate (Figure 3.15-Bottom panel). For the in phase coupling case, the average sandbar cross-shore location is more offshore and the preceding wave energy is quite severe (typhoon Goni). But the response of the shoreline seems to be not always so coherent for all the length of Anmok beach. In the images of Figure 3.24, A and D, the type and magnitude of the shoreline response vary across the beach. There seems to be again a strong dependency between the shoreline response (magnitude of perturbations) and the sandbar's distance from the shoreline.

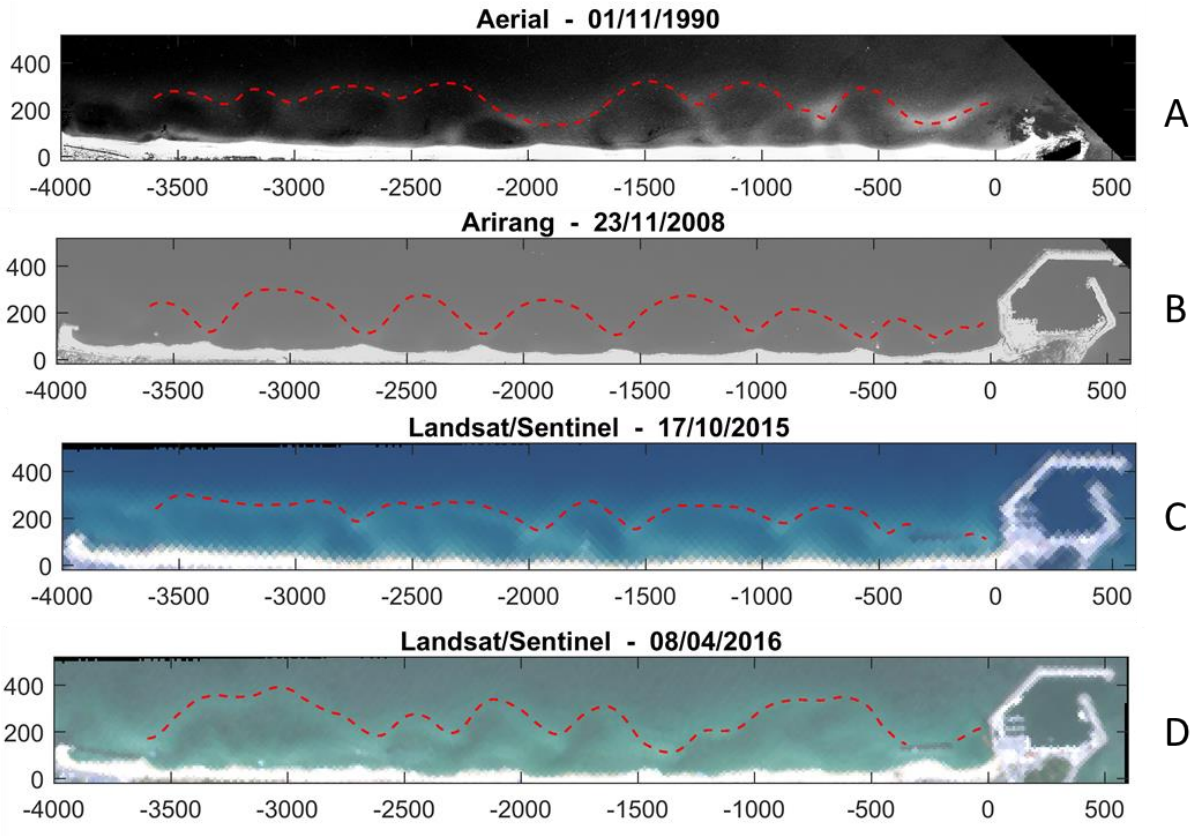

Figure 3.24: Satellite and aerial images where different kinds of sandbar and shoreline coupling are visible.

3.5.2 Linear dependency in cross-shore location

For the period of 2008-2017 the available sandbar and shoreline observations presented in the previous chapters are checked to find concurrent data. As the source of the shoreline and sandbar observation differ except the case of Sentinel and Arirang imagery it was difficult to find observations that are concurrent. For this reason, a constraint of ±10 days is used. This resulted in 37 couples of sandbar-shoreline observations. For each couple the linear dependency between the sandbar and shoreline cross-shore distances is calculated using the Pearson correlation coefficient:

$$r(t) = \frac{1}{N-1}\sum_{i}^{N}\left(\frac{x_b(y,t) - \overline{x_b(t)}}{s_{x_b}(t)}\right)\left(\frac{x_s(y,t) - \overline{x_s(t)}}{s_{x_s}(t)}\right) \tag{3.4}$$

Where N is the alongshore grid length and s is the standard deviation.

A negative correlation will indicate an out of phase coupling while a positive one, an in phase coupling. In Figure 3.25 the calculated correlation coefficient for the available data can be found. Furthermore, for these observations the separation between the sandbar and the shoreline is calculated. In accordance to previous observations, out of phase coupling is present for a small distance between the sandbar and the shoreline. As previously mentioned during the period 2008-2010 there is a strong out of phase coupling (Figure 3.26-Top) whereas during the typhoon season of 2015 there is a moderate in-phase coupling (Figure 3.26-Bottom).

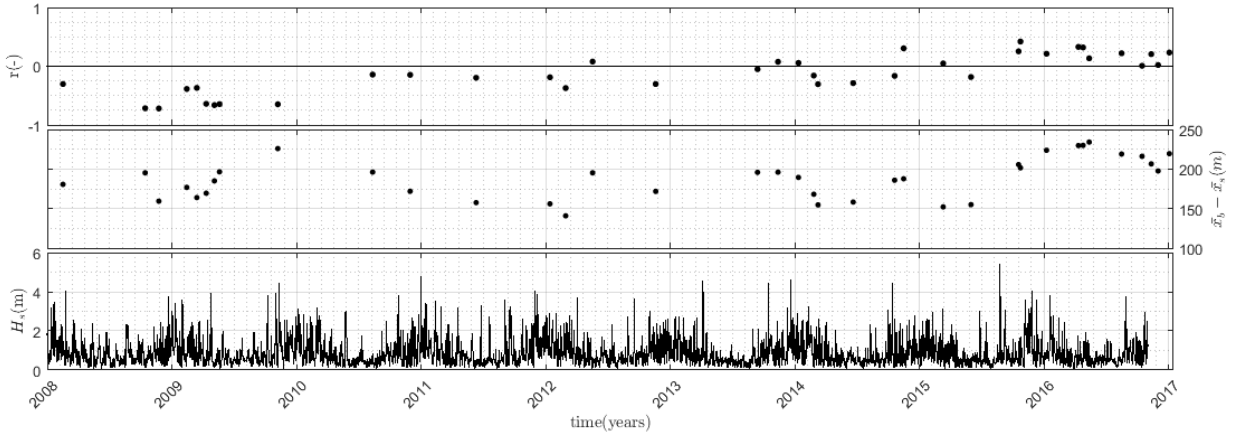

Figure 3.25: (Top) Pearson correlation coefficient r for the available shoreline-sandbar patterns, (middle) Distance between the alongshore average sandbar and shoreline position, (bottom) Significant wave height at W1.

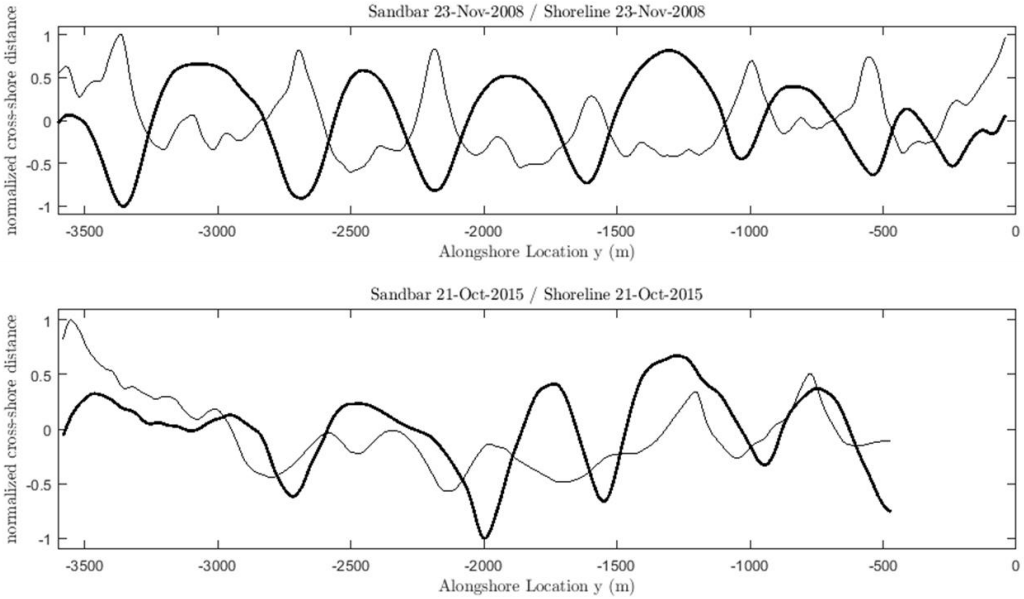

Figure 3.26: (Top) Example of high negative correlation of r=-0.72 showing out of phase coupling, (Bottom) Example of highest observed positive correlation r=0.42 showing in phase coupling. The sandbar is represent with the thick black line while the shoreline with the thin one. Both patterns have been normalized.

It is important to mention that correlation close to zero does not mean that the sandbar and shoreline are independent. It has been already mentioned that there might be in and out of phase coupling at the same time at Anmok beach, something that cannot be calculated with a linear correlation as they will cancel out leading to a value close to zero. Additionally, the presence of an inner bar at some areas during some periods introduces a different forcing on the shoreline.

3.6 Conclusion

Twenty seven years of satellite and in situ surveys are examined to describe the sandbar patterns at Anmok beach in the last decades. First of all, the sandbar's position is investigated for the study period of 1990-2017 and found to maintain its crescentic shape through all the period, while the patterns are mostly symmetric. Sandbar's cross-shore position is related to the concurrent wave conditions and showed not to respond linearly to incoming wave energy, while antecedent morphology is likely to be of importance. The alongshore migration of the sandbar characteristics is found to follow the general long term trends of the alongshore wave energy component, meaning that the alongshore current is capable of migrating the sandbar characteristics in the alongshore direction.

Different parameters of the sandbar are calculated for the study period in order to be used as indicators of sandbar response. These parameters change between pre and post human intervention periods, showed that the port construction affected the adjacent sandbar position by suppressing its crescentic shape (A and L) to smaller magnitudes.

Furthermore, the typhoon and storm events of the second half of 2015 seem to have changed abruptly the beach's nearshore morphology in comparison to all previous observations. This highlights the potential of consecutive high energy events for the sandbar response.

The mean alongshore sandbar's cross location $\overline{x_b}$ and the crescentic amplitude α are calculated for all of the available observations. These two parameters are used to model the sandbar response to changing wave conditions (Chapter 4).

Moreover, the connection between the sandbar and shoreline position is preliminary investigated from the observations. During some periods, clear out of phase coupling patterns are observed, but most of the times there is not a coherent response of the shoreline through all of its length. Factors that seem to be of importance in governing the response of the shoreline are identified as:

- Sandbar cross-shore distance from the shore
- Alongshore variability of the sandbar
- Incoming wave height
- Wave angle of incidence
- Presence of human made structures

These factors can act as systems controls for creating different scenarios to investigate the effect of the sandbar patterns on the alongshore sediment transports and study the coupling between the sandbar and the shoreline, using a numerical model (Chapter 5).

4. Predicting sandbar response to wave forcing

4.1 Introduction

This chapter deals with the investigation of the use of an empirical model that can predict the sandbar response to changing wave conditions. Having a predicting capability of the sandbar cross-shore location can provide insight for future wave climate scenarios. Furthermore, establishing a connection between the sandbar and the shoreline (Section 5.5) can eventually indicate what kind of response is expected at the shoreline according to the location of the sandbar. Two approaches are followed; one taking into account the alongshore variability of the sandbar and one that does not. The empirical models are calibrated and then tested for the Anmok beach dataset. Additionally, an assimilation algorithm, with an extended Kalman filter is used in order to verify the capability of the models to describe the sandbar system.

4.2 Model description

In order to reduce the dimensionality of the problem, two approaches are used. One is 1-D horizontal (1DH) and is based on Plant et al. (Plant et al., 1999), where the cross-shore sandbar migration is modelled in response to the wave forcing. The other one is a 2-D horizontal (2DH) and is based on Plant et al. (2006), where the dynamic relationship between the alongshore variable morphology and the sandbar cross-shore position is taken into account. Both approaches are based on an equilibrium response of the bar to changing wave conditions.

4.2.1 **1-DH Approach**

In the 1-DH model, cross-shore sandbar migration is specified as the difference between the mean cross-shore sandbar location $\overline{x}_b$ and the equilibrium location x_{eq} at time t, times the inverse of the response time τ:

$$\frac{d\overline{x}_b(t)}{dt} = \frac{1}{\tau}\left(x_{eq}(t) - \overline{x}_b(\mathrm{t})\right) \tag{4.1}$$

Assuming that the cross-shore migration is a function of the wave height raised in a power p, equation 4.1 can be rewritten as:

$$\frac{d\overline{x}_b(t)}{dt} = \mathrm{b}_1 + \mathrm{b}_2\overline{x}_b(\mathrm{t}) + \mathrm{b}_3\mathrm{F}(\mathrm{t}) \tag{4.2}$$

Where, $F(t) = H_s^p$ and b_1, b_2, b_3 are fixed parameters that can be determined with a least-squares fit to the observations.

4.2.2 2-DH Approach

In this approach the change in the mean alongshore sandbar cross-shore position $\overline{x}_b$ and the change in the crescentic amplitude α, depend on each other and on the incident wave height, following the linearized feedback model:

$$\begin{bmatrix} \frac{d\overline{x}_b}{dt} \\ \frac{d\alpha}{dt} \end{bmatrix} = A\begin{bmatrix} \overline{x}_b \\ \alpha \end{bmatrix} + B\begin{bmatrix} 1 \\ F \end{bmatrix} \tag{4.3}$$

Where A (2x2) and B (2x2) are coefficient matrices determined by linear regression to the available observations. The matrix A describes the interaction between $\overline{x}_b$and α, while matrix B describes the linear response of the system to the forcing plus a constant to account for non-zero mean values of $\overline{x}_b and\ \alpha$ (Plant et al., 2006).

The equilibrium values of $\overline{x}_b$ and α can be determined by setting the left hand side of equation 4.5 to zero:

$$\begin{bmatrix} x_{eq} \\ \alpha_{eq} \end{bmatrix} = -A^{-1}B\begin{bmatrix} 1 \\ F \end{bmatrix} = B_0\begin{bmatrix} 1 \\ F \end{bmatrix} \tag{4.4}$$

4.3 Calibration and results

4.3.1 1-DH Model

The coefficients b_1, b_2 and b_3 are determined with a least-squares fit to the observations for the study period. Different values for the power p of the wave height are tested with p=3 giving the best prediction skill. The linear regression is poor (R^2 is 0.04) and results in the values, $b_1 = 0.527\ md^{-1}, b_2 = -0.0028\ d^{-1}$ and b_3=0.034 $(m^2 d)^{-1}$.

The model is tested for the period of 2000-2016 by initialization with the first observations of x_b and the driven forward with the observed wave heights and a time step of 1 day. The results in Figure 4.1 show a very low predictive skill of $\overline{x}_b$ (R^2=0.05 and RMSE=22.5m).

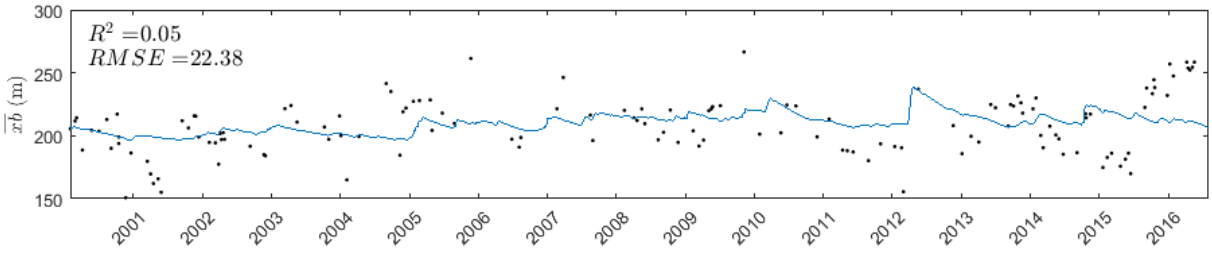

Figure 4.1: Model predictions (blue lines) and observations (black dots) of the alongshore average sandbar cross-shore location $\overline{x}_b$ for the period of 2000-2016.

4.3.2 **2-DH Model**

In order to account for the dynamical coupling between the sandbar cross-shore position and its alongshore variability the 2-DH model presented in Section 4.2.2 is used as well. The coefficient matrices A and B are estimated by integrating equation 4.5 over successive observations for the study period (Figure 3.15) and fitting the model to the observed changes in x_b and α using linear regression. Different values for the power p of the wave height are tested with p=3 giving the best prediction skill. The linear regression is poor (R^2 is 0.05 and 0.02 for $\overline{x}_b and\ \alpha$ respectively) and results in the coefficients:

$$A = \begin{bmatrix} -0.0023\ \{d^{-1}\} & -0.0110\ \{d^{-1}\} \\ -0.0003\ \{d^{-1}\} & 0.0007\ \{d^{-1}\} \end{bmatrix}$$

$$B = \begin{bmatrix} 0.6099\ \{md^{-1}\} & 0.0343\ \{(m^2d)^{-1}\} \\ -0.0726\ \{md^{-1}\} & -0.0013\ \{(m^2d)^{-1}\} \end{bmatrix}$$

The model is tested for the period of 2000-2016 by initialization with the first observations of $\overline{x}_b and\ a$ and the driven forward with the observed wave heights and a time step of 1 day. The results in Figure 4.2 show a very low prediction skill of $\overline{x}_b$ (R^2=0.18 and RMSE=21m) and no skill for α.

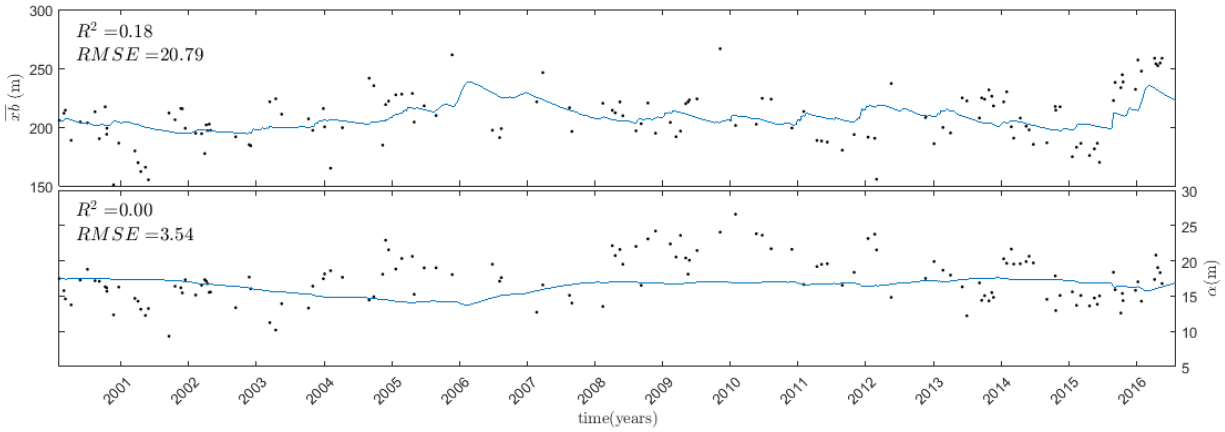

Figure 4.2: Model predictions (blue lines) and observations (black dots) of the alongshore average sandbar cross-shore location $\overline{x}_b$(top panel) and the crescentic amplitude α (bottom panel) for the period of 2000-2016.

As a test, the model is simplified by taking the crescentic amplitude α out of the prediction process, and taking into account only the one way influence of α on $\overline{x}_b$. This is realized by fitting a high order polynomial to the available observations of α, in order to have its values in each time step.

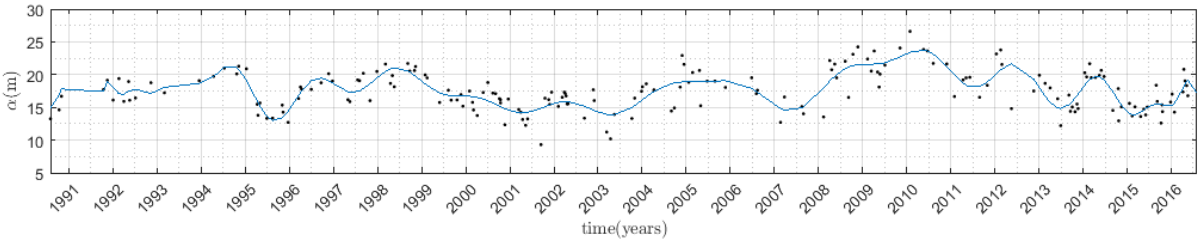

Figure 4.3: Observations of crescentic amplitude α for the study period (black dots) and polynomial high order fit (blue line)

Then the model is described only by the first equation of the equation system 4.3, and is initiated from the starting observation of $\overline{x}_b$ and moved forward with the observed wave height and crescentic amplitude α. The results are less accurate than the dynamically coupled case, producing no skill in the prediction of $\overline{x}_b$ (Figure 4.4).

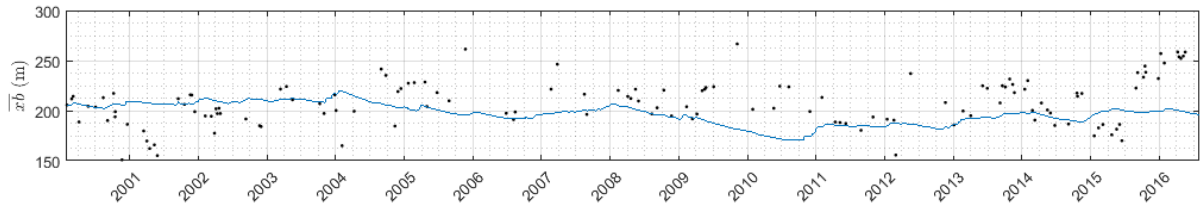

Figure 4.4: Model predictions (blue line) and observations (black dots) of $\overline{x}_b$ for the model without the dynamic coupling.

4.3.3 **Results interpretation**

The two empirical modelling formulations presented have been previously applied with success by producing predictive skill for different sandbar systems (Plant et al., 1999, 2006; Pape et al., 2010; Splinter et al., 2011). In all these applications, the sandbar observations came from processing video imagery from the sites with coherent and frequent intervals.

The bad prediction skill of both the modelling approaches for the case of Anmok beach can be connected with either the quality of the dataset, concerning both spatial accuracy and temporal resolution, or the simplicity of the model itself. To this end, the behavior of the sandbar at Anmok beach might not follow the schematization of the model. In order to test if the influence of the port on the sandbar might disrupt the simple behavior of the empirical model, the model was applied again but only for the part of Anmok beach that is out of the ports influence. The results showed no improvement in comparison to the previous application on all the length of the beach.

4.4 Extended Kalman filter framework

4.4.1 **Description**

As showed in chapter 4.3, the two model approaches that are used, fail to produce any predictive skill for the case of Anmok beach. Predictions errors can be a result of bad model parameterizations and inaccurate initial or boundary conditions. One approach that can deal with these kinds of problems is an assimilation algorithm that uses the available observations to update the model's forecast and to estimate the model's parameters. This way whenever an observation is available, the model "resets" itself

according to that and avoids carrying further accumulated errors from previous estimates. Long and Plant (2012) used an extended Kalman filter as an assimilation method for a shoreline change model, predicting the shoreline position at two time scales and estimating the non-observable parameters of the model. The assimilation algorithm is presented in the next chapter for the 1-DH model. For the 2-DH model the same procedure is followed.

4.4.2 **Assimilation Algorithm**

Following equation 4.2, there is one state ($\overline{x}_b$) and three parameters (b_1, b_2, b_3) that need to be estimated by the assimilation of the model and the observations of sandbar cross-shore position. This results in a state vector ψ:

$$\psi=\begin{bmatrix}\overline{x}_b\\ b_1\\ b_2\\ b_3\end{bmatrix} \tag{4.5}$$

In order to propagate each of the variables through time four equations are defined, according to equation 4.2 and assuming the parameters fixed:

$$\begin{aligned}\frac{d\overline{x}_b}{dt} &= \mathrm{b}_1 + \mathrm{b}_2\overline{x}_b + \mathrm{b}_3\mathrm{F} \quad , \quad \mathrm{F} = \mathrm{H}_s^3\\ \frac{db_1}{dt} &= 0\\ \frac{db_2}{dt} &= 0\\ \frac{db_3}{dt} &= 0\end{aligned} \tag{4.6}$$

This resulted in the following forecast equations f:

$$\psi_k^- = f(\psi_{k-1}, F_{k-1}) \;\Leftrightarrow\; \begin{bmatrix}\overline{x}_{b\,k}^-\\ b_{1\,k}^-\\ b_{2\,k}^-\\ b_{3\,k}^-\end{bmatrix} = \begin{bmatrix}\overline{x}_{b\,k-1} + \Delta\mathrm{t}(b_1 + b_2\overline{x}_b + b_3F)_{k-1}\\ b_{1_{k-1}}\\ b_{2_{k-1}}\\ b_{3_{k-1}}\end{bmatrix} \tag{4.7}$$

Where k is the discrete time step index, Δt is the discrete time step and ψ_k^- the a priori state estimate. The a priori error covariance is given by:

$$P_k^- = J_k P_{k-1} J_k^T + Q_{k-1} \tag{4.8}$$

where Q is the process noise covariance, which is assumed constant here and is chosen according to the values of Long and Plant (Long & Plant, 2012), giving a higher uncertainty on the model predictions in the state than in the parameters :

$$Q = diag\begin{bmatrix}1e^{-1}\\ 1e^{-5}\\ 1e^{-5}\\ 1e^{-5}\end{bmatrix}^2$$

The extended Kalman filter performs a first-order linearization of the forecast equations at each time step. This is done with the Jacobian matrix J of partial derivatives of the forecast equations f with respect to ψ:

$$J_{i,j} = \frac{\partial f_i}{\partial \psi_j} \tag{4.9}$$

The time step of the assimilation algorithm is defined as Δt=0.25 days. At each time step the algorithm checks if an observation is available.

- If yes, the state estimate is updated according to:

$$\psi_k = \psi_k^- + K_k(d_k - H\psi_k^-) \tag{4.10}$$

where ψ is the posterior corrected state. The correction is applied by the difference between the observation d and the modeled state $H\psi_k^-$ and it's commonly called innovation. As only $\overline{x}_b$ observations are available:

$$H = [1 \quad 0 \quad 0 \quad 0] \tag{4.11}$$

The Kalman gain weights the innovation according to the error covariance of the predicted state P_k^- and the observed state R_k using the following equation:

$$K_k = P_k^- H_k^T (H_k P_k^- H_k^T + R_k)^{-1} \tag{4.12}$$

R_k is defined according to the observation grading that has been described in Appendix A. After the forecast update the error covariance of the posterior state is updated as well, according to:

$$P_k = (I - K_k H) P_k^- \tag{4.13}$$

- If no, the forecasted state is equal to the a priori state estimate and the error covariance to the a priori one, as no update occurs :

$$\psi_k = \psi_k^- \tag{4.14}$$

$$P_k = P_k^- \tag{4.15}$$

In order to initialize the algorithm a starting state vector is defined according to the first observation and the results of the previous modelling approach, while the starting error covariance vector is defined from the observations accuracy and the uncertainty of the parameters:

$$\psi_{t_0} = \begin{bmatrix} 185 \\ 0.525 \\ -0.0028 \\ 0.034 \end{bmatrix} \qquad P_{t_0} = diag \begin{bmatrix} 5 \\ 1 \\ 1 \\ 1 \end{bmatrix}^2$$

4.4.3 **Results and interpretation**

1-DH approach

Based on the choices of error covariance matrices for the measurements and the model predictions described in the previous chapter the extended Kalman filter is "following" the measurements. This means that the model coefficients are adapting according to the sandbar position observations. From Figure 4.5, the model parameters appear not to converge in some specific values, which can mean that the system cannot be described by fixed model parameters for the study period.

2-DH approach

For the 2-DH empirical model, the same approach as for the 1-DH case is followed in order to build the assimilation algorithm. The results are shown in Figure 4.6. Again the model parameters do not seem to converge to some standard values. Moreover, their

values are not of the same scale as the results from the linear regression, which was expected from the low regression analysis at the previous step.

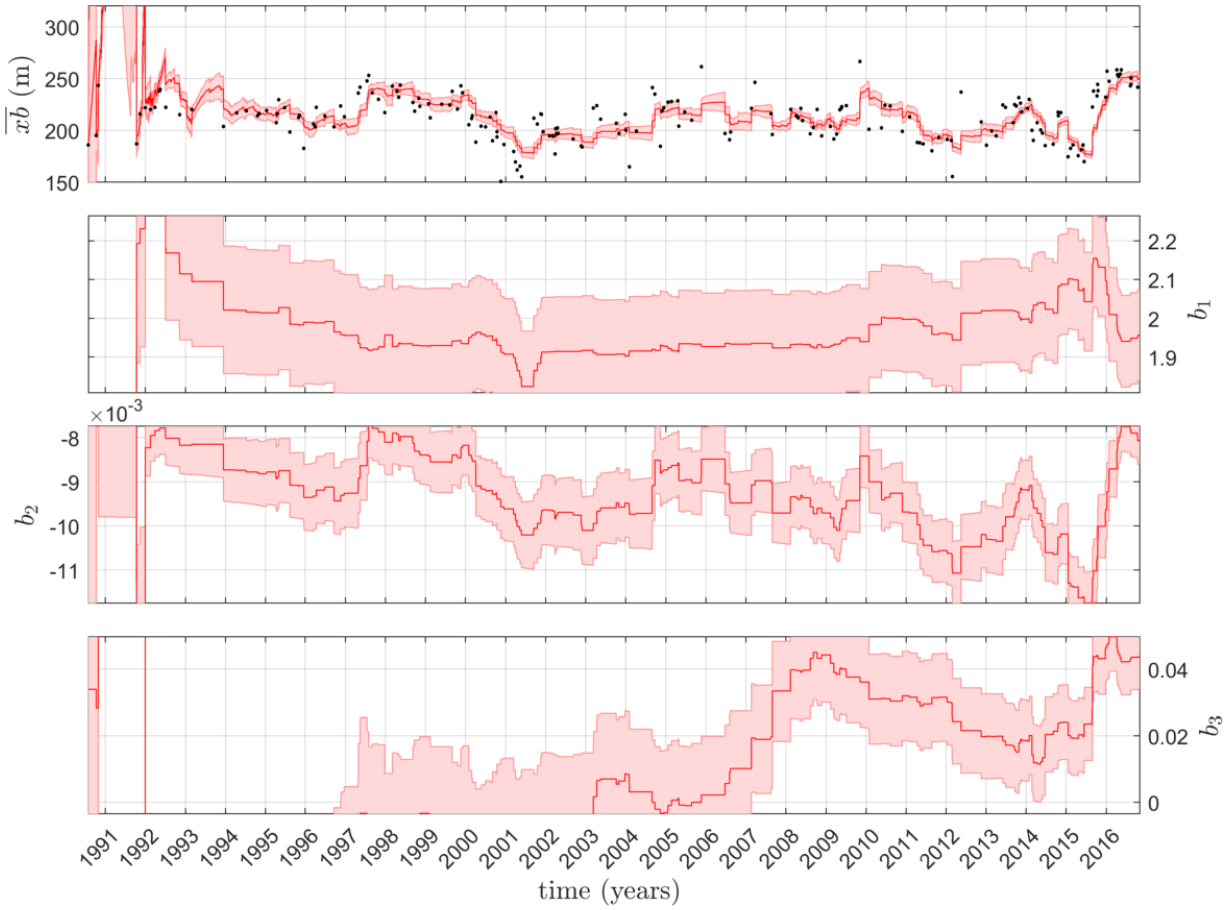

Figure 4.5: Results of the model-data assimilation algorithm. (top to bottom) Alongshore averaged cross-shore sandbar position (x_b), and coefficients b_1, b_2 and b_3. The solid red line describes the modelled results while the shaded area represents the uncertainty of the results (square root of error covariance diagonal values).

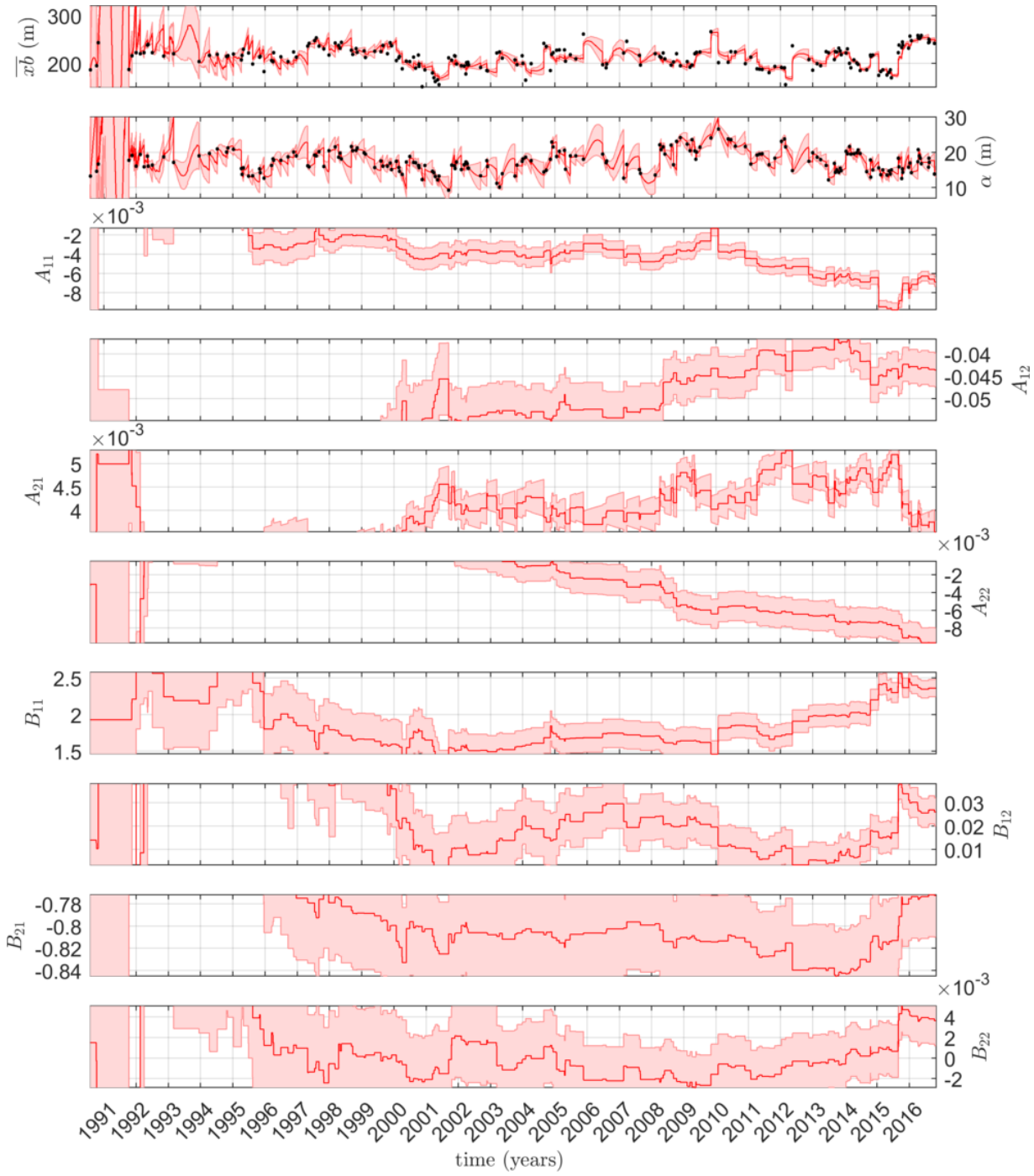

Figure 4.6: Results of the model-data assimilation algorithm. (Top to bottom) Alongshore averaged cross-shore sandbar position (x_b), crescentic amplitude α, and coefficients A and B. The solid red line describes the modelled results while the shaded area represents the uncertainty of the results (square root of error covariance diagonal values).

4.5 Conclusion

The results from the empirical modelling of the sandbar response at Anmok beach are unsatisfactory, at least with the dataset and the model approaches that are used in this study. Possible factors that are identified, concerning the bad prediction skill of the empirical models are:

- Not coherent and high interval between observations, which can mask the response of the sandbar to the forcing. For example, the integration of wave energy between to observations with a time interval of 2 months cannot resolve the individual storms in between.
- Spatial accuracy of the observations from satellite imagery is not good enough for the linear regression and derivation of the model coefficients.
- Mean alongshore sandbar's cross-shore position in this study is calculated from a fixed reference line, while in previous approaches it was determined in reference with the coastline.
- The model from Plant et al. (2006) includes a linearized formulation which is valid for small perturbation about a mean and for short records (Splinter et al., 2011).
- The assumption of fixed model coefficients, which might be invalid especially for longer time scales Pape et al. (2010) showed that treating the coefficients as variable according to the wave height can produce better results. This approach needs an extensive dataset which is not available in this case.
- Errors in the model (parameters or boundary conditions) at a specific time step are carried to the next predictions as well.
- Finally, there is always the possibility that the sandbar system in Anmok beach is quite complex in order to be described by these kind of simplified parametric models. Other forcing parameters like the wave angle or the wave period might be of importance for the behavior of the sandbar.

5. Modelling sandbar and shoreline interactions

5.1 Introduction

In this chapter the processes behind the shoreline and sandbar interactions are investigated with the use of numerical modelling. A Delft3D model for Anmok beach has been set-up and calibrated during previous phases of the CoMIDAS project (Deltares, 2016; Ton, 2017). Here, it is used to identify the nearshore hydrodynamic patterns under various synthetic wave conditions on bathymetries created from available surveys. This step is essential to understand the underlying processes and investigate how different wave conditions and bathymetries change the hydrodynamic patterns. These bathymetries are chosen according to the analysis of the available observations from Chapter 3.

Furthermore, a new Delft3D model is created to study the influence of the sandbar characteristics on the alongshore sediment transports by means of schematized bathymetries and yearly averaged wave climates. The schematized bathymetries are created according to the analysis of the sandbar position in Anmok beach through the study period and available surveys (Chapter 3). This approach investigates the impacts of the sandbar variability on the net alongshore sediment transport rates. Additionally, a study on how different sandbar patterns can affect the shoreline response is performed.

5.2 Hydrodynamic processes at Anmok beach

5.2.1 General model information

In order to compute the hydrodynamics and sediment transports, a Delft3D(2DH) numerical model is used (Lesser et al., 2004). To this end, the modules Delft3D-WAVE (Deltares, 2014b) and Delft3D-FLOW (Deltares, 2014a) are used in an online coupled way. The Delft3D-WAVE module uses the 3rd generation SWAN model to compute wave transformation and breaking though the domain. The model is based on the discrete spectral action balance equation and is fully spectral both in frequencies and directions. The Delft3D-FLOW module solves the unsteady shallow-water equations in two (depth-averaged) dimensions. The current velocities are calculated using the non-linear shallow

water equations. This way the wave-driven alongshore current and residual circulations and rip-currents due to water level set-up are resolved.

5.2.2 **Model domain and specifications**

The Delft3D model domain for the Anmok case, both for the WAVE and the FLOW model can be seen in Figure 5.1. This model has been set-up and calibrated during previous phases of the CoMIDAS project (Deltares, 2016; Ton, 2017). The WAVE domain extends about 300m around the FLOW domain to account for erroneous results close to the wave module boundaries. The grid resolution is finest at the nearshore area, with a grid size of approximately 5x5m. The resolution decreases towards the alongshore and offshore model extents to approximately 20x15m.

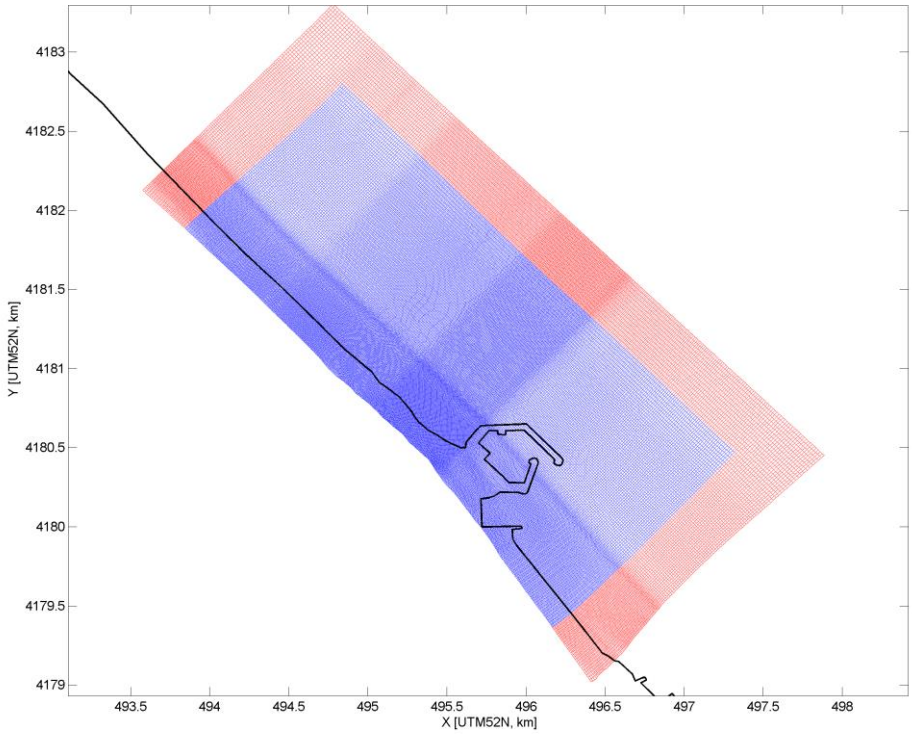

Figure 5.1: Delft3D-Wave model domain (red grid) and Delft3D-FLOW domain (blue grid) for the Anmok case

The boundary conditions of the FLOW model are specified with a water level of ζ=0m for all times as the influence of tide is not taken into account due the small tidal range of the area. At the lateral boundaries, Neumann boundary conditions are specified. According to the calibration of Ton, (2017), the harbour is represented as an obstacle for the wave module and with thin dams in the flow module. The following physical parameter settings are applied:

- Gravitational acceleration: 9.81 m/s^2
- Water density: 1025 kg/m^3
- Bed roughness: Chézy roughness of 65 $m^{1/2}/s$ is applied to the entire domain, except the locations of the SBW and the harbour where it is increased to 35 $m^{1/2}/s$.
- Horizontal eddy viscosity: To avoid instabilities because of variations in bathymetry along the boundaries, the horizontal eddy viscosity is adjusted at a

band with a width of 60 to 90 meters along the boundaries from the default of 1.5 m^2/s to 100 m^2/s.

- Sediment Parameters:
  - D_{50} of 400μm
  - Specific density of 2650 kg/m^3
  - Dry bed density of 1600 kg/m^3
- Transport and morphology parameters
  - Transport computed based on the TRANSPOR2004 formulation (Van Rijn et al., 2004; van Rijn, 2007a, 2007b)
  - Wave related transport factors set to 0.2
  - No bed level updating

The model is run for 12 hours with a time step of 6 seconds, which is sufficient to obtain a steady flow state.

5.2.3 **Bathymetry**

The bathymetries that are used in the Delft3D model are created from available surveys and shoreline measurements. Specifically, from section 3.5.1, two different nearshore beach states where identified, which included different sandbar configurations and shoreline states. The available surveys, for these two states where from September 2008 and August 2015 (Figure 5.2). September 2008 bathymetry presented a quite pronounced RBB state with sandbar-shoreline out of phase coupling appearing. On the other hand, the bathymetry from 2015 is described by a TBR state, with oblique rip channels formed. Furthermore, it presents a moderate in-phase sandbar-shoreline coupling.

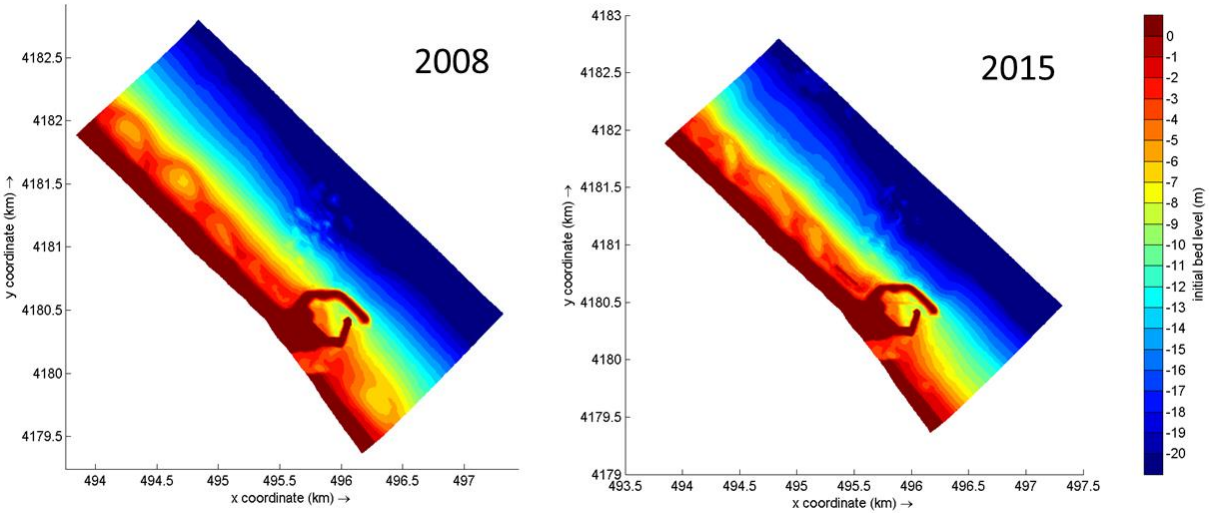

Figure 5.2: Bathymetries for the two beach states under consideration. (Left) September 2008, (Right) August 2015.

5.2.4 **Hydrodynamic study**

In order to understand how the sandbar system and the wave conditions influence the local hydrodynamics some synthetic wave conditions are chosen according to the wave time series available. The boundary conditions that are chosen can be seen in Table 5-1,

with main focus in investigating the influence of the wave height and angle of incidence. The wave direction that are tested are normal to the shore (43.5° N) and ±13.5 °. Wave period is assumed not so important and kept a typical value for the case study of 7s. The forcing is chosen as uniform along all the open boundaries and a JONSWAP spectrum is assumed.

Table 5-1: Test simulations performed with the boundary conditions that are used

Test id	Bathymetry	H_s (m)	T_p (s)	Dir (deg N)
test1	2008	1.5	7	43.5
test2	2008	3	7	43.5
test3	2008	1.5	7	30
test4	2008	1.5	7	57
test5	2015	1.5	7	43.5
test6	2015	1.5	7	30
test7	2015	1.5	7	57

The stationary results of the WAVE module for the test1 simulation can be seen in Figure 5.3. Along the sandbar wave shoaling can be identified while at the locations of the sandbar horns (shoals) there is a significant amount of wave breaking occurring. On the other hand, at the bays, the waves continue relatively undisturbed and break only when they reach close to the shoreline. Due to refraction, the wave's directions changes when they pass through the crescentic sandbar bathymetry. Landward of the sandbar horns the waves are focusing.

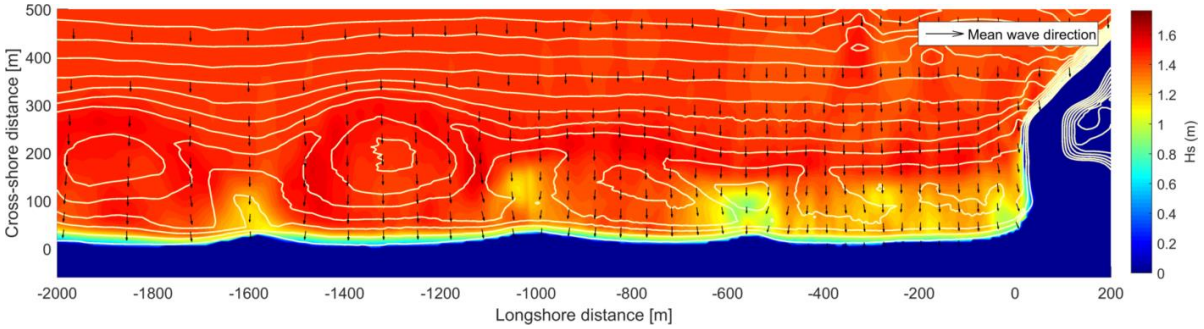

Figure 5.3: Significant wave height Hs (m) for test1 simulation. Vectors indicate the mean wave direction while contours the bed level with respect to MSL, from 0m MSL to -12m MSL and every 1m.

The results of the test1 simulation (Figure 5.4-top), which is forced with waves arriving perpendicular to the coast, show an onshore directed flow over the sandbar horns. Due to continuity, this onshore flow results in an offshore directed flow (rip current) at the bay of the sandbar. Close to the shoreline the flow patterns change directions with an alongshore flow convergence being observed at the horn locations at y=-550m, -1000m and -1600m. The colour alternation in the velocity fields of Figure 5.4 landward of the horns locations shows a convergence of the flow patterns which can indicate an accretional hotspot, thus a shoreline horn. Plotting the water levels (Figure 5.5) shows that landward of the sandbar bays location the set-up is almost double in comparison to

the areas landwards of the sandbar horns. Consequently, the pressure gradients along the coastline can explain the convergent flow patterns that appear.

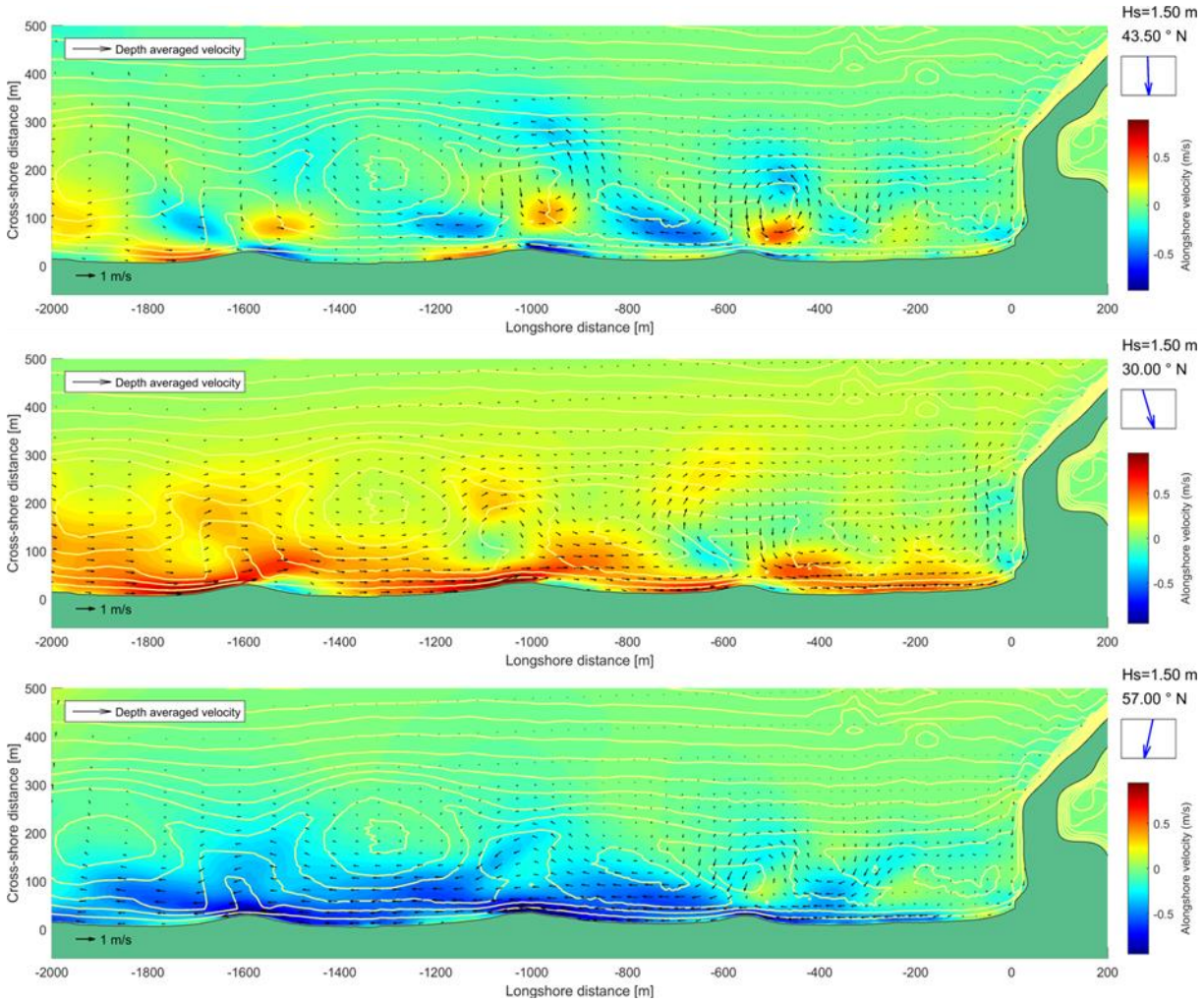

Figure 5.4: Alongshore velocity (GLM) component fields for test1, test3 and test4 (From top to bottom). Vectors indicate the depth averaged velocities while contours the bed level with respect to MSL, from 0m MSL to -12m MSL and every 1m.

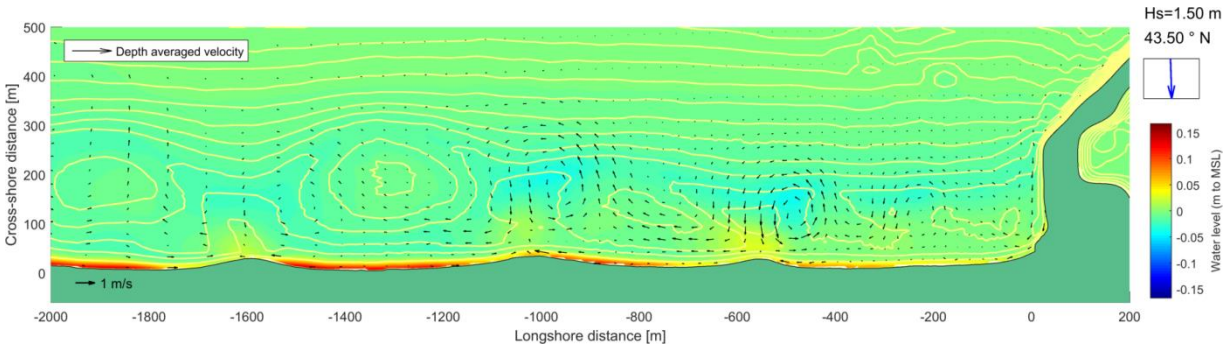

Figure 5.5: Water level with respect to MSL field for test1. Vectors indicate the depth averaged velocities while contours the bed level with respect to MSL, from 0m MSL to -12m MSL and every 1m.

Raising the wave height (test2) shows only an increase of the magnitude of the velocities but the general hydrodynamic patterns stay the same as test1. Changing the incoming wave direction seems to have different effects according to the side relative to the

normal to the shore. For an anti-clockwise rotation of the wave forcing (test3) the flow follows a meandering current pattern at the location of the sandbar. Closer to the shore, the convergence of flow at the horns location still exists, but the magnitude of the alongshore velocities down drift of the horn is far smaller than in test1. On the other hand, for a clockwise rotation of the wave direction (test4) the hydrodynamic converging patterns close to the shoreline do not appear at all. This is speculated to be connected with the shape of the bathymetry which shows a small anti-clockwise obliqueness in respect to the normal to the coast.

For the 2015 case (Figure 5.6) the sandbar horns are obliquely connected to the shoreline. The hydrodynamic patterns follow the rip channels that are imprinted in the nearshore morphology when the waves are normal to the shore or coming from Southeast. When the waves arrive perpendicularly to the coast there is again an alternation of alongshore flow direction near the coastline. The flow converges where the rip currents are formed and then follows the rip channels. Again, as for the bathymetry of 2008 when the wave come from the Northeast (test5) there is still the converging cell patterns appearing close to the shoreline. On the other hand, when the waves are approaching from Southwest the hydrodynamic patterns are directed only to the North.

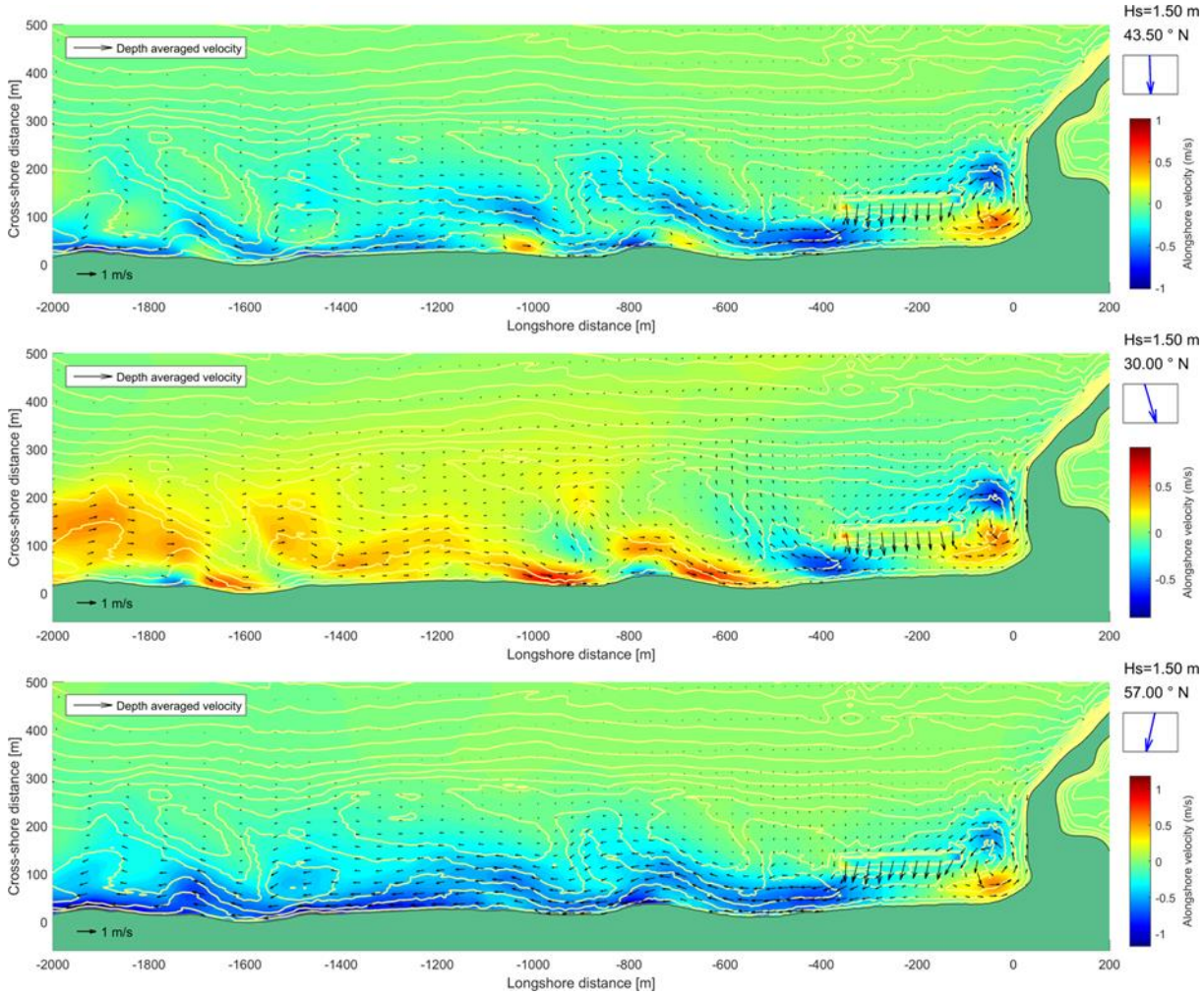

Figure 5.6: Alongshore velocity (GLM) component fields for test5, test6 and test7 (From top to bottom). Vectors indicate the depth averaged velocities while contours the bed level with respect to MSL, from 0m MSL to -12m MSL and every 1m.

5.3 Schematized scenarios

5.3.1 Model domain and specifications

The Delft3D model domain for the schematized cases, both for the WAVE and the FLOW model can be seen in Figure 5.7.

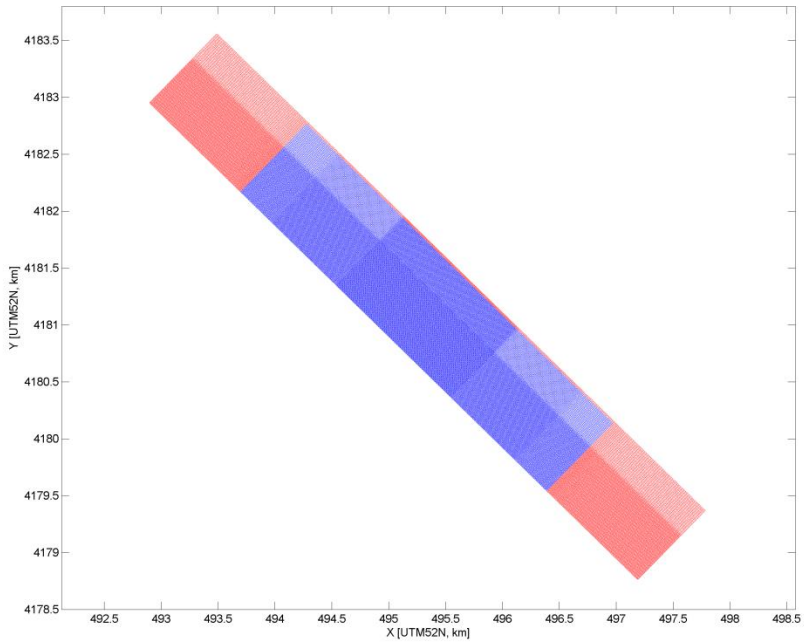

Figure 5.7: Delft3D-Wave model domain (red grid) and Delft3D-FLOW domain (blue grid) for the schematized cases

The domain consists of a rectangular grid that has the same orientation as Anmok beach (43.5° N). The FLOW grid has a length of 4km while the WAVE grid extends to the sides by 1km to account for boundary effects. The width of the domain is about 800m.The grid resolution is fine the center of the domain (5x5m), while it decreases towards the extents (20x5m). The parameters configuration of the model is chosen exactly the same as for the Anmok case model (Section 5.2.2).

5.3.2 Bathymetries

The idealized-schematized bathymetries in this step are created according to one real bathymetry of Anmok beach from the survey of September 2008 and the statistical analysis of the available observations of the sandbar horizontal location (Chapter 3). Through this approach, the natural variability of the sandbar patterns that has been observed at the study area and the resulting effects on the nearshore morphology can be further studied. At the same time, specific characteristics of the sandbar configuration can be isolated and tested individually, for a sensitivity analysis.

The horizontal position of the sandbar crest line for the schematized bathymetries is configured according to the three characteristics of the sandbar that are specified in Section 3.3:

- The sandbar mean cross-shore location $\overline{x}_b$
- The amplitude A of the crescents
- The length scale L of the crescents

The cross-shore profile of the bed-level is created using a mean profile and a sandbar profile. The mean profile z_{bmean} is specified from the profile of the September 2008 survey (Figure 5.8). The sandbar profile z_{sb} is specified according the barred profile given by (Roelvink & Reniers, 2012):

$$z_{sb} = A_b exp(-\left(\frac{(x - x_b)}{R_b}\right)^2) \tag{5.1}$$

Where:

- A_b the height of the sandbar
- x_b the cross-shore location of the sandbar crest and
- R_b the cross-shore length scale of the sandbar

In order to have schematized bathymetries that represent the natural morphology of Anmok beach, equation 5.1 is calibrated with the help of the 2008 survey. It is found that cross-shore length scale of the sandbar is different for the landward and seaward side. For this reason R_b seaward is defined as alongshore variable according to the sandbar crest-line cross-shore location. After this calibration the agreement between the survey and schematized cross-shore profiles at the location of a horn and a bay is apparent (Figure 5.9).

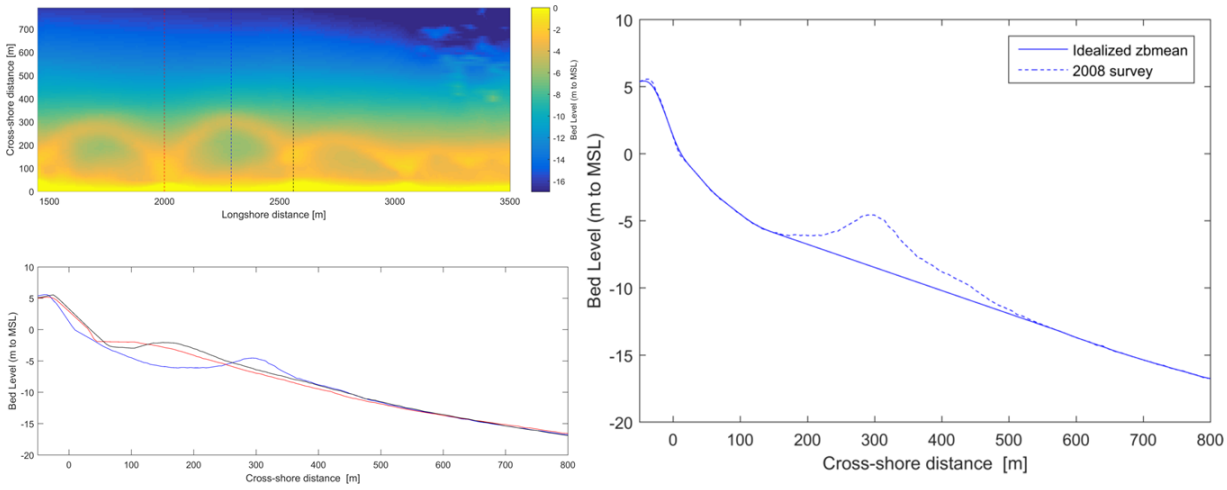

Figure 5.8: (Top left) Bathymetry from September 2008 survey, (Bottom left) Cross-shore profiles at the locations that are visible in the plan view, (Right) Cross-shore profile of the bed level at a sandbar bay location (dashed blue line) and mean cross-shore profile used for the schematized bathymetries (solid blue line).

In order to test the importance of the sandbar characteristics different scenarios are constructed according to the statistical analysis of the available observations (Figure 3.16) as can be seen in Table 5-2. For the investigation of the importance of the sandbar's variability scenarios s1, s2, s5 and s3, which have the same cross-shore position (mean value) and same length scale (peak value) are defined. The base case scenario (s1) presents an alongshore uniform bathymetry while the alongshore variability (described by A) is varied by one standard deviation value from its mean (Figure 3.16). For the investigation of the importance of the sandbar's mean cross-shore location scenarios s4, s5 and s6 which that have the same variability (mean value) and same length scale (peak

value) are defined. The length scale of the rhythmicity is tested with scenario s7 which presents smaller scale crescents while the mean values of $\overline{x}_b$ and A are kept the same.

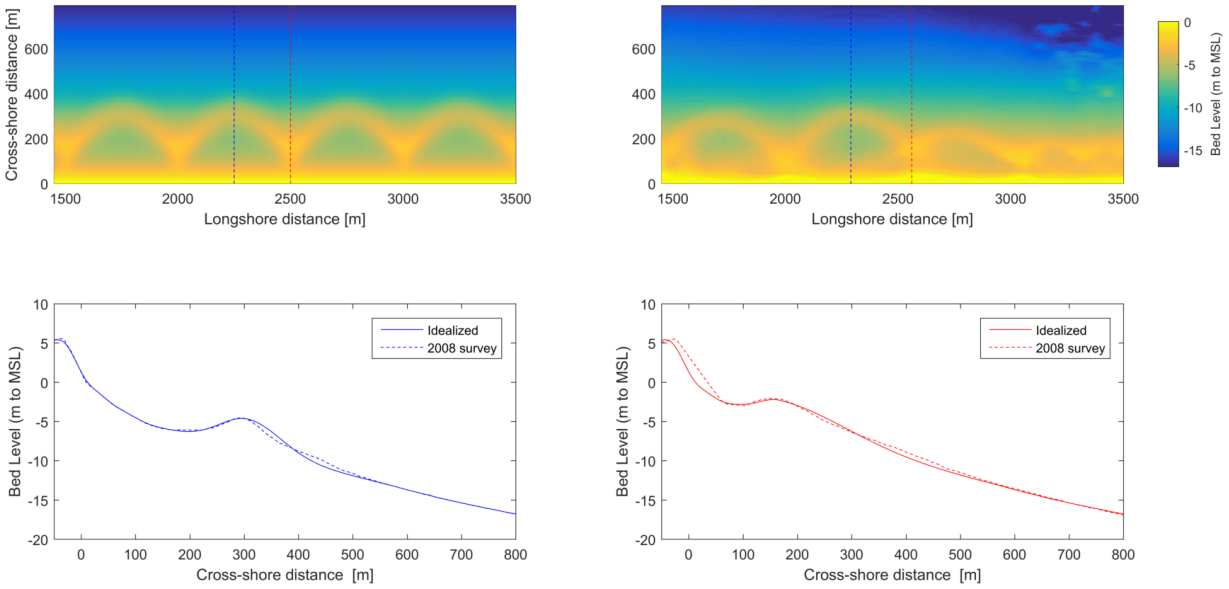

Figure 5.9: Validation of bed level profiles at a horn and bay location between the schematized bathymetry and the 2008 survey.

Moreover, two extra scenarios are defined according to the mean values of the available observations at the area close to the port, for the two ten year periods before and after the port construction (Figure 3.21). These scenarios are named p1 and p2 respectively and indicate the change in the sandbar characteristics from the port construction as it is described in Section 3.3.6.

Table 5-2: Schematized scenarios and their sandbar characteristics for the creation of the bathymetries to be tested

Scenario id	$\overline{x}_b$ (m)	A (m)	L (m)
s1	213	0	0
s2	213	29	450
s3	213	64	450
s4	191	47	450
s5	213	47	450
s6	235	47	450
s7	213	47	300
p1	202	56	418
p2	183	39	336

5.3.3 **Wave and wind boundary conditions**

The schematization of the offshore wind and wave climate at Anmok has previously been performed (Deltares, 2016) using WAM data from the period 1979-2008 (Figure C-1). The classification was performed based on wave height, wave direction, wave steepness and wind direction boundaries. This resulted in 241 classes, for which the representative wave and wind condition is determined by averaging the conditions within each bin. These conditions are used in a SWAN model of the larger Gangneung domain, to calculate the 2D wave spectra at an offshore location at Anmok beach with the same depth (~16.5m) as the offshore boundary of the schematized model (Figure 5.10).

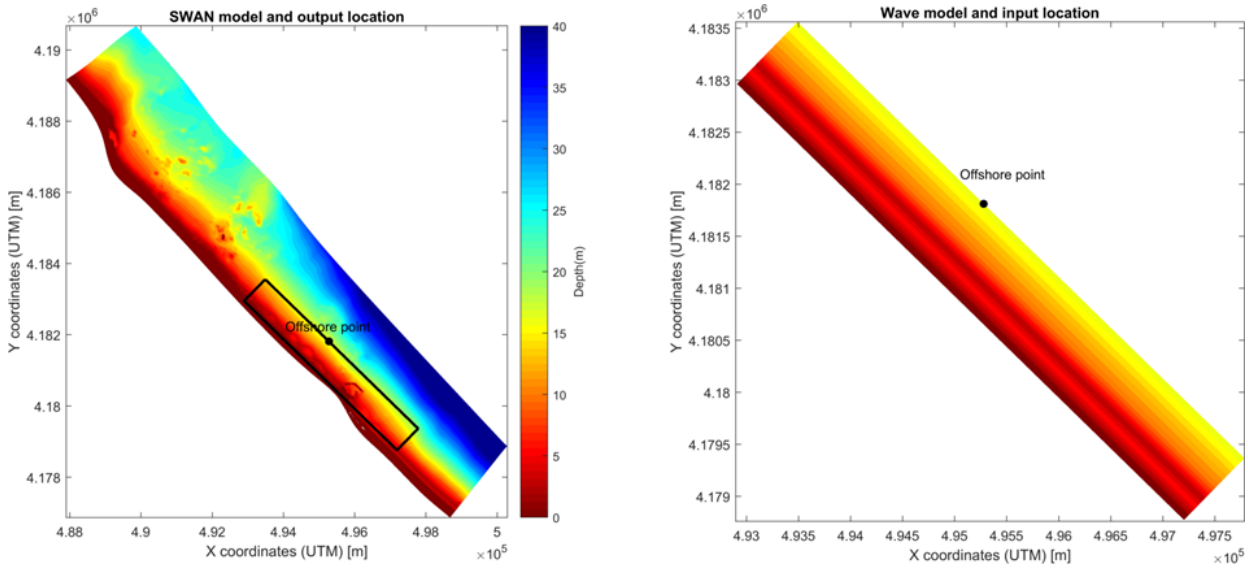

Figure 5.10: (Left) Large Gangneung SWAN model domain, (Right) Schematized WAVE model domain.

These 241 conditions describe the offshore wave climate and can be used for sediment transport analysis. The annual conditions are a function of the wave height, wave period, wave direction and wind speed and direction. A further reduction of the representative conditions is performed according to conditions that are not expected to contribute to significant sediment transports. These are the conditions with a wave height smaller than 0.5m and the offshore directed waves. This results in 154 conditions that are considered the most relevant for the sediment transport dynamics.

Each of these conditions is forced in the schematized models. The incoming waves are defined by 2D spectrums, uniform across the open boundaries, while the wind is assumed uniform across the domain. The quasi-stationary instantaneous sediment transports are transformed into annual transports based on their annual occurrence (duration).

5.3.4 **Hydrodynamic Results**

The Delft3D model described previously (Section 5.3.1) is used to compute the wave propagation through the bathymetric scenarios and the currents due to the wave- driven processes. The nearshore wave results are shown in Figure 5.11 for a wave condition with incoming angle relatively normal to the coast and a wave height of 1.75m and period 9.5s. The general wave propagation, transformation and breaking processes seem to follow the same patterns as for the real Anmok bathymetries (Section 5.2.4). Most of the wave dissipation takes place close to the shore line due to wave breaking. But as the

sandbar variability increases or the mean cross-shore distance of the sandbar from the shore decreases, there are pronounced patterns of wave dissipation formed at the location of the sandbar horns. Furthermore, due to wave refraction and focusing of wave energy there is a wave height enchantment spotted landward of the horns, while the wave arrive at the shoreline obliquely due to refraction.

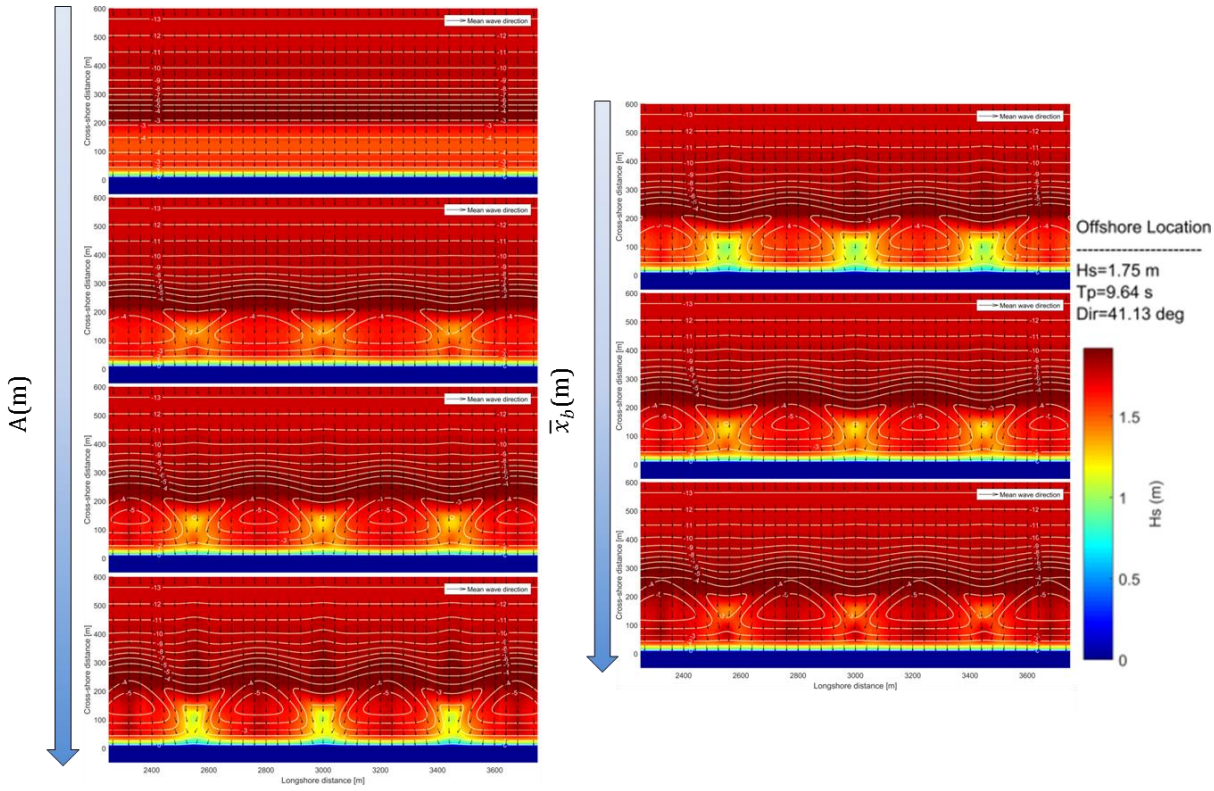

Figure 5.11: Significant wave height H_s (m) for the schematized scenarios testing the sandbar variability (left) and mean cross-shore position (right). The wave forcing is described by one wave condition relatively normal to the shore. Vectors indicate the mean wave direction while contours the bed level with respect to MSL, from 0m MSL to -13m MSL and every 1m.

The current patterns for two selected wave conditions and the s2 scenario are shown in Figure 5.12. Due the schematization of this idealized scenario the flow patterns that are developed are more distinct than the real Anmok bathymetry cases (Section 5.2.4). When waves approach normal to the shore, the 4-cell patterns at the sandbar area are again observed, while offshore directed rip currents are formed at the bays location. This alternation of current direction close to the shoreline may be connected to the local refraction of the waves which changes locally the angle of incidence when they break close to the shore. When the angle of incidence is increased the flow patterns form a meandering longshore current that has an enchanted magnitude, landward of the horns. These results of the schematized cases are in agreement with the results for the real bathymetries at Anmok (Section 5.2.4) and provide confidence for the natural representation of the study case.

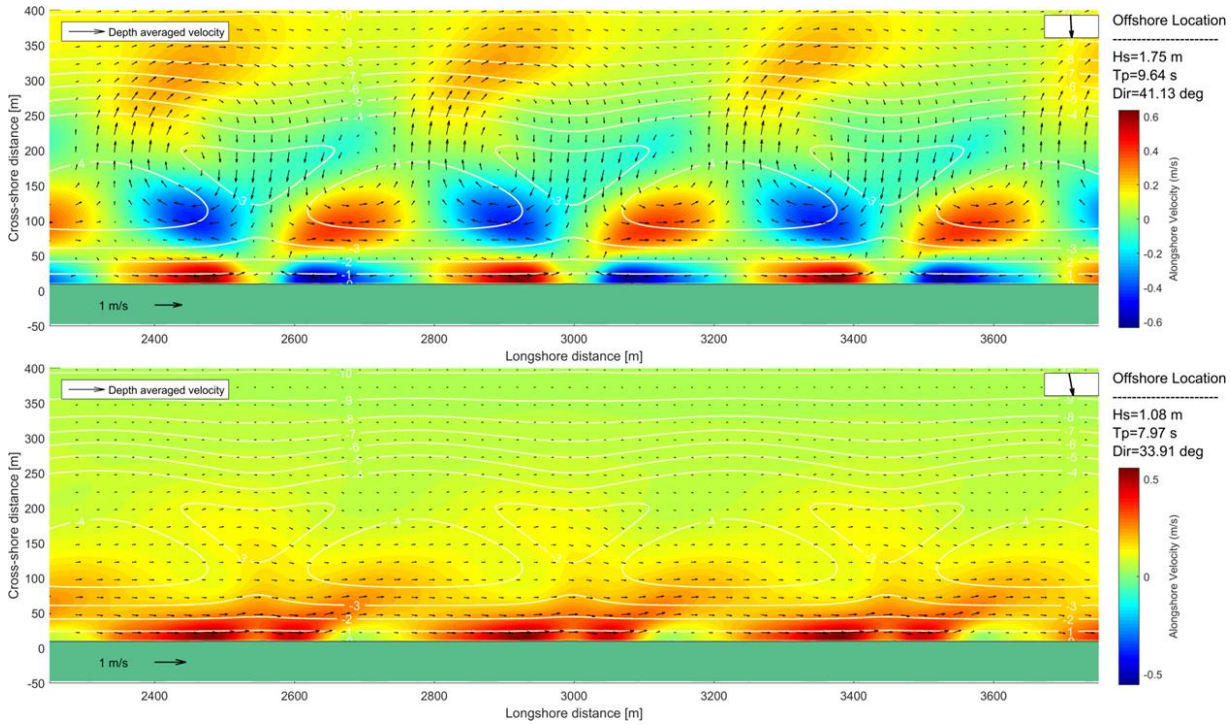

Figure 5.12: Alongshore velocity (GLM) component fields for s2 scenario and two wave conditions. Top: Relatively normal to the shore. Bottom: Angle of incidence almost 10 degrees from the North. Vectors indicate the depth averaged velocities while contours the bed level with respect to MSL, from 0m MSL to -13m MSL and every 1m.

5.3.5 **Sediment transport rates assessment**

The effect of the various sandbar configurations on the net alongshore sediment transport is assessed by computing the "beach state averages" alongshore transport rates (Huisman et al., 2017) for each of the considered bathymetric scenarios and wave conditions. First, the alongshore sediment transport rates q_s are integrated over the cross-shore direction, according to:

$$Q_S(x) = \int_{y=0}^{y=400} q_S(x,y)dy \tag{5.2}$$

Where x is the alongshore direction and y the cross-shore. Then the cross-shore integrated alongshore sediment transport rates $Q_S(x)$ are averaged over the length of two crescents in the middle of the domain according to:

$$Q_{S,AVG} = \frac{1}{2L}\int_{-L}^{L} Q_S(x)dx \tag{5.3}$$

The unweighted alongshore sediment transport fields, cross-shore integrated alongshore sediment transports $Q_S(x)$ and beach state averaged $Q_{S,AVG}$ can be seen in Figure 5.13 for the s2 scenario and the same wave conditions as in Figure 5.12 . The sediment transports are mainly generated close to the shoreline and at the location of the sandbar horns where the wave dissipation is high. Plotting the cross-shore integrated alongshore sediment transports shows repetitive patterns across the beach with quite high local gradients.

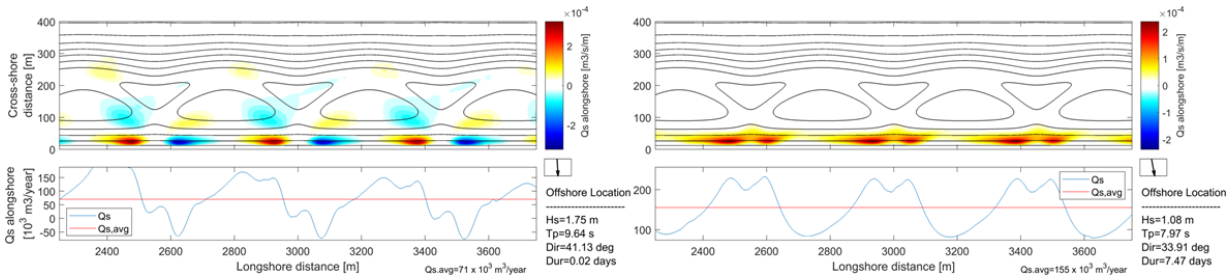

Figure 5.13: Computed unweighted alongshore transport rates for s2 scenario and two wave conditions. Left: Relatively normal to the shore. Right: Angle of incidence almost 10 degrees from the North. Upper panel: Spatial transport fields of the alongshore sediment transport component (positive directed to the South). Bottom panel: Cross-shore integrated alongshore transports $Q_S(x)$ (blue line) and beach state averaged transport $Q_{S,AVG}$ (red line).

Adding up all the quasi-stationary sediment transports fields calculated for each of the 154 conditions weighted by their annual duration results in the net annual sediment transports for each of the schematized bathymetry scenarios. Furthermore, all conditions that create a positive beach state averaged transport are added up to get the gross positive beach state averaged transport. The same is performed for the gross negative transports.

5.4 Sandbar variability and net alongshore sediment transports

Increasing the alongshore variability of the sandbar, starting from an alongshore uniform case and computing the annual alongshore sediment transports (scenarios s1, s2, s5 and s3) results in Figure 5.14. The net alongshore sediment transports for all the scenarios all quite low but are in line with previous sediment transports modelling studies at Anmok beach (Deltares, 2016). For the alongshore uniform sandbar scenario the annual alongshore sediment transports are concentrated at the seaward side of the sandbar while close to the shore they have quite low values. For an alongshore uniform sandbar there are no circulations formed in the flow as for the alongshore variable case. On the contrary, an alongshore current uniformly directed to the Northwest (left side of Figure 5.14) or to the Southeast (right side of Figure 5.14) is formed. As a result, the gross-positive and gross-negative alongshore sediment transports cancel each other near the shoreline.

On the other hand, for the scenarios with sandbar alongshore variability included, there are circulations patterns formed at the sandbar horns locations, when the waves come relatively normal to the coast. Moreover, even when the waves come with higher angle, the alongshore current takes a meandering shape which introduces local gradients in the depth averaged velocities (Figure 5.12 and Figure 5.13). As a result, the annual alongshore sediment transports computed, present quite high local gradients at the locations of the circulations. These gradients become more intense as the variability of the sandbar grows. This appears to be the effect of the sandbar horns being closer to the shore, leading to higher velocities of the circulation patterns formed.

Plotting the beach state averaged sediment transport rates (Figure 5.15) shows that even though there is a trend of the gross sediment transports getting lower as the variability increases, this change is quite small and equivalent to a maximum 8% for the highest

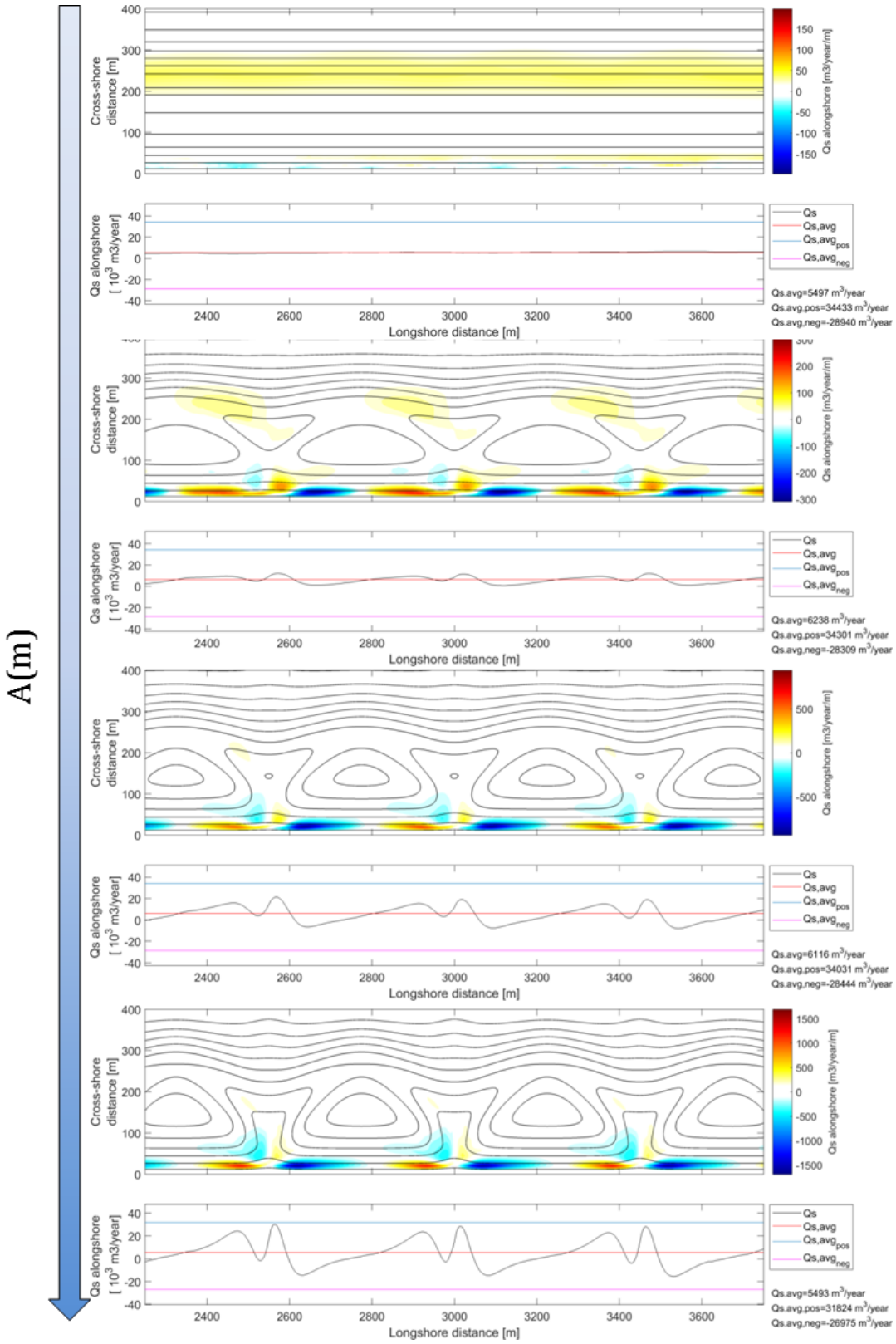

Figure 5.14: Computed net and gross annual alongshore transport rates for (From top to bottom) s1, s2, s5 and s3 scenarios. Upper panel: Spatial transport fields of the annual alongshore sediment transport component (positive directed to the South). Bottom panel: Cross-shore integrated net alongshore transports $Q_S(x)$ (black line) and net beach state averaged transport $Q_{S,AVG}$ (red line). Gross-positive (blue line) and gross-negative (purple line) beach state averaged transports are plotted as well.

variability scenario. Moreover, the net sediment transports demonstrate changes of the same scale (≈10%).

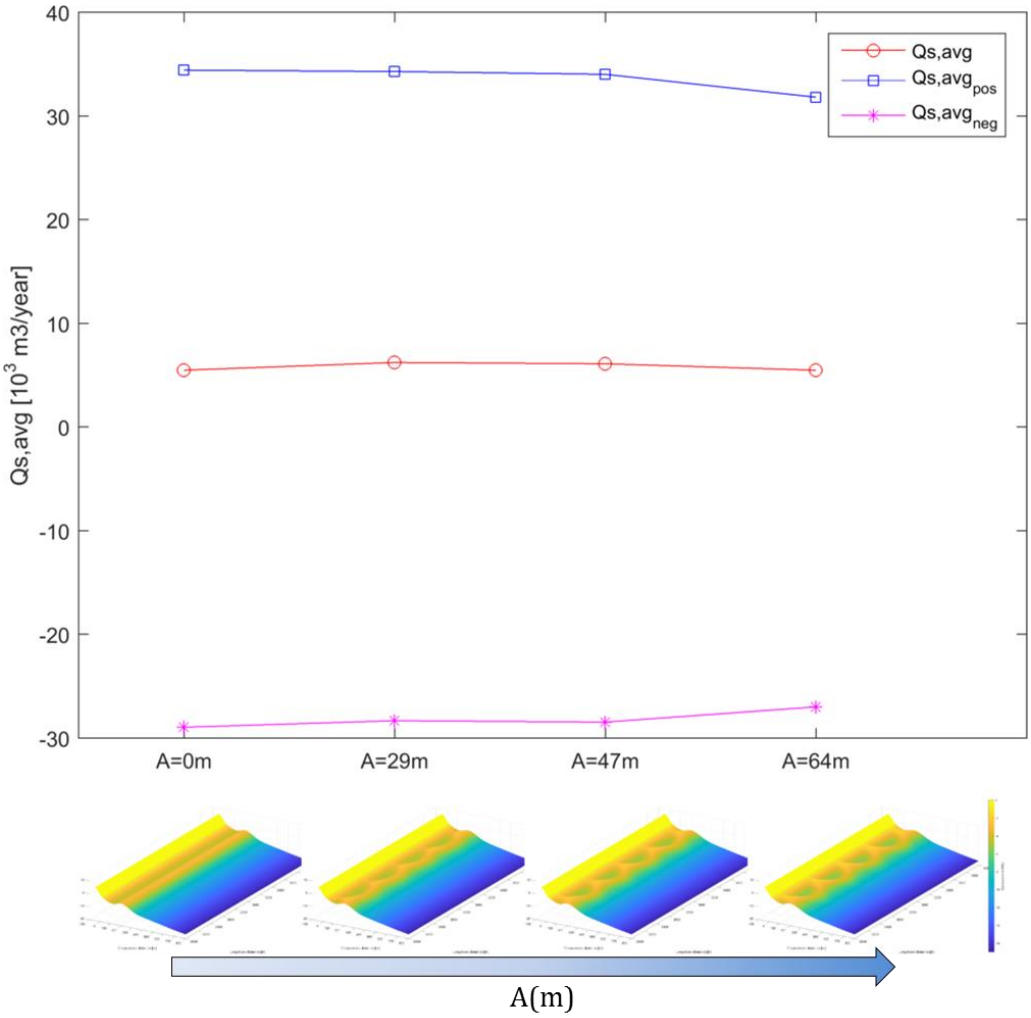

Figure 5.15: Beach state annual averaged net alongshore sediment transports (red line) for scenarios (From left to right) s1, s2, s5 and s3. The blue line represents the gross positive beach state alongshore sediment transports while the purple line the negative.

In order to check the sensitivity of these results to the wave climate, the same bathymetric scenarios are forced with an altered wave climate. This alteration included a rotation of the directions of the incoming waves clockwise and anticlockwise by 6 degrees. The results can be seen in Figure 5.16. The changes in the net and gross alongshore sediment transports follow the same trends and are of the same scale (≈7-13%) as for the normal Anmok yearly wave climate. This means that disregarding the wave climate main direction the changes of the net alongshore sediment transports when variability is included keep low values, in the order of 10%.

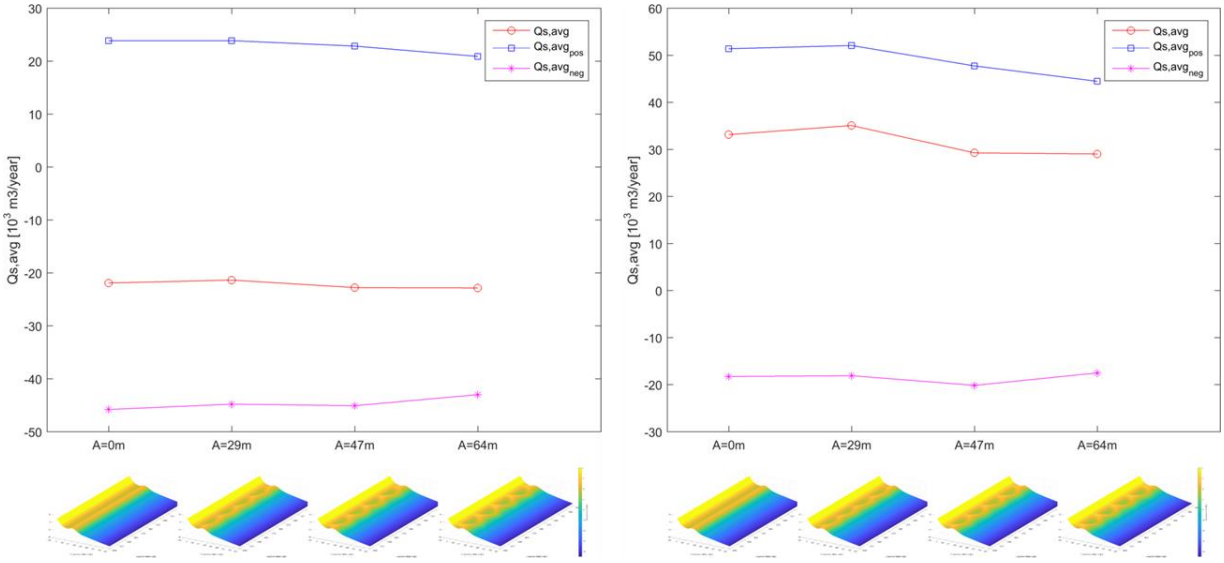

Figure 5.16: Beach state averaged net alongshore sediment transports (red line) for scenarios (From left to right) s1, s2, s5 and s3. The blue line represents the gross positive beach state alongshore sediment transports while the purple line the negative. Left panel: Clockwise rotation of the wave climate by 6 degrees. Right panel: Anticlockwise rotation of the wave climate by 6 degrees.

Concerning the influence of the crescentic length scale L, the net annual sediment transports of scenarios s7 (Figure 5.17) are investigated. The difference between the s7 and s5 scenarios is in the order of 20%, but this is mainly an effect of the wave climate and the relatively small net alongshore sediment transports. For the rotated climates this difference is a lot smaller (≈2-7%).

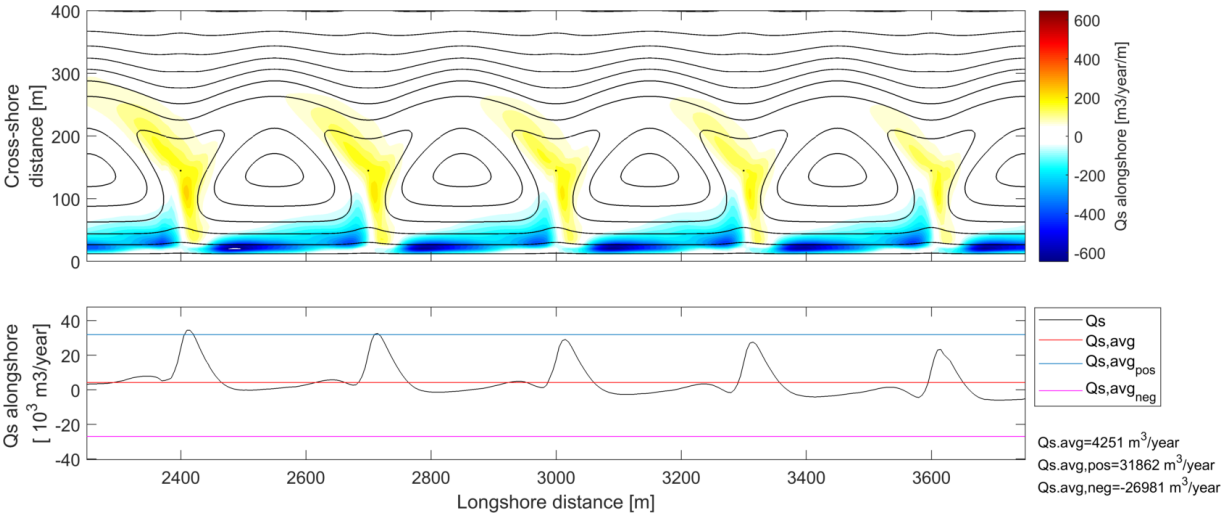

Figure 5.17: Computed annual alongshore transport rates for s7 scenario. Upper panel: Spatial transport fields of the annual alongshore sediment transport component (positive directed to the South). Bottom panel: Cross-shore integrated alongshore transports $Q_S(x)$ (black line) and beach state averaged transport $Q_{S,AVG}$ (red line). Gross-positive (blue line) and gross-negative (purple line) beach state averaged transports are plotted as well.

5.5 Sandbar cross-shore position and shoreline response

In this section the local sedimentation or erosional areas at the shoreline that have been observed in Chapter 3 are qualitatively studied in relation to the sandbar characteristics. From the results of the previous section, it is observed that the alongshore sediment transport direction can be variable in the cross-shore. This is the effect of circulation patterns that occur due to the presence of the crescentic sandbars. It is expected that the coastline perturbation are a result of the sediment transports gradients close to the shore. To this end, for the calculation of the shoreline response, cells are defined that expand 20 m offshore (roughly at the -1m MSL contour) from the shoreline, every 25 m in the alongshore direction (Figure 5.18). The sedimentation or erosion volume in each cell is defined as the difference between the left and right side alongshore sediment transports integrated over the cell cross-shore distance. Higher confidence is expected for the alongshore sediment transports close to the shoreline in Delft3D, while for most of the coastline line studies only the alongshore sediment transport rates are used. To this end, the cross-shore transports at the seaward side of the cells are neglected.

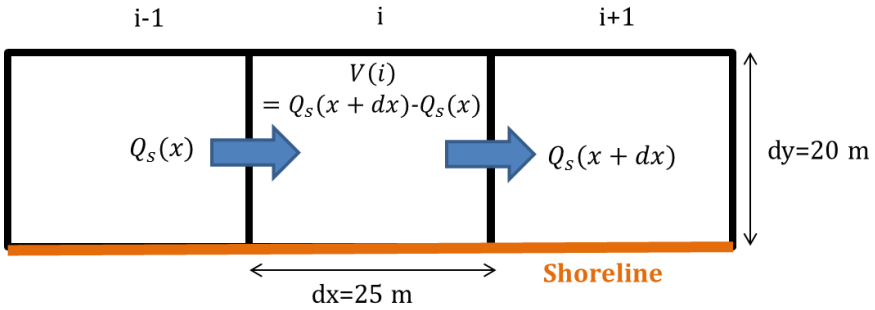

Figure 5.18: Definition of the sedimentation/erosion volumes in each cell. Where Qs(x) is the alongshore sediment transport rates integrated over dy=20m.

Therefore, the volumes V(i) that are calculated for each cell represent a qualitative result, indicating the location of possible sedimentation/erosion and its relative magnitude for comparisons between the different scenarios.

In Section 3.5, it is proposed that the cross-shore location of the sandbar is quite critical for the response of the shoreline. Therefore, the alongshore cells erosion sedimentation is computed for the previously specified bathymetric scenarios. The importance of the cross-shore location of the sandbar is verified with this approach as well, showing that the closer the sandbar is to the shoreline, the more intense the sedimentation and erosion patterns are (Figure 5.19). This agrees with the observation from the satellite images (Figure 3.24-B). Furthermore, it can be observed that the more offshore the sandbar is located the more influence the predominant wave direction has. It is found that the net alongshore sediment transport is directed to the Southeast (right side of the plots). When the sandbar is located close to the shoreline the sedimentation is concentrated landward of the sandbar horn (Figure 5.19-top plot). This is the case for the rotated wave climates as well (Figure C-2). But when the sandbar is located at a relatively offshore location the sedimentation area is moved to the Southeast. This effect appears to be connected with the predominant directions of the incoming waves and the cross-shore distance between the sandbar shoals and the shoreline. For the rotated wave climates, for which the predominant incoming waves arrive in an angle higher to the normal to the shore this effect is more clear (Figure C-3).

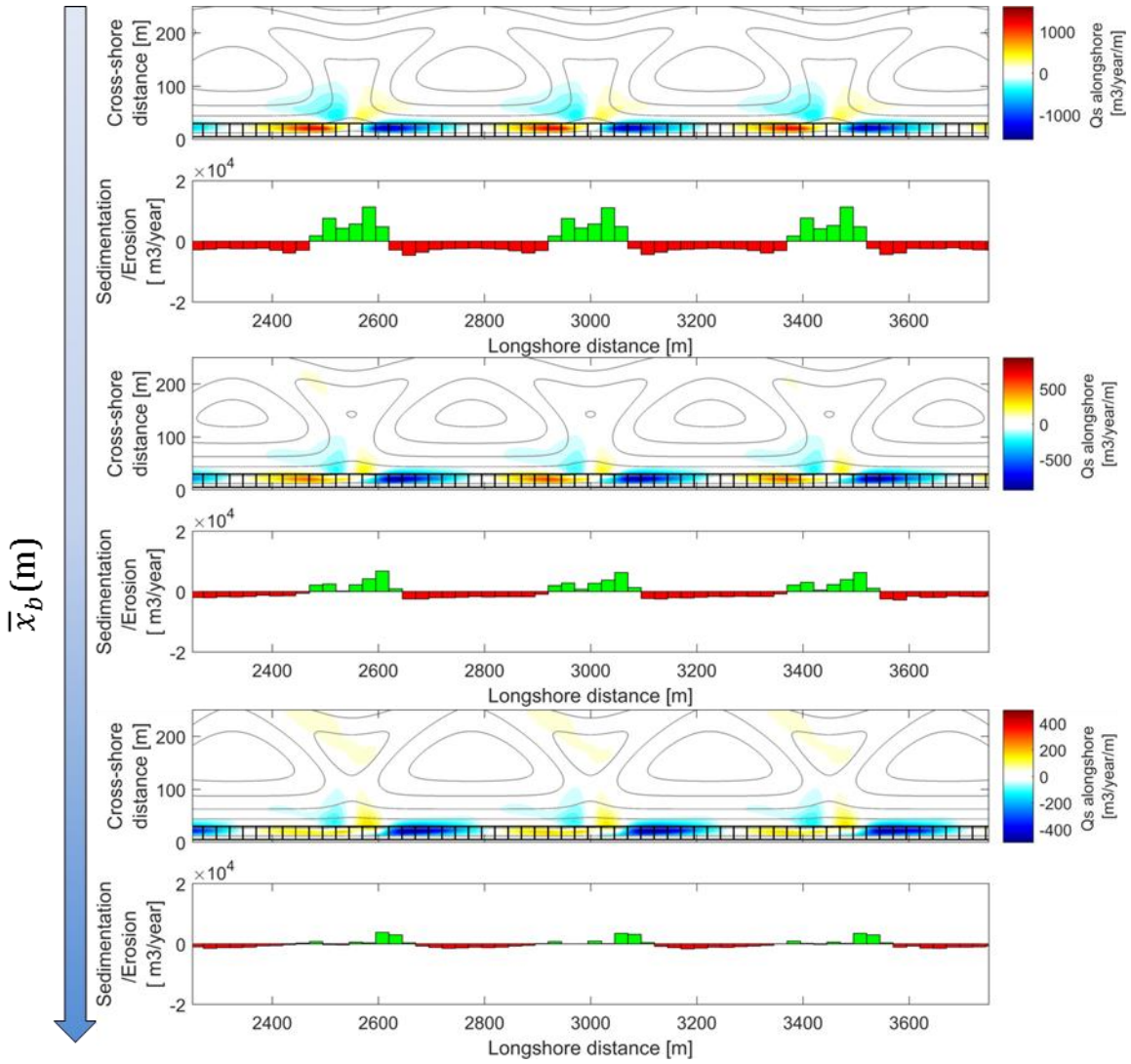

Figure 5.19: Computed annual alongshore transport rates for (From top to bottom) s4, s5 and s6 scenarios. Upper panel: Spatial transport fields of the annual alongshore sediment transport component (positive directed to the South). Black lines indicated the cells used for the computations. Bottom panel: Sedimentation (green) or Erosion (red) volumes calculated for each cell.

Plotting the same graphs for the sandbar variability scenarios as well (Figure C-4) it can appears that as expected for the alongshore uniform case s1 there is no erosion-sedimentation patterns observed at the shoreline. But when the variability becomes higher, the shoreline response becomes more intense. This is again connected with the cross-shore distance of the sandbar horns to the coastline.

5.6 Pre and post port scenarios

It has been verified (Section 3.3.6) that the port construction has influenced the average characteristics of the sandbar close to the port breakwater. In this section, we investigate the influence of the schematized pre and post port averaged sandbar configurations (Section 5.3.2) on the net alongshore sediment transport rates and shoreline response. To construct these sandbar configurations, the sandbar characteristics ($\overline{x}_b$, A, L) are defined according to their mean values for the area close to the shore and the two

periods prior and after the port construction. The port is not included in the bathymetries, as in this test the aim is to investigate the effects of the changed bathymetry due to the port, on the shoreline response. The direct influence of the port construction has already being investigated in previous studies both by means of coastline models and process based models (Deltares, 2016). Forcing the two bathymetry scenarios with the annual wave climate resulted in small differences between the beach average net sediment transports of about 10% (Figure 5.20). The shoreline for the post-port scenario has perturbations with smaller magnitude than the prior one. Additionally, due to the smaller length scale the shoreline features are positioned closer to each other.

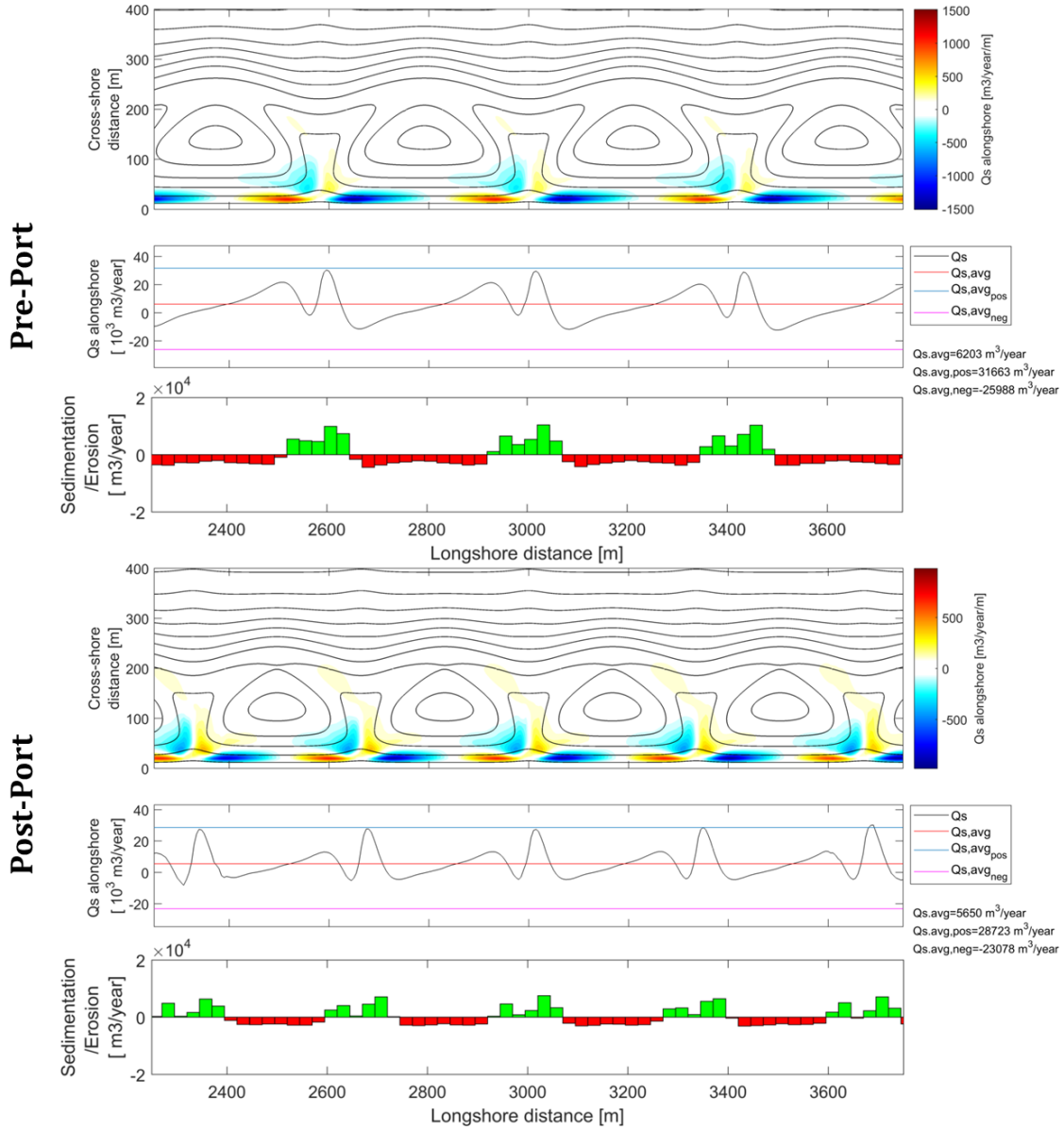

Figure 5.20: Computed annual alongshore transport rates for p1(top figure) and p2(bottom figure) scenarios. Upper panel: Spatial transport fields of the annual alongshore sediment transport component (positive directed to the South). Middle panel: Cross-shore integrated alongshore transports $Q_S(x)$ (black line) and beach state averaged transport $Q_{S,AVG}$ (red line). Gross-positive (blue line) and gross-negative (purple line) beach state averaged transports are plotted as well. Bottom panel: Sedimentation (green) or Erosion (red) volumes calculated for each cell.

5.7 Conclusion

The influence of a crescentic sandbar bathymetry on the local hydrodynamics and annual sediment transports is investigated by means of the physical process model Delft3D. It is found that the sandbar variability significantly changes the local hydrodynamics depending on the wave conditions. For waves coming relatively normal to the shore, 4-cell circulation patterns develop which can explain the observed shoreline response at the horns location (sandbar-shoreline out of phase coupling). For waves with higher incoming angle, the alongshore current created takes a meandering shape which introduces local gradients in the alongshore velocities at the horns locations.

Moreover, using an annual wave climate and schematized bathymetries, the influence of the sandbar variability on the beach average net alongshore sediment transports is investigated. The changes of the sediment transports, when alongshore variability is included, mainly involves the introduction of local alongshore gradients. On the other hand, the change in the beach averaged net alongshore transports is in the order of 10% with respect to a base case with alongshore uniform bar. This deviation is in the order of the model results uncertainty and shows that at least for the symmetric crescents that are investigated, the sandbar variability does not influence severely the annual sediment transports from a beach average perspective. This agrees with the results from Huisman et al. (2017), where the importance of the rip channel obliqueness was highlighted for changes in the sediment transport rates.

Additionally, the local alongshore sediment transport gradients are investigated by dividing the surf zone area close to the shoreline in cells and calculating the expected accreted or eroded volumes in a year. This study shows that these gradients actually can cause erosion and sedimentation patterns across the coastline similar to the ones observed by the satellite images (Section 3.5). The magnitude of these shoreline perturbations seems to be directly connected with the distance of the sandbar relative to the shoreline. Furthermore, the location of these erosional or accretional hotspots changes according to the predominant annual wave direction and the location of the sandbar.

Finally, the average sandbar configurations close to the port and for the two periods, before and after its construction are analysed. The resulted beach state averaged sediment transports shows a small difference between the two scenarios. The shoreline response shows smaller perturbations for the post-port scenario related to the smaller variability of the sandbar. However, it should be accounted for in the interpretation of the results that the port construction has changed the wave climate at the area next to it, which is not represented in this study.

6. Discussion

The previous chapters have focused on presenting the approaches followed and their results, in order to answer the research questions defined in Section 1.3. During this process, various decisions and assumptions are made related to the approaches used, empirical or numerical model parameters and sandbar characteristics taken into account. In this chapter these approaches and assumptions are further discussed and analyzed, while suggestions for other studies are made.

6.1 Use of satellite imagery for the extraction of the sandbar horizontal position

As the available 14 surveys at Anmok beach cover only the periods of 2007-2008 and 2013-2016 with a season temporal resolution, additional data sources are needed to study the long-term sandbar dynamics. To this end, freely available satellite images are used to manually extract the sandbar horizontal position. This approach extends the temporal coverage of the dataset to 27 years and increases the temporal resolution. A comparison of the manually extracted sandbar positions with 11 available bathymetric surveys shows fair to good agreement (r^2=0.5-0.85).

So far, in literature, various studies concerning the dynamics of sandbars have used mainly video monitoring systems (van Enckevort et al., 2004; Plant et al., 2006; Orzech et al., 2010; Pape et al., 2010; Splinter et al., 2011; Price et al., 2013; van de Lageweg et al., 2013) or surveys (Plant et al., 1999) to derive the sandbar location though time. The study sites they used though, concerned beaches where either camera systems have been set up for some time (decade or more) or sites where frequent surveying is performed. Yet, at most of the study sites around the globe, these extended datasets are not or scarcely available. On the other hand, the use of freely available satellite images forms an approach that can be used at almost every study site and has proven its potential for deriving the characteristics of a sandbar and studying its dynamics. The capabilities of this method lie mainly in the availability of images and its spatial and temporal coverage. Satellite images from the Landsat 4,5,7,8 (U.S Geological Survey) and Sentinel 2 (EU Copernicus Services) missions are freely available. These missions cover almost Earth's entire surface and have a pixel resolution of 30m and 10m respectively. Their temporal coverage starts from 1985, astonishingly earlier than any other in-situ data that might be available. The images frequency varies according to periods and satellite problems from

1 day to some months. As expected, during the last decade, when more satellites are available the frequency is quite higher and in the order of 8 days.

Certainly, the other methods may have higher accuracy or better temporal resolution. For example, in situ surveys can provide far more accurate data with bed level information included. Moreover, video monitoring systems can provide data on the horizontal position of the sandbar with really high frequency (order of hours), but only during daylight. The latter approach uses the areas of intense wave breaking in time-averaged images as a proxy for nearshore morphology (Lippmann & Holman, 1989). However, conducting surveys is a quite expensive procedure, and most importantly surveys or camera monitoring systems are not always available at the study sites that they are needed as previously mentioned. Additionally, even when they are available their temporal coverage is far inferior to that of satellite images. The drawbacks using the freely available satellite imagery mainly concern the resolution of the images and the manual extraction of the sandbar position, which can affect the accuracy of the extracted data. Furthermore, a lot of the available images are not clear enough to extract the sandbar location. This is connected most of the times with the presence of clouds or intense wave breaking, which hides the location of the sandbar. Hence, the frequency of the usable satellite images is sometimes quite variable and the dynamics of the sandbar might be masked in between. Yet, they can still provide a more extensive dataset than any of the other conventional methods.

6.2 Empirical modelling of sandbar position

From the available observations it appears that the sandbar mean cross-shore position and its variability are of importance for the shoreline response. To this end, a model that can predict these sandbar characteristics in response to changing wave conditions in the future is useful. Previous attempts to model the sandbar response to wave forcing using process based numerical models (Reniers et al., 2004; Smit et al., 2010) showed that even though they can reproduce some of the bulk characteristics of the 2DH morphology they lack the predictive skill. For this reason, in this study, it is chosen to use two alternative parametric approaches proposed by Plant et al. (1999) and Plant et al. (2006). The results of the validation of these models at Anmok beach are unsatisfactory. Both these models are simplistic concerning the way they describe the nearshore morphology (two parameters of the sandbar) and the wave forcing (only H_s). This is at the same time their advantage and drawback. From one point of view, these simplifications can allow the modelling of nearshore sandbars in a straight forward way without the demand of extensive computational power and input data. On the other hand, in systems where the sandbar response is more complex and is potentially connected with additional parameters of the wave forcing (like wave period or angle of incidence) or the presence of human structures, they lack the relevant processes.

The unsatisfactory results of the use of these models in the present study can be attributed either to the simplification of the models themselves or the temporal resolution and spatial accuracy of the dataset. In studies where datasets with high temporal resolution and high spatial accuracy are available, these empirical models can be proven useful for the prediction of the sandbar position. Care should be taken, in the historic sandbar dynamics as well, and their relationship with wave forcing.

The assumption of fixed model coefficients might be invalid as well. Especially for longer time scales Pape et al. (2010) showed that treating the coefficients as variable according to the wave height can produce better results. This approach needs an extensive dataset which is not available for the present case. One other approach that is used in the present is an assimilation algorithm (extended Kalman filter) framework integrating the empirical models and the available observations. This showed that the model coefficients do not attain specific values throughout the study period.

6.3 Use of schematized bathymetries for numerical modelling

As the available surveys at Anmok beach did not incorporate all the observed sandbar configurations from the satellite images, schematized bathymetries are used for the application of a sensitivity analysis of the sandbar 2DH characteristics on the alongshore sediment transports and the shoreline response. The importance of these characteristics for the shoreline response is highlighted during the data analysis of the available observations (Section 3.5). The calibration of the schematized bathymetries to an in-situ survey provides confidence that the resulting bathymetries incorporate the natural characteristics of the nearshore morphology at Anmok beach.

Yet, as mentioned the 3D aspects of the sandbar are fixed according to only one survey from the study site. It is expected, that the 3D characteristics of the sandbar, like the depth of the crestline or the seawards and landward sandbar slopes can be important attributes as well. These characteristics are expected to play an important role in the transformation of the waves coming to the shore and thus the hydrodynamic patterns appearing in the surf zone. A sensitivity analysis of these sandbar characteristics on the alongshore sediment transports and the shoreline response can indicate their importance.

Furthermore, the shape of the individual crescents in Anmok beach is found to be symmetrical most of the times through the study period, as is presented in Section 3.3.1. This means that the formed rip channels are relatively normal to the shore. This is an effect of the wave climate and its predominant direction which is normal to the shore, resulting in the small magnitude of net alongshore sediment transports (~6000 m^3/year). Still, in August of 2015, the nearshore morphology at Anmok beach developed oblique rip channels in response to the oblique wave angle of incidence of a big typhoon. This asymmetry of the crescentic characteristics is not investigated in this study concerning its sediment transport potential, but has been previously indicated as a culprit for changes in alongshore sediment transports (Huisman et al., 2017). From their results they concluded that the obliqueness of the rip channels in the nearshore morphology enhances or decreases the alongshore sediment transports according to the wave angle of incidence. In this study, as most of the observations at Anmok beach included symmetrical shaped crescents, this asymmetry is not tested. Yet in areas where oblique rip channels are usually encountered at the nearshore morphology, this should be taken into account.

6.4 Numerical model settings and results

In this study, a Delft3D model is used for the computation of the annual sediment transport rates for a set of schematized bathymetries at Anmok beach. Due to the

extensive number of simulations, it was decided not to use the roller model of Delft3D. The roller model can improve the representation of the wave breaking in the surf zone by including the turbulence induced by the rollers in the water column. Therefore, the use of this setting is thought to be the most accurate approach. Huisman et al. (2017), mention in their study that the resulting hydrodynamic patterns were the same but the impacts were more pronounced using the roller model. This can be of relevance for the results of the present study as well, as using the roller model might result in higher differences in the net sediment transports.

In this study the influence of the sandbar variability on the sediment transports is investigated from a net (or gross) annual sediment transport point of view. This was decided in order to understand the influence of the morphology on the annual sediment transports and is thought to be valid due to the slow response of the sandbar system at Anmok beach which changed annually only due to high wave energy events. For this case the influence of the sandbar variability was found minor. Yet, for the individual wave conditions the difference in the computed sediment transport rates might be more pronounced. An analysis, where schematized wave conditions are used is advised in order to indicate the importance of the wave parameters on the resulting differences in the sediment transport rates.

Tide is not included in any of the numerical models used in this study. This was chosen due to the small tidal range (a few decimeters) at the study case. Tide can be an important parameter as it can influence the water levels and wave breaking patterns at the surfzone. Additionally, tidal currents can influence the importance of the wave generated alongshore currents on the sediment transport rates. In cases with higher tidal ranges, it is advised to investigate its potential by including in the numerical simulations.

For the representation of the shoreline response, the cells are defined close to the shoreline. These cells are defined according to the cross-shore area that the circulation patterns are more pronounced. It is chosen to compute the changing volumes only using the ingoing and outgoing alongshore sediment transports of each cell. This is decided due to the higher reliability of Delft3D for the computation of alongshore sediment transports. As a result, the magnitude of the computed volumes is not realistic but still provides qualitative results for the initial shoreline response. As the bathymetries are schematized, no validation is possible, so the qualitative results are thought to be enough for the extraction of conclusions regarding the shoreline response.

6.5 Crescentic sandbars in coastal engineering studies

In coastal engineering studies for areas where crescentic sandbars are present, special care should be taken in the modelling approaches and coastal zone policies. In order to understand the system and provide prediction for the shoreline location, the following steps can be considered:

Data Analysis

As a starting point, it is recommended to analyze the long-term sandbar and shoreline position. Except any available surveys or shoreline measurements, freely available satellite images can be used as showed in the present study to extend the temporal coverage and increase the temporal frequency of observations. With this approach, the natural variability of the sandbar and shoreline characteristics can be obtained. Furthermore, a bandwidth of the shoreline perturbations can be computed from the

available shoreline observations. Additionally, the effects of implemented human interventions on the sandbar position can be identified and can be used as a proxy for future planning of interventions. Knowing how an intervention can affect the nearshore morphology can help in predicting how it will affect the shoreline as well.

Coastline Modelling

The present study showed that, in case the shape of the crescents is symmetrical, the use of coastline models that assume alongshore uniform bathymetry to predict the shoreline position is expected to be valid. If the bathymetry is composed by asymmetrical crescents and oblique rip channels, process based modelling should be introduced as well. The influence on the alongshore sediment transports can then be evaluated. If it is found pronounced, it can be incorporated by adjusting the coastline model settings. Finally, the bandwidth of the shoreline perturbations found in the data analysis should be added to the coastline position calculated by the coastline model. This results not in a single coastline but a range of possible position that should be taken into account for the expected beach width and any developments by the policy makers and managers.

An overview of the aforementioned approach can be seen in Figure 6.1, while a general schematization based on Anmok beach can be found in Figure 6.2. The blue line indicates the large scale reorientation of the coastline that can be predicted from a coastline model under the influence of human interventions or changes on the annual wave conditions. In the presence of crescentic sandbars this line can be replaced by a bandwidth based on the available observations of shoreline perturbations. This bandwidth (dashed red line) indicates the maximum/minimum expected position of the coastline due its rhythmicity. This schematization can help decision makers in coastal zones to incorporate these shoreline undulations when planning the construction of infrastructure or recreational areas.

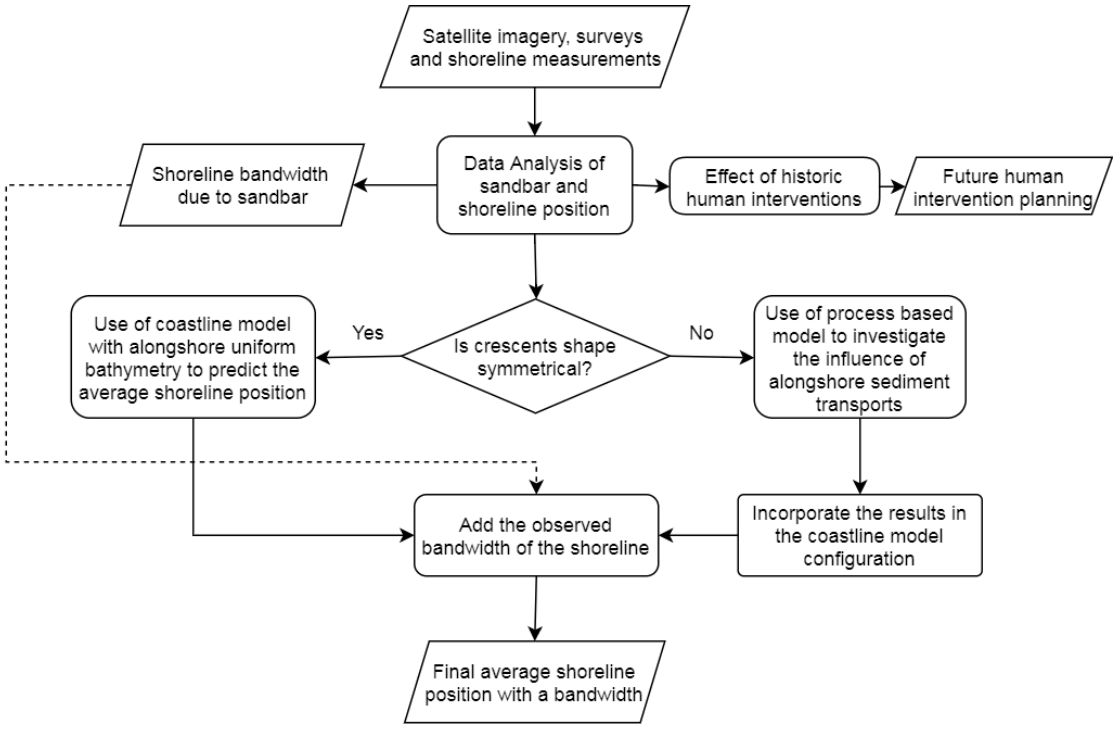

Figure 6.1: Flow chart of steps that can be followed in a coastal study with crescentic sandbars presents.

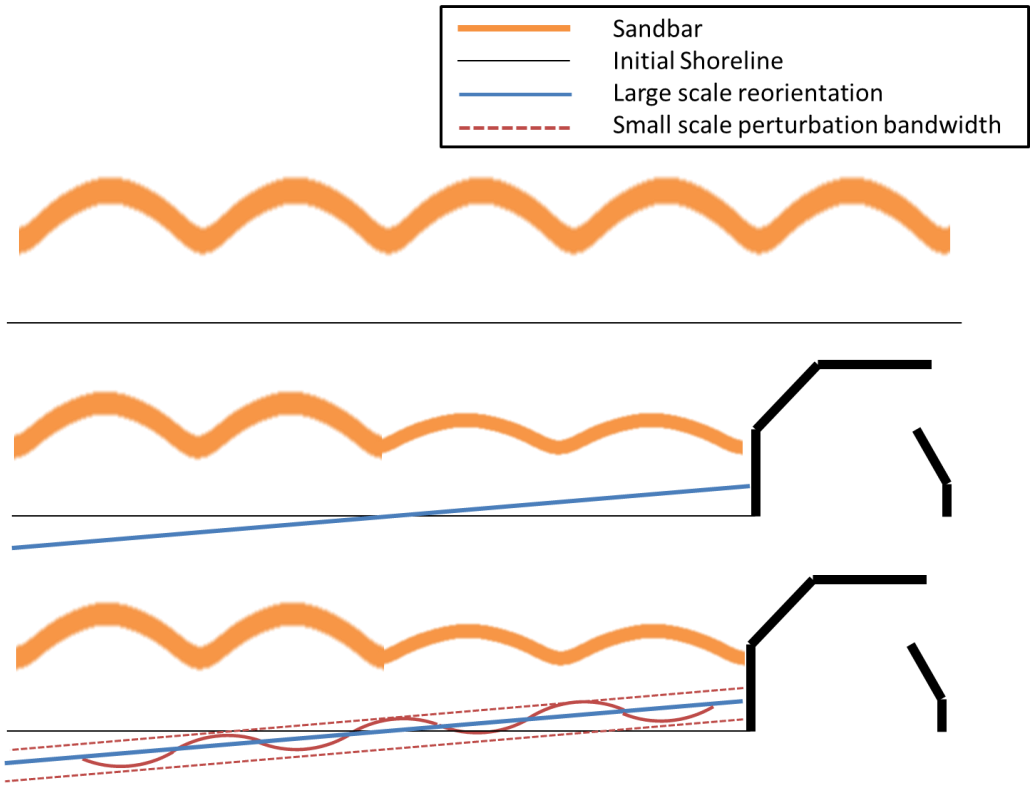

Figure 6.2: Schematization based on Anmok beach of a coastal engineering approach for a case with crescentic sandbars

7. Conclusions and Recommendations

Understanding crescentic sandbars systems is crucial for coastal zone management; as they form a natural coastal feature quite commonly encountered around the globe, which can affect the shoreline position. The coastline position is directly connected with the beach width and can endanger any infrastructure located at the shore or downgrade any recreational activities taken place there. In this study, insight is gained into the dynamics of rhythmic sandbars and its interaction with the shoreline and human interventions at Anmok beach at the South Korean East coast (Figure 7.1), based on analysis of satellite images, surveys, and modelling. This study site is located at a micro-tidal and wave dominated coast, where human interventions (port and SBW) have taken place.

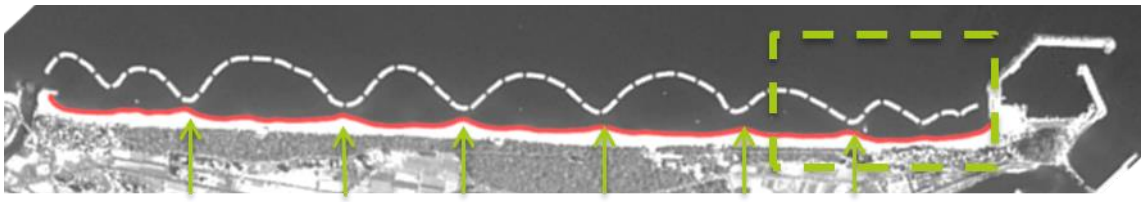

Figure 7.1: Anmok beach field case (Arirang 2 sattelite image from 23/11/2008). White dashed line indicates the sandbar crest line. Red line shows the coastline position. Green arrow point the location of sandbar and shore line horns. The green area presents the area of influence of the sandbar close to the port.

In order to answer the research questions defined in Section 1.3, the use of diverse approaches is decided, while taking into account the advantages and drawbacks of the individual methods. First, data analysis is performed on a dataset of the sandbar and shoreline position (obtained from satellite imagery and surveys) in order to gain insight on the system. At the study site only a number of surveys are available, while no camera monitoring system is placed. To this end, freely available satellite images are used to derive the sandbar horizontal position. Then, an empirical modeling attempt of the sandbar's response to wave forcing is explored, in pursuit of a predictive capability for future wave scenarios. For these purpose two empirical models found in literature (Plant et al., 1999, 2006) are tested. In the end, numerical modelling of the sediment transports for schematized bathymetric scenarios provides insight on the effects of the sandbar alongshore variability on the longshore sediment transport rates. This approach aims to test the use of coastline models that don't account for the alongshore variable

bathymetry for the calculation of sediment transport rates. Furthermore, the response of the small scale shoreline perturbations to different sandbar configurations is investigated to verify possible system controls, some of which, have been identified in the observations analysis phase.

The present chapter comprises the concluding remarks about the present study by answering the research questions defined in Section 1.3. Additionally, recommendations regarding future work are presented.

7.1 Conclusions

7.1.1 What are the characteristics of the sandbar patterns at Anmok beach over the last decades?

Satellite imagery and in situ surveys covering a period of 27 years are examined to describe the sandbar patterns at Anmok beach over the last decades. The extraction of the sandbar location from satellite imagery is the key factor that contributes to this high temporal coverage and allows for the study of the influence of the port and the sandbar-shoreline coupling. The characteristics of the sandbar can generally be described as follows:

- The crescentic (rhythmic) shape of the sandbar is present constantly throughout the study period, with no reset events being observed (at least in the available satellite images and surveys). The observed crescentic characteristics of the sandbar vary spatially over Anmok beach and temporally through the study period.
- The amplitude A (Section 3.3.1) of all the individual crescents observed has a mean value of almost 45m and a standard deviation of about 15m. The amplitude is found on average to be smaller at the northern part of Anmok beach.
- For the length scales L (Section 3.3.1) of the individual crescents two peaks are identified in the histograms with values of 300m and 450m. The length of the crescents is on average smaller at the northern part of the beach as well.
- The mean alongshore cross-shore position $\overline{x}_b$ of the sandbar from a reference line defined at the shore (Section A.2) is found to vary from its mean value, which is equal to 210m with a standard deviation of about 20m. The sandbar appears to migrate onshore quite slowly (years) while when it migrates offshore its response is faster (days to month).
- The shape of the crescents is found to be quite symmetrical for most of the study period (max value of asymmetry $\bar{S}$ is 0.2), while only during the typhoon and storm period of the second half of 2015, asymmetry is developed.

7.1.2 What is the correlation between the position of the sandbar and the local wave conditions at Anmok beach?

The response of the sandbar (cross-shore migration, alongshore migration or alongshore rhythmicity) are studied with respect of the wave height computed at a depth of 17m (Location W1). The main findings are the following:

- The response of the sandbar to wave forcing is found not to be governed by the concurrent wave conditions, besides some high energy events (big winter storms and typhoons). During these events, the sandbar response is to migrate offshore.
- The initial location of the sandbar is expected to be of importance for the response to the wave forcing. For periods with high wave energy events and an offshore located sandbar the response is minor. On the other hand, there are events with lower wave energy that the sandbar migrates offshore, when its initial location is closer to the shoreline.
- The sequencing of the wave forcing can be important for the resulting morphological changes. During the second half of 2015, a sequence of a typhoon and several winter storms with offshore wave heights up to 4m changed the morphological patterns abruptly, creating larger scale rhythmicity in the order of 1km, besides the smaller crescents.
- Additionally, the alongshore migration of the sandbar features is studied with respect to the alongshore wave induced current for the study period. It is observed that the fluctuations of the alongshore component of the wave energy flux have an annual cycle due to the change of the predominant wave direction at Anmok between summer and winter. Interestingly, when the alongshore wave energy component is cumulative summed, there are trends of unidirected net alongshore wave energy over periods of 5-10 years. The same trends are observed at the alongshore overall sandbar migration time series when they are cumulative summed. Their linear correlation reached values of r=0.79. This highlights the potential of the alongshore wave induced current to migrate the sandbar rhythmic features in the alongshore direction.

7.1.3 **What are the estimated effects of the harbour and breakwater construction on the sandbar position?**

The effects of the human interventions (port and SBW) are studied by means of sandbar comparisons for pre and post construction periods:

- It is found that the average length and amplitude of the crescents over an area 600-700m away from the port's breakwater are reduced by almost 30% after its construction. This difference does not represent the natural variability of the crescent characteristics at Anmok beach, as for the other part of the beach (Northern part) the average values of the crescents characteristics stayed the same over these two periods. This behavior of the sandbar is expected to be connected with the sheltered zone that the port's breakwater creates and the reduction of the hydrodynamic circulations in this area.
- Furthermore, the sandbar at the area of the SBW at Anmok beach slowly disappeared almost 4 months after its construction. This is expected to be connected with the blocking of the return current induced by the SBW, which is likely to be the driving force for the creation and conservation of the sandbar.

7.1.4 **What is the expected shoreline response to different sandbar horizontal patterns and wave conditions?**

The shoreline response to different sandbar patterns is investigated through available observations and numerical modelling:

- From the available observations, the shoreline is found to present perturbations in the scale of 20-30m from its mean position. Their alongshore location is found to be connected with the sandbar alongshore location, with sometimes linear correlation reaching values of r=-0.8. The negative correlation indicates an out of phase coupling, meaning the sandbar horns are faced landward by shoreline horns. In phase coupling is observed scarcely and attains much smaller values (r=0.45). The shoreline sometimes appears to present a non-coherent response throughout its length due to different sandbar configuration in the alongshore direction.
- The importance of the cross-shore position of the sandbar for the intensity of the shoreline perturbations is indicated from the satellite images. This is further tested, using schematized bathymetry scenarios and calculating the annual sedimentation or erosion volumes in cells that are specified close to the shoreline. To this end, the alongshore net annual sediment transports rates computed with Delft3D are used. It is found that the closer the alongshore averaged cross-shore position of the sandbar is to the shoreline, the more intense the sedimentation-erosion patterns are. Furthermore, the higher the cross-shore distance of the sandbar from the coastline, the more important the predominant wave direction is for the location of the patterns.
- The indirect effect of the port construction to the shoreline, by changing the sandbar configuration appears not to be significant. This is tested by using two pre and post port schematic bathymetries with the period average crescentic characteristics. It is found that the location of the shoreline perturbation will change according to the length scales and location of the sandbar characteristics but the magnitude difference of the shoreline undulations is not expected high. Yet, these results are potentially connected with the quite small annual alongshore sediment transport rates at Anmok beach.

7.1.5 **Is it possible to predict the sandbar's horizontal position based on the local wave conditions?**

The use of two empirical model approaches for the prediction of the sandbar response to wave forcing produced unsatisfactory results and therefore no predictive skill. The calibration of the models parameters for the Anmok beach case, using linear regression analysis, resulted in quite poor values (R^2=0.04-0.05). These results can be associated with the dataset accuracy or the models simplifications.

The data-set of sandbar position extracted mainly from the satellite images proves to be valuable for investigating the sandbar system. But, its spatial accuracy and temporal resolution may not to be adequate for the calibration of the empirical models. Moreover, the models that are used assume constant model coefficients for all of the study period, which might not be the case for Anmok beach. Having variable model coefficients according to wave height requires an extended data-set , which was not available for the present work.

7.1.6 **What is the importance of the sandbar alongshore variability for the alongshore sediment transport rates?**

The present study showed that the effects of the sandbars alongshore variability on the beach average sediment alongshore sediment transports are not pronounced, at least for the dominant sandbar configuration (symmetric shape) found at Anmok beach. The

differences of the beach averaged alongshore sediment annual transports are at maximum in the order of 10% compared to an alongshore uniform base case, both for the gross and net transports. This is validated for the reduced annual wave climate computed at Anmok, and for wave data covering the period 1979-2008. The results are the same even when the wave climate is rotated by 6 degrees in both directions. This outcome indicates that the application of coastline models, which assume alongshore uniform bathymetry, in study cases with relative symmetric crescentic sandbars can be valid. This mainly concerns the large scale reorientation of the coastline. Smaller scale perturbations though (shoreline horns and embayments), due to localized sediment transport gradients, are actually affected by the variability of the sandbar and cannot be resolved by coastline models. Yet, they can be accounted for by calculating a bandwidth of the shoreline undulations based on available shoreline observations.

7.2 Recommendations

7.2.1 Satellite Imagery and extraction techniques

The manual extraction of the sandbar position from the satellite images enabled us to study the long-term sandbar dynamics and investigate the effects of the port. To this end, this technique proved quite useful in its present state. Yet, it is recommended to improve the extraction technique from the satellite imagery by introducing automatic detection methods and avoid the extraction bias. This can improve its spatial accuracy. In this study the majority of the satellite images have a resolution of 30m (Landsat missions); therefore a manual approach for the extraction of the sandbar position is used. Following the improvement of the quality of the freely available satellite imagery in the last years (Sentinel 2 mission), new automatic detection approaches can be tested. The satellite imagery obtained from Sentinel 2 mission has a resolution of 10m and a smaller revisit period. Using this dataset, automatic techniques that identify the sandbar position through pixel color intensity can be developed. Automatic extraction techniques that have been used for camera images or shoreline extraction can be investigated. Creating a more accurate and coherent dataset of the sandbar location might help in improving the understanding of the sandbar dynamics and recalibrate and validate the empirical models that are tested in the present study.

7.2.2 Sensitivity analysis of the 3D aspects of morphology

As mentioned in the discussion section, in this study it is chosen to study some specific characteristics of the sandbar mainly connected with its horizontal position. In next studies it could be insightful to investigate the effect of the 3D features of the sandbars. A sensitivity analysis could be performed for the characteristic of the sandbar, like the depth of the crestline or the landward and seaward slope of the sandbar. For the creation of schematized bathymetries the available surveys at Anmok beach can be used to identify the natural variability of these characteristics. Then the scripts developed in the present study can be used to create schematized bathymetries according to the surveyed data. A study like this can indicate how important these features are for the transformation of the waves and the resulting hydrodynamics and sediment transports.

7.2.3 Seasonal wave forcing and sensitivity analysis of wave conditions

In the present study the longshore sediment transports and shoreline response were computed in response to the average annual wave forcing. It would be interesting to

repeat the present analysis, but at a seasonal scale, to determine if the results will show a diverse response through the year.

Additionally, in this study the importance of the wave forcing (especially concerning the wave height and wave direction) for the shoreline response and the longshore sediment transport rates was highlighted. However, it was not explicitly studied, as a local wave climate in the form of representative wave conditions was used. An analysis with schematized wave conditions on the developed schematized bathymetries can indicate the importance of the wave parameters as controls for the response of the shoreline and the generations of longshore sediment transports.

7.2.4 **Human interventions effects at other sites**

The present study highlights the potential of the freely available satellite imagery for the investigation of the effects of historic human intervention on the sandbar characteristics. This approach can be used at other sites with human interventions to investigate the effects and understand how site specific the results from this study are. Especially at the East coast of South Korea both crescentic sandbars and human interventions are commonly encountered, as mentioned in Chapter 1. Thus, it can provide a lot of study sites for the effects of human interventions on sandbars to be verified.

7.2.5 **Sandbar configuration and extreme events**

The importance of the crescentic bathymetry during extreme events is another subject that is worth to be investigated. Processes like wave grouping, long waves and swash zone dynamics and their response to crescentic sandbars bathymetry can be important to understand the shoreline response during extreme conditions. This can be realized by modelling the initial response of the shoreline without bed level changes using a model like XBeach, while using the same bathymetric scenarios that are used in the present study. This approach can be quite useful for producing an integrated framework for the prediction of coastline retreat including extreme events as well.

References

Arifin, R. R., & Kennedy, A. B. (2011). The evolution of large scale crescentic bars on the northern Gulf of Mexico coast. *Marine Geology*, *285*(1–4), 46–58. https://doi.org/10.1016/j.margeo.2011.04.003

Bosboom, J., & Stive, M. J. F. (2012). *Coastal Dynamics I: Lectures Notes CIE4305*. VSSD.

Bowen, A. J., & Inman, D. L. (1971). Edge waves and crescentic bars. *Journal of Geophysical Research*, *76*(36), 8662–8671.

Caballeria, M., Coco, G., Falqués, a., & Huntley, D. a. (2002). Self-organization mechanisms for the formation of nearshore crescentic and transverse sand bars. *Journal of Fluid Mechanics*, *465*, 379–410. https://doi.org/10.1017/S002211200200112X

Castelle, B., & Bonneton, P. (2006). Nearshore waves and currents over crescentic bars. *Journal of Coastal Research*, *2*(January 2004), 687–691.

Coco, G., & Murray, A. B. (2007). Patterns in the sand: From forcing templates to self-organization. *Geomorphology*, *91*(3–4), 271–290. https://doi.org/10.1016/j.geomorph.2007.04.023

de Schipper, M. A., Ranasinghe, R., Reniers, A., & Stive, M. (2011). On the initiation of nearshore morphological rhythmicity. *Coastal Engineering Proceedings 1.32*, 1–14.

Deltares. (2014a). *Delft3D-FLOW, User Manual, Simulation of multi-dimensional hydrodynamic flows and transport phenomena, including sediments*. version: 3.15.34158.

Deltares. (2014b). *Delft3D-WAVE, User Manual, Simulation of short-crested waves with SWAN*. version: 3.05.34160.

Deltares. (2016). *CoMIDAS-East Coast Case: Numerical model study of Anmok Beach*.

Falqués, A., Coco, G., & Huntley, D. A. (2000). A mechanism for the generation of wave-driven rhythmic patterns in the surf zone. *Journal of Geophysical Research*, *105*(October), 24071. https://doi.org/10.1029/2000JC900100

Huisman, B. J. A., Vargas Solis, A., de Schipper, M. A., Radermacher, M., & Ranasinghe, D. (2017). Impact of beach states on alongshore transport. *Proceedings of Coastal Dynamics 2017 : Helsingør, Denmark*, 996–1006. Retrieved from https://repository.tudelft.nl/islandora/object/uuid:55a3db01-9a23-4815-be17-90a74562d523?collection=research

Lesser, G. R., Roelvink, J. A., van Kester, J. A. T. M., & Stelling, G. S. (2004). Development and validation of a three-dimensional morphological model. *Coastal Engineering*, *51*(8–9), 883–915. https://doi.org/10.1016/j.coastaleng.2004.07.014

Lippmann, T. C., & Holman, R. a. (1990). The spatial and temporal variability of sand bar morphology. *Journal of Geophysical Research*, *95*(C7), 11575. https://doi.org/10.1029/JC095iC07p11575

Lippmann, T. C., & Holman, R. A. (1989). Quantification of sand bar morphology: A video technique based on wave dissipation. *Journal of Geophysical Research: Oceans*, *94*(C1), 995–1011. https://doi.org/10.1029/JC094iC01p00995

Long, J. W., & Plant, N. G. (2012). Extended Kalman Filter framework for forecasting shoreline evolution. *Geophysical Research Letters*, *39*(13), 1–6. https://doi.org/10.1029/2012GL052180

Orzech, M. D., Reniers, A. J. H. M., Thornton, E. B., & MacMahan, J. H. (2011). Megacusps on rip channel bathymetry: Observations and modeling. *Coastal Engineering*, *58*(9), 890–907. https://doi.org/10.1016/j.coastaleng.2011.05.001

Orzech, M. D., Thornton, E. B., MacMahan, J. H., O'Reilly, W. C., & Stanton, T. P. (2010). Alongshore rip channel migration and sediment transport. *Marine Geology*, *271*(3–4), 278–291. https://doi.org/10.1016/j.margeo.2010.02.022

Pape, L., Plant, N. G., & Ruessink, B. G. (2010). On cross-shore migration and equilibrium states of nearshore sandbars. *Journal of Geophysical Research: Earth Surface*, *115*(3), 1–16. https://doi.org/10.1029/2009JF001501

Plant, N. G., Holland, K. T., & Holman, R. A. (2006). A dynamical attractor governs beach response to storms. *Geophysical Research Letters*, *33*(17), 1–6. https://doi.org/10.1029/2006GL027105

Plant, N. G., Holman, R. A., Freilich, M. H., & Birkemeier, W. A. (1999). A simple model for interannual sandbar behavior. *Journal of Geophysical Research: Oceans*.

Price, T. D., Castelle, B., Ranasinghe, R., & Ruessink, B. G. (2013). Coupled sandbar patterns and obliquely incident waves. *Journal of Geophysical Research: Earth Surface*, *118*(3), 1677–1692. https://doi.org/10.1002/jgrf.20103

Price, T. D., Ruessink, B. G., & Castelle, B. (2014). Morphological coupling in multiple sandbar systems – A review. *Earth Surface Dynamics*, *2*(1), 309–321. https://doi.org/10.5194/esurf-2-309-2014

Reniers, A. J. H. M., Roelvink, J. A., & Thornton, E. B. (2004). Morphodynamic modeling of an embayed beach under wave group forcing. *Journal of Geophysical Research*, *109*(C1), 1–22. https://doi.org/10.1029/2002JC001586

Ribas, F., Garnier, R., Ojeda, E., Falqués, A., Guillen, J., & Calvete, D. (2007). Observation and modeling of crescentic bars in Barcelona embayed beaches. *Coastal Sediments*, *7*.

Roelvink, J. A., & Reniers, A. J. H. M. (2012). *A Guide to Modeling Coastal Morphology* (Vol. 12). World Scientific.

Smit, M., Reniers, A. J. H. M., & Stive, M. J. F. (2010). What determines nearshore sandbar response? *Coastal Eng. 2010*, 1–7.

Splinter, K. D., Holman, R. A., & Plant, N. G. (2011). A behavior-oriented dynamic model for sandbar migration and 2DH evolution. *Journal of Geophysical Research: Oceans*, *116*(1), 1–21. https://doi.org/10.1029/2010JC006382

Tiessen, M. C. H., van Leeuwen, S. M., Calvete, D., & Dodd, N. (2010). A field test of a linear stability model for crescentic bars. *Coastal Engineering*, *57*(1), 41–51. https://doi.org/10.1016/j.coastaleng.2009.09.002

Ton, A. M. (2017). *Process-based modelling of hydro- and morphodynamics around the Anmok submerged breakwater*. TU Delft. Retrieved from http://repository.tudelft.nl/islandora/object/uuid:810e6874-f5a1-4eff-9e77-459b80ebc0cf?collection=education

van de Lageweg, W. I., Bryan, K. R., Coco, G., & Ruessink, B. G. (2013). Observations of shoreline-sandbar coupling on an embayed beach. *Marine Geology*, *344*, 101–114.

https://doi.org/10.1016/j.margeo.2013.07.018

van Enckevort, I. M. J., Ruessink, B. G., Coco, G., Suzuki, K., Turner, I. L., Plant, N. G., & Holman, R. A. (2004). Observations of nearshore crescentic sandbars. *Journal of Geophysical Research*, *109*(C6), C06028. https://doi.org/10.1029/2003JC002214

van Rijn, L. C. (2007a). Unified View of Sediment Transport by Currents and Waves. I: Initiation of Motion, Bed Roughness, and Bed-Load Transport. *Journal of Hydraulic Engineering*, *133*(6), 649–667. https://doi.org/10.1061/(ASCE)0733-9429(2007)133:7(776)

van Rijn, L. C. (2007b). Unified View of Sediment Transport by Currents and Waves. II: Suspended Transport. *Journal of Hydraulic Engineering*, *133*(6), 668–689. https://doi.org/10.1061/(ASCE)0733-9429(2007)133:7(776)

Van Rijn, L. C., Walstra, D. J. R., & Van Ormondt, M. (2004). *Description of TRANSPOR2004 and Implementation in Delft3D-ONLINE*.

Wright, L. D., & Short, A. D. (1984). Morphodynamic variability of surf zones and beaches: A synthesis. *Marine Geology*, *56*(1–4), 93–118. https://doi.org/10.1016/0025-3227(84)90008-2

Yates, M. L., Guza, R. T., & O'Reilly, W. C. (2009). Equilibrium shoreline response: Observations and modeling. *Journal of Geophysical Research: Oceans*, *114*(9), 1–16. https://doi.org/10.1029/2009JC005359

Appendix A - Sandbar position extraction

A.1. Introduction

In order to study how the sandbar at Anmok beach behaves and moves through the study period an estimation of the sandbar crest line is needed. Usually during the research conducted so far regarding the dynamics of sandbars, data from video observation and a frequency of one hour during daylight (time exposure images) are used (van Enckevort et al., 2004; Plant et al., 2006; Price et al., 2013; van de Lageweg et al., 2013). For this study case, as no camera was positioned at the South Korean East coast, the only source to extract the sandbar position are satellite (or aerial) images and surveys.

A.2. Data sources

For the extraction of the position of the sandbars crest line during the study period different data sets of satellite images, aerial images and surveys are used. An overview of the available data and their specifications can be found in Table A-1.

Table A-1: Overview of available data for the extraction of sandbar position, including their source, spatial resolution and quantity.

Type & Source		Spatial Resolution	Quantity	Description
Satellite imagery	Landsat 4,5,7,8 (U.S Geological Survey)	30m	507	True colour satellite images covering the period from 1985 onwards with varying intervals.
	Sentinel 2 (EU Copernicus Services)	10m		
	Arirang 1,2 (KIOST)	1m and 6.6m	20	Panchromatic satellite images covering the periods of 2000-2006 and 2008-2014 with varying intervals.
Aerial Imagery supplied by KIOST		0.5-1m	5	Panchromatic aerial images from 1972-2005 with long intervals
Surveys supplied by KIOST		5m x 50m (cross-shore x alongshore)	14	Surveys bathymetric data conducted in 2007-2008 and 2013-2016

The Landsat and Sentinel freely available satellite imagery for the area of interest is obtained using the eeFEX application (to be published in Deltares Report 2017). This application uses the Google Earth Engine platform to download all the available images from Landsat 4,5,7,8 and Sentinel 2 missions, for the area and period specified that meets the cloud coverage value selected (Figure A-1). Furthermore, before downloading, the coordinate reference system (CRS) of the extracted images can be chosen. For the case

study, acceptable cloud coverage is set at 25% and the UTM CRS is chosen. This resulted in 507 satellite images.

Figure A-1: eeFEX download panel with area of interest and satellite missions to be used selected.

As automated methods for the bar position extraction are not able to produce reliable results a manual approach is followed. For the case of the satellite imagery downloaded with eeFEX, the images are checked one by one in their true colour format in order to draw manually the sandbar crest position for the cases that this is feasible regarding the visibility of the sandbar (Figure A-2). The sandbar crest line is defined as the centre of the bars width visible. This is the case for 175 of the images that resulted in the same number of sandbar crest line position polylines with UTM coordinates. During the sandbars position manual extraction, these 175 images are graded regarding their quality, as will be explained in the following.

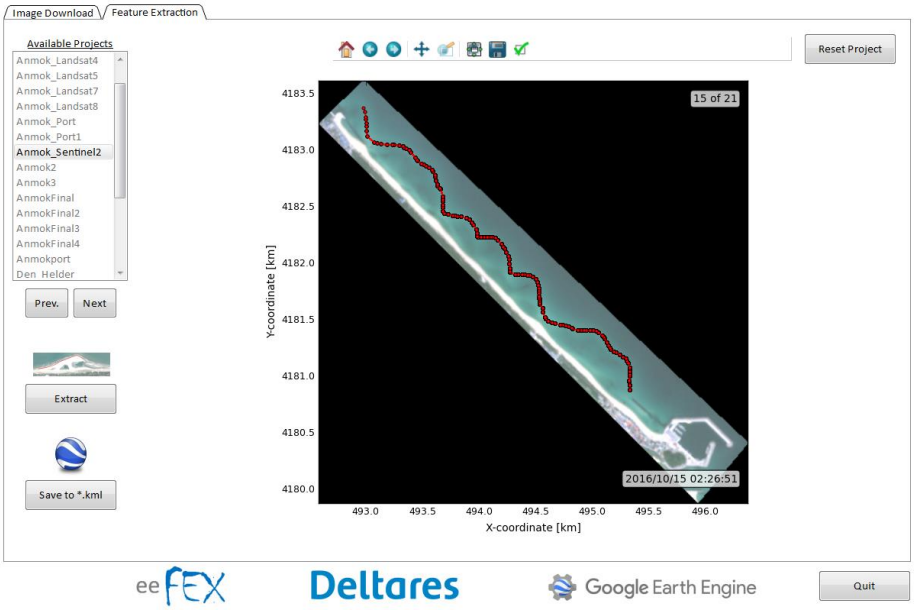

Figure A-2: eeFEX feature extraction procedure with sandbar polyline sketched on the picture.

In some of the images differences in the horizontal position of the Gangneung port are detected, which can be attributed to inconsistencies in the satellite projection of the satellite image sets. To attribute for this mismatches, a manual correction calculated based on the position of the port is applied to all the images and polylines after the port's construction.

Additionally, for the satellite imagery from the Korean satellites Arirang 1 and Arirang 2 the images are georeferenced in the UTM CRS and the polyline of the sandbar's position are extracted manually in the same way as before for nine of them, when the sandbar is visible. The same is performed for the three aerial images of the five available that are in the period of interest. Additionally, for the 14 surveys that are available the sandbar crest line is extracted manually, as the attempt to extract the crest line position from finding peaks at cross-shore transects method didn't produce continuous location results.

The end result is a set of 201 sandbar positions polylines with UTM coordinates for the period 1990-2017. All this polylines are graded from 1 to 4 according to their quality as following:

Table A-2: Extraction sandbar location grading description

Grade	Description
1	All of the surveys, as there are thought to be the best quality data available for the study regarding the location of the sandbar. The aerial and Arirang Imagery that are clear enough to identify the sandbar location and due to their high spatial resolution.
2	The Sentinel satellite imagery that are clear and without waves. The most clear Landsat satellite imagery that the sandbar is easily distinguished. The aerial and Arirang imagery that is less clear.
3	The Landsat satellite imagery that the sandbar is not really visible at some location or wave breaking is present
4	The Landsat satellite imagery with the sandbar not being easy to distinguish. Includes images of Landsat 7 with black stripes due to sensor problems, where the sandbar is not visible at some locations.

A reference line is defined parallel to the coast with its origin (0, 0) at the point with UTM coordinates 495507E, 4180473 N. The angle of the reference line and thus the coastline is calculated as 313.5^{o} to the North direction. For each of the polylines with UTM coordinates previously extracted, the following steps are applied:

1. The coordinates of the origin are subtracted in order to get their coordinates in reference to the origin.
2. The local coordinates are rotated around the origin with a transformation matrix with angle -43.5^{o}.
3. The cross shore distance of the sandbar crest from the reference line is linearly interpolated in an alongshore grid of 10m interval in the 3.6km coastal stretch of Anmok beach.
4. The sandbar crest line is finally smoothed using a moving average to take into account small perturbation due to the manual drawing phase.

Repeating this procedure for all available observations resulted in the matrix $x_b(y,t)$, where x_b expresses the observed cross shore distance of the sandbar crest from the reference line at alongshore distances y and at time t.

A.3. Sandbar position accuracy

The satellite images from the Landsat missions have a spatial resolution of 30m while the ones from the Sentinel 2 mission have a resolution of 10m. This made the detection of the sandbar less accurate for the Landsat images. To estimate the accuracy of the manual extraction method the available surveys are used. For all of the 14 available surveys, satellite images that were temporally close to the survey dates are chosen (maximum 20 days). This is the case for 11 of the surveys. In a preliminary qualitative check the extracted sandbar crest line seems to be in agreement with the surveys (Figure A-3).

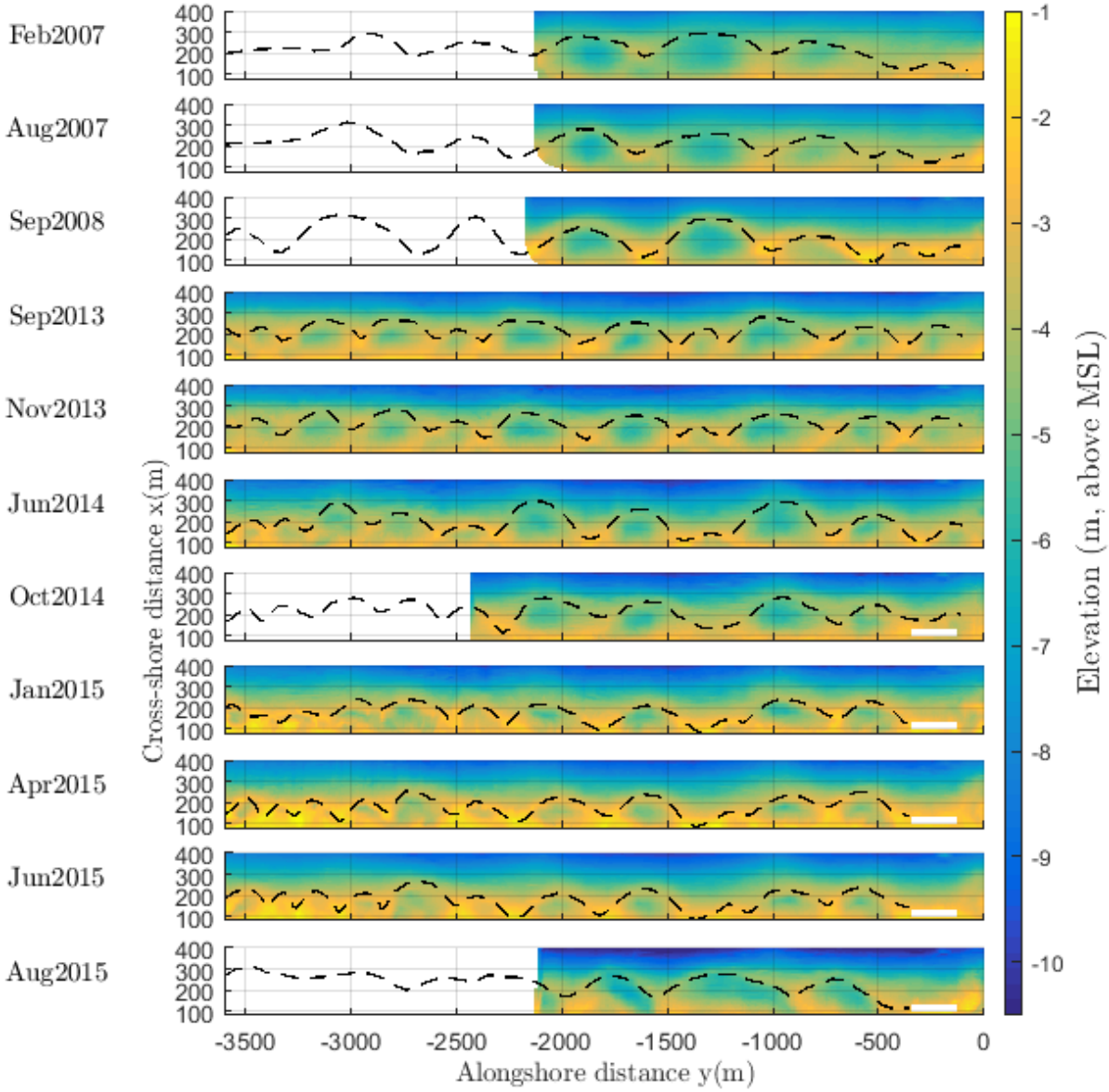

Figure A-3: Bathymetries created from the available surveys with the sandbar crest line detected manually from the satellite images plotted on them

In order to quantify the accuracy of the extracted sandbar position estimation an attempt to extract the sandbar crest line position from the surveys is made. This is performed by

normalizing every cross-shore profile with the mean beach profile of each survey (Figure A-4). Then the local maxima are identified and the cross-shore position and depth are calculated. Sadly, due to the spatial accuracy of the surveys and the failure of detection at some cases, the results are not continuous, while some errors in the detection are present due to the normalization of the bathymetry.

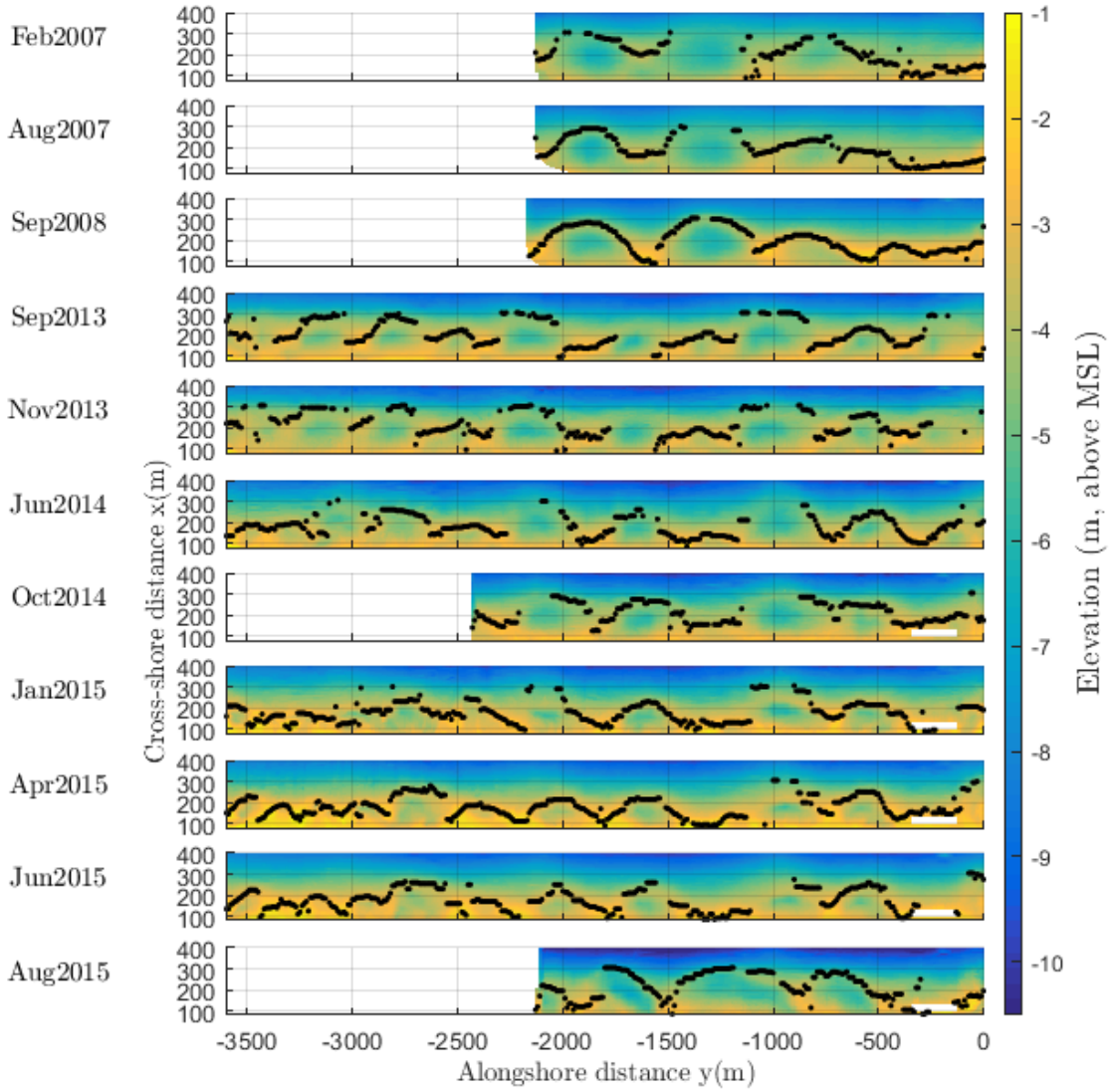

Figure A-4: Sandbar crest line position detected for each of the normalized profiles from the bathymetric data.

Regarding each of the 11 available survey detected and satellite detected sandbar position the results are compared for all the alongshore points that estimations from both methods exist. The R^2 ranged from 0.5 to 0.85 for the available observations, while the RMSE from 25m to 45m (Figure A-5). It's important to point out that this error estimation does not only include the error from the manual extraction. It contains differences regarding the temporal gaps between the surveys and the satellite images. Moreover, it contains erroneously detected sandbar position from the surveys because of the normalization procedure.

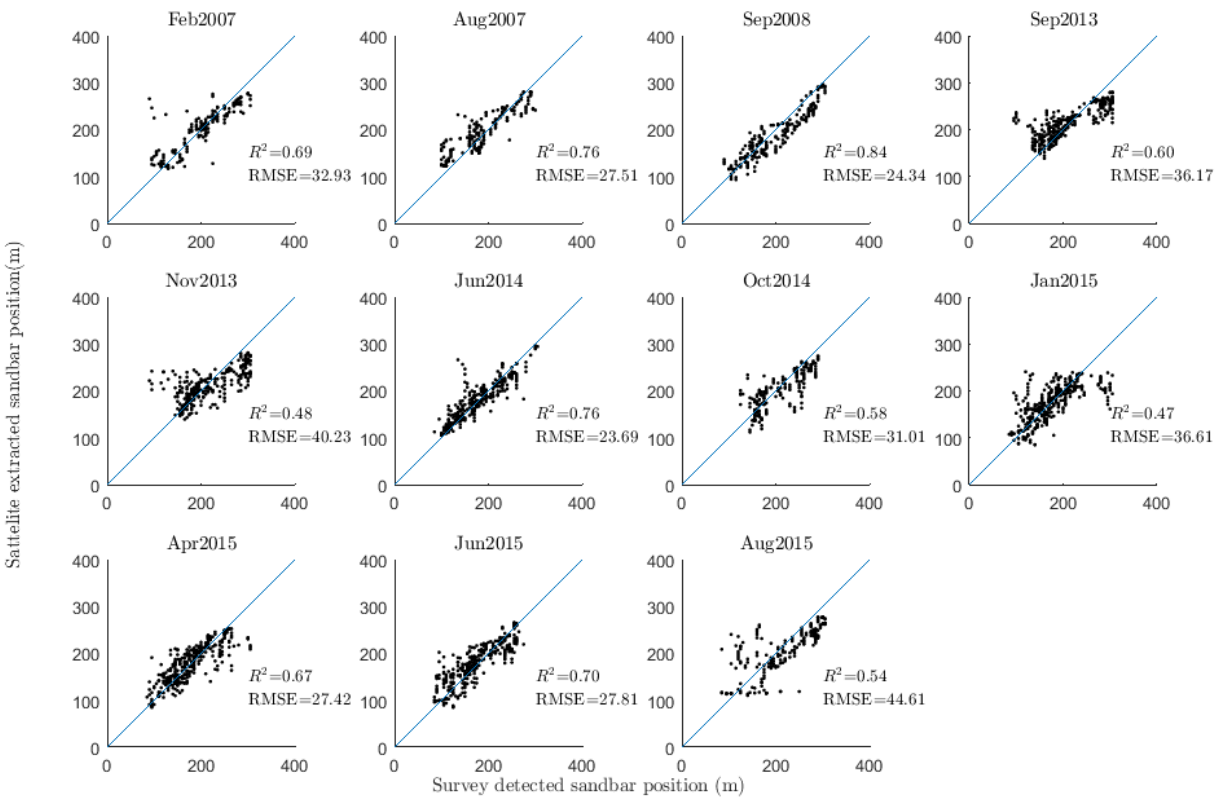

Figure A-5: Scatter plots of the survey detected sandbar cross-shore position (x-axis) vs. the satellite detected one (y-axis) for each of the available observations.

Due to lack of time, it is chosen not to try and improve the sandbar position detection method from the surveys. Furthermore, the depth of the detected sandbar position is plotted against the cross-shore position in order to estimate a linear relationship between the two parameters (Figure A-6).

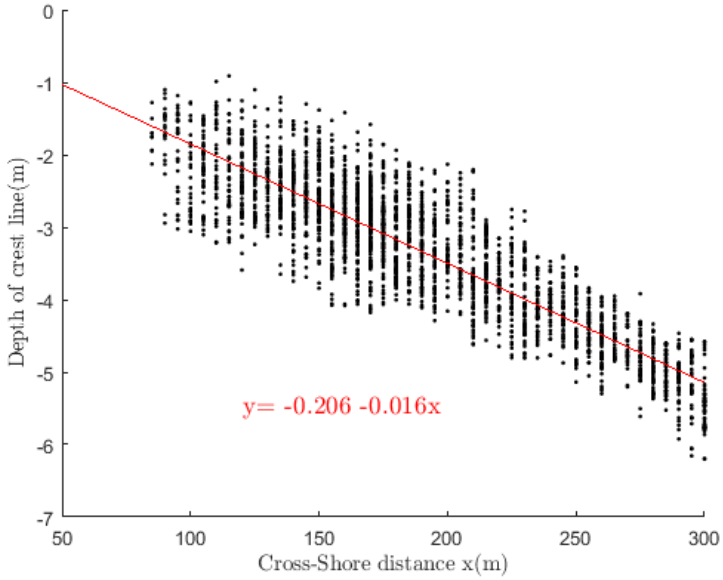

Figure A-6: Scatter plot of the cross-shore location of the sandbar (x-axis) vs. the depth at the same point (y-axis). The red line represents the best linear f

Appendix B - Nearshore wave time series

B.1. Introduction

As highlighted in Chapter 2, waves are the main forcing mechanism that initiates changes in the nearshore morphology in Anmok beach. In order to understand how the sandbar system changes through the study period, knowing the nearshore wave conditions is crucial. To this end, hindcasted offshore wave time series are used in combination with previous wave transformation modelling results.

B.2. Approach

Hindcasted wave data from a WAM (Wave Modelling Group) wave model are provided by KIOST for the period of 1979-2008 for several offshore locations around Gangneung. The data are generated by the KIOST research group using ECMWF wind data to determine the wave climate around the whole Korean peninsula. During previous phases of the CoMIDAS project, in order to determine the nearshore wave climate a SWAN wave propagation model was set up. The offshore wave time series are classified in about 241 classes according to their wave height, direction, period, steepness and wind direction. Then, scenarios are defined for each class as the average values of the time series falling in the class and then introduced as boundary conditions in the wave propagation model.

As these wave data span a period until 2008, while in this study the biggest part of the available sandbar and shoreline data are available after 2008, it is chosen to use a different offshore wave dataset, generated from the ECMWF's ERA-Interim model, which covers all the study period. In order not to run another SWAN model with the new boundary data, which would have been time consuming, the previous transformations are used in order to identify relationships between the offshore hindcasted WAM wave scenarios and nearshore computed wave conditions. In order to do this the ORCA software is used. ORCA is a toolbox for classification and transformation of metocean data, developed by Deltares. The procedure that is followed can be schematised as in Figure B-1.

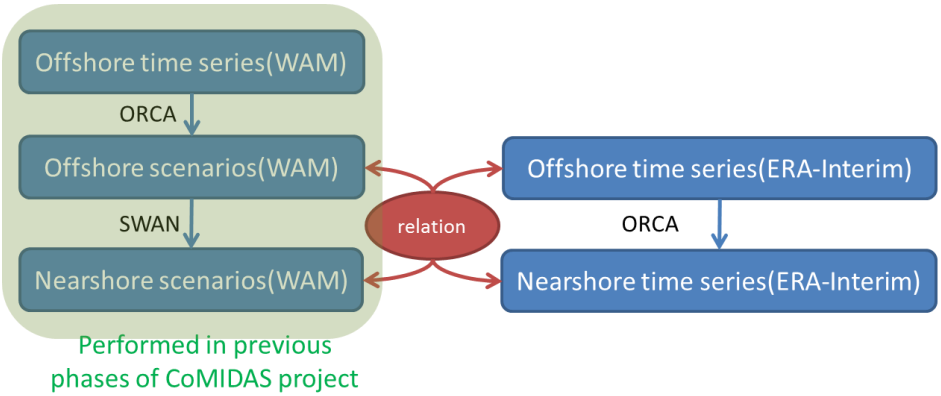

Figure B-1: Description of the procedure followed to obtain the nearshore wave time series for the period of study.

The main steps in order to obtain the nearshore time series include:

1. Calculation of relations between offshore and nearshore conditions. In this step using ORCA toolbox, the relationships between the offshore and nearshore parameters that are chosen to be transformed (H_s, T_m and mean wave direction) are defined in the form of ratios for wave height and period and differences for the directions. The nearshore location is specified as the location of W1 measurements to provide validation potential.
2. Interpolation between relations. As expected the offshore time series parameter values will lay between the scenario parameters values. This makes interpolation necessary. Using ORCA toolbox this interpolation is performed using two parameters, the wave height and the wave direction. The results are three transformation matrices (one for each parameter).
3. Transformation of the offshore time series to nearshore. During this step the nearshore time series are constructed be multiplying (or adding in case of directions) the offshore parameters values with the values of the corresponding values of the transformation matrix.

In Figure B-2 the available WAM and ERA-Interim offshore wave data for the area can be seen. Additionally, one year measured wave data are available for Anmok beach, at the location named W1, and at a water depth of about 17m (Figure B-3). As it is easily observed, the spatial coverage of the available ERA-Interim data is far less extensive in comparison to the WAM data. The two ERA-Interim locations 12 and 17 lay in the desired area of interest. The same procedure is applied for the transformation of the offshore wave time series to nearshore for both locations.

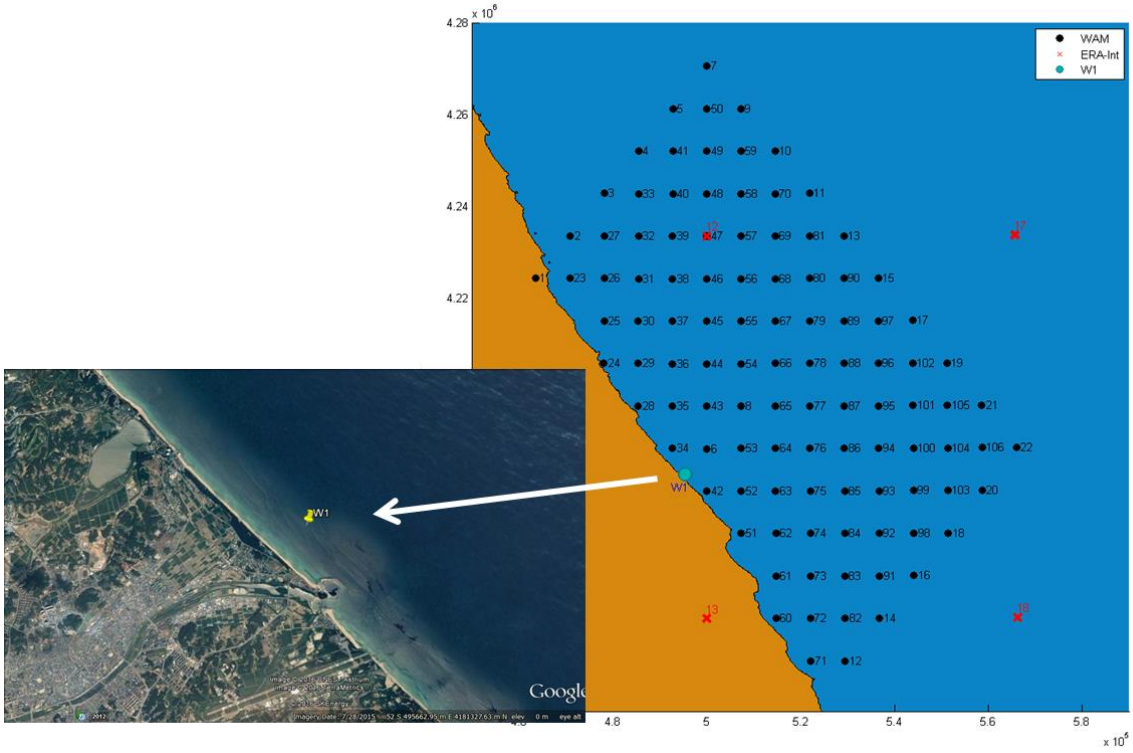

Figure B-2: Overview of the available offshore WAM and ERA-Interim wave data locations. Furthermore the location W1 of the available wave measurements can be seen.

The results of the transformation showed larger consistency with the measured data for the case of location 17, even though the WAM location used for the transformation is in a different location. This is expected to be the case, because of the orientation of the coast and this point being at the perpendicular line, thus realizing the wave directions in a better way. The results presented in the following include only the ERA-Interim location 17 transformation.

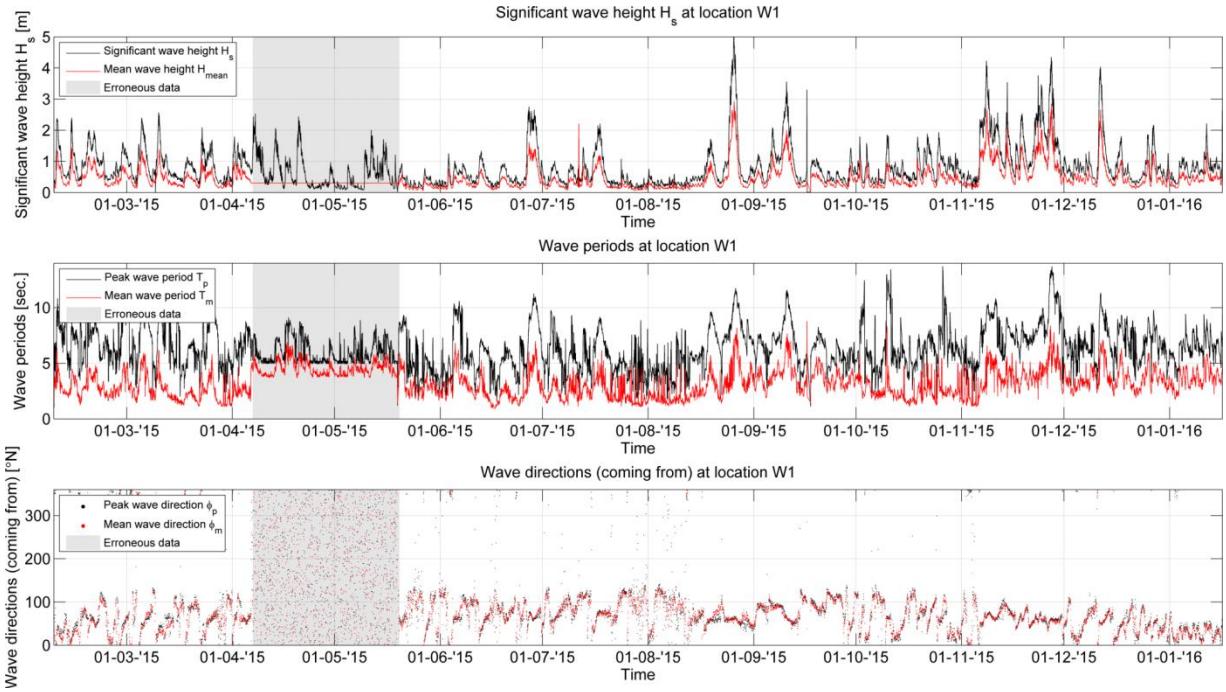

Figure B-3: Overview of the available offshore WAM and ERA-Interim wave data locations. Furthermore the location W1 of the available wave measurements can be seen.

B.3. Validation

The transformed significant wave height H_s (m), mean wave period T_m (s) and mean wave direction Dir (°) at location W1 are validated with the measurements available for the period of the year 2015. The wave roses of the wave height for the measured and computed data for that period can be seen in Figure B-4.

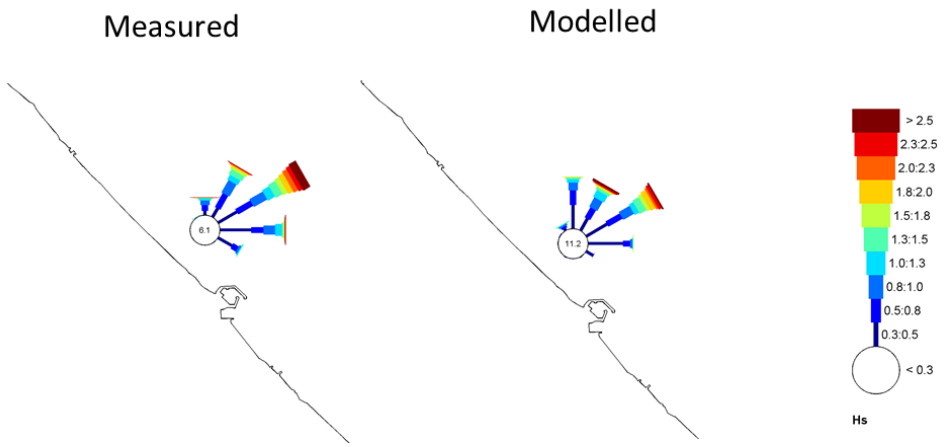

Figure B-4: Wave roses of significant wave height for modelled and measured wave data at location W1 for the period of 2015.

Overall the computed results show good agreement with the measured data, from a first quality check of the wave roses. The dominant wave come from the NE sector with similar distribution of the wave heights. There seems to be an underestimation of the higher wave heights. Moreover the wave energy coming from the N sector is overestimated while the one coming from E is underestimated. To gain a quantitative insight, scatter plots are obtained with ORCA toolbox for each of the three parameters (Figure B-5). From these plots, it is observed that the higher wave height are indeed underestimated while the largest mean wave periods are overestimate a little bit. The same observation as from the wave plots can be derived for the scatter plots for the wave directions computed.

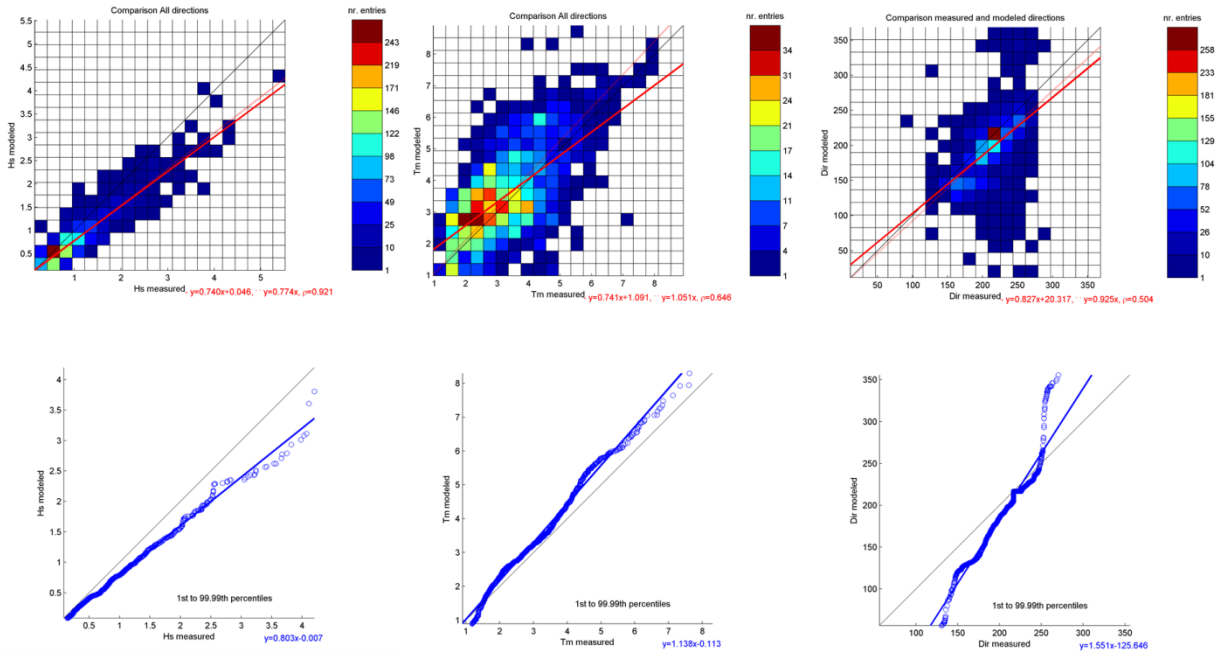

Figure B-5: Density scatter plots (top panels) and quintile plots (bottom panels) of the observed (horizontal axis) and modelled (vertical axis) wave heights (left) wave period (middle) and wave direction (right). Mind that the wave's directions are relative to the shore normal with direction landwards.

B.4. Correction

The linear fit angles without intesects that are calculated for the density scatter plots are used as a correction factor for the wave height and wave period. For the wave direction a clockwise turn of 3 degrees is applied to account for the underestimation of the eastern sector. It is assumed that using all the 2015 year measurements for the correction is valid as it includs seasonal data.

The corrected data scatter plot can be seen in Figure B-6. As expected the agreement between the observed and modelled wave height and period is much higher than before. The regression between the corrected modelled and the measured data gave an $r^2 = 0.85$ for the wave height and a $r^2 = 0.42$ for the wave period. For the wave direction an extra check is performed by plotting the scatterplots of the directions excluding the small wave heigth (Hs<0,4 m). This gaves a far better agreement with the observed data with an $r^2 = 0.53$ and a slope of 0.93. For the case of this study it is expected that the smaller wave heights are not that critical concerning the morphological changes of the beach.

B.5. Final results

The final time series of the wave weight, period and angle of incidence relative to the shore at the location of W1 and at a depth of almost 17m are presented in Figure B-7.

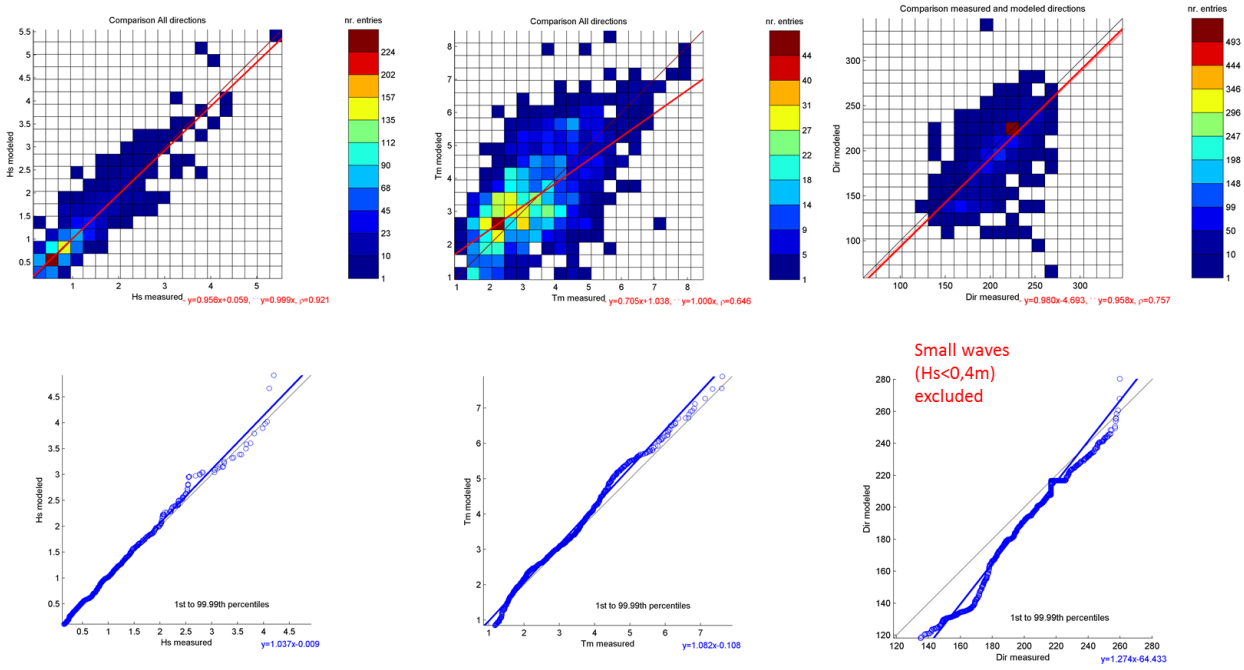

Figure B-6: Density scatter plots (top panels) and quintile plots (bottom panels) of the observed (horizontal axis) and corrected modelled (vertical axis) wave heights (left) wave period (middle) and wave direction (right). Mind that the wave's directions are relative to the shore normal with direction landwards and that for the direction plot the wave heights with Hs<04m have been excluded

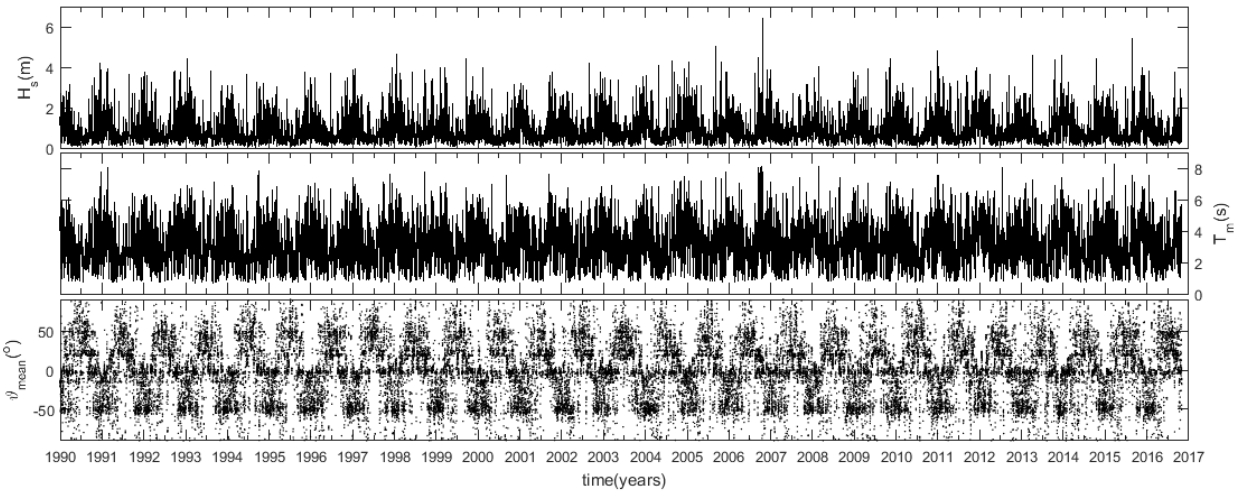

Figure B-7: Final time series of significant wave height Hs (top), mean wave period Tm (middle) and mean wave angle of incidence θmean (bottom).

Appendix C - Delft3D Results

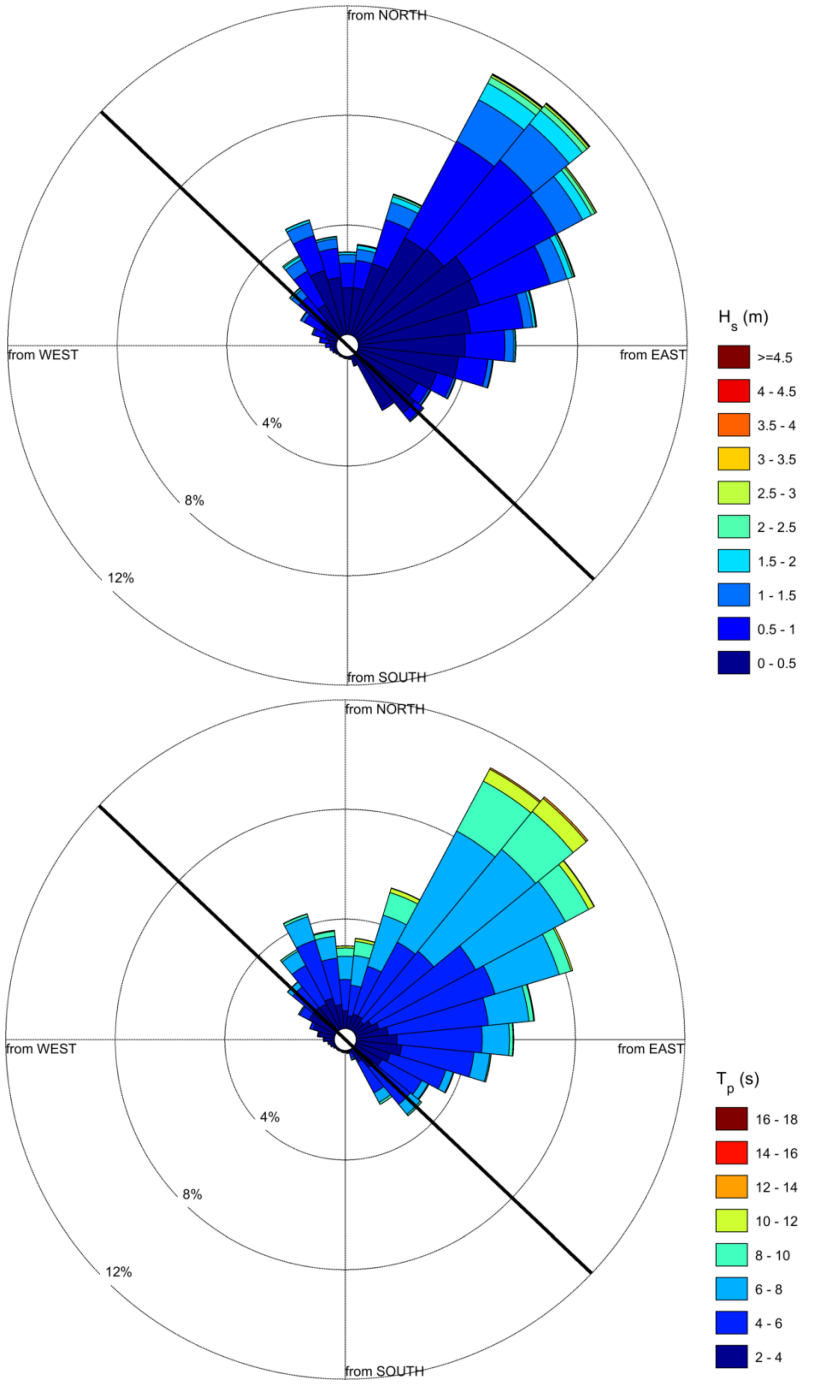

Figure C-1: Wave rose plot at offshore location (129.00° E, 37.83° N) presenting the significant wave height (top) and peak wave period (bottom) for the period of 1979-2008. Thick black line represents the orientation of the coastline at Anmok beach (43.5° N)

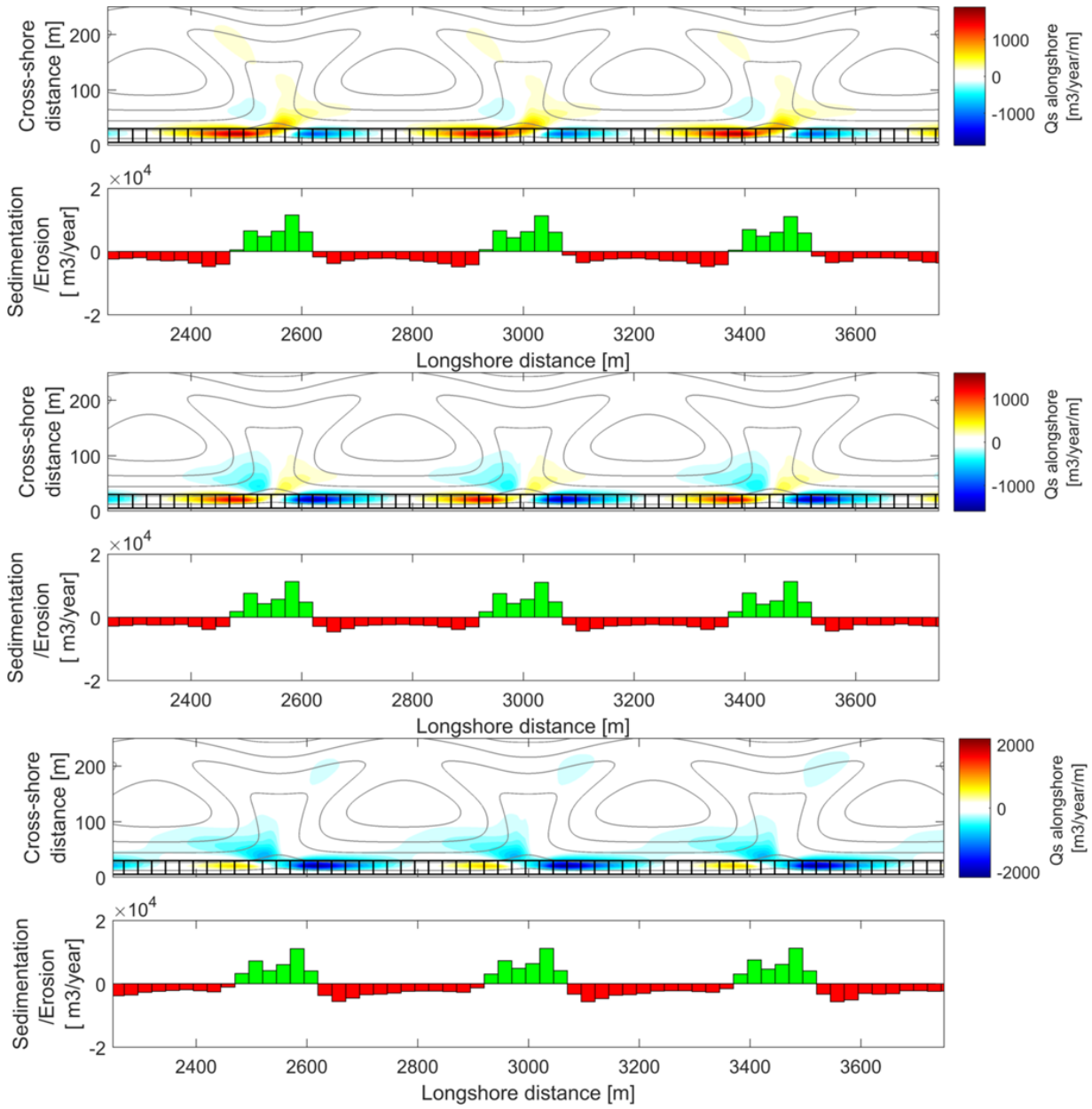

Figure C-2: Computed annual alongshore transport rates for s3 scenario and the (from top to bottom) WAM-6deg, WAM and WAM+6deg. Upper panel: Spatial transport fields of the annual alongshore sediment transport component (positive directed to the South). Black lines indicated the cells used for the computations. Bottom panel: Sedimentation (green) or Erosion (red) volumes calculated for each cell.

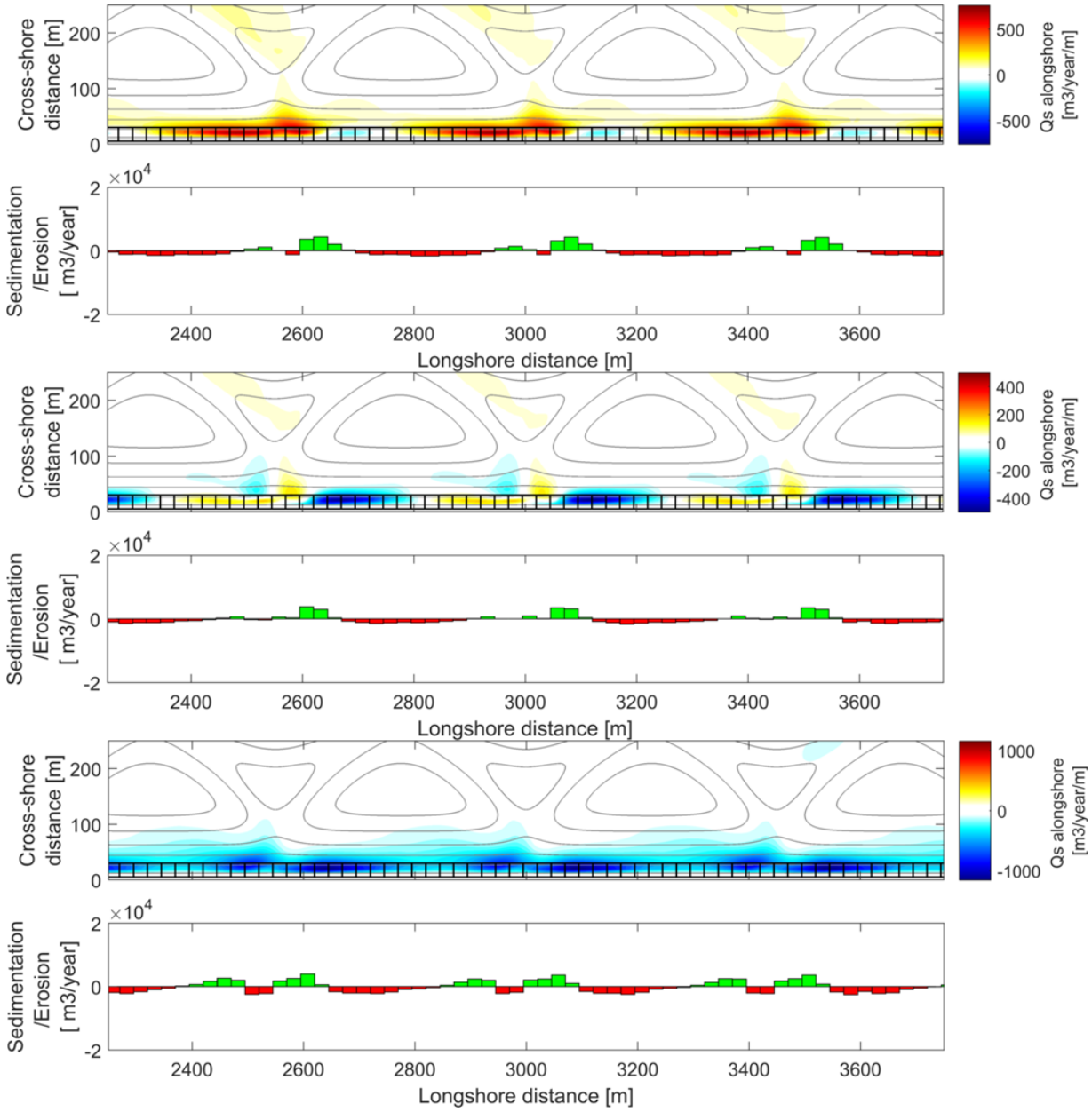

Figure C-3: Computed annual alongshore transport rates for s6 scenario and the (from top to bottom) WAM-6deg, WAM and WAM+6deg. Upper panel: Spatial transport fields of the annual alongshore sediment transport component (positive directed to the South). Black lines indicated the cells used for the computations. Bottom panel: Sedimentation (green) or Erosion (red) volumes calculated for each cell.

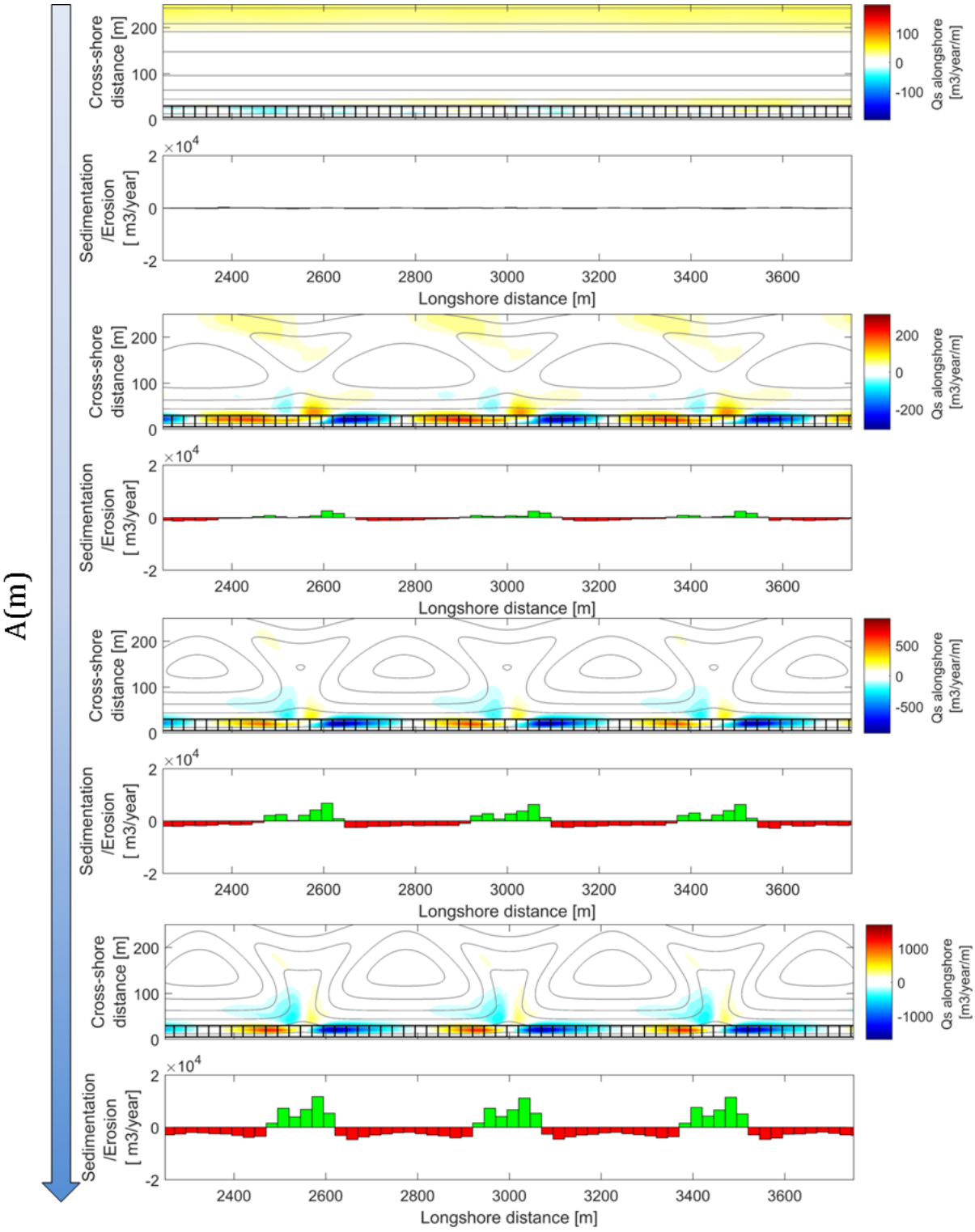

Figure C-4: Computed annual alongshore transport rates for s1, s2,s5 and s3 scenarios. Upper panel: Spatial transport fields of the annual alongshore sediment transport component (positive directed to the South). Black lines indicated the cells used for the computations. Bottom panel: Sedimentation (green) or Erosion (red) volumes calculated for each cell.

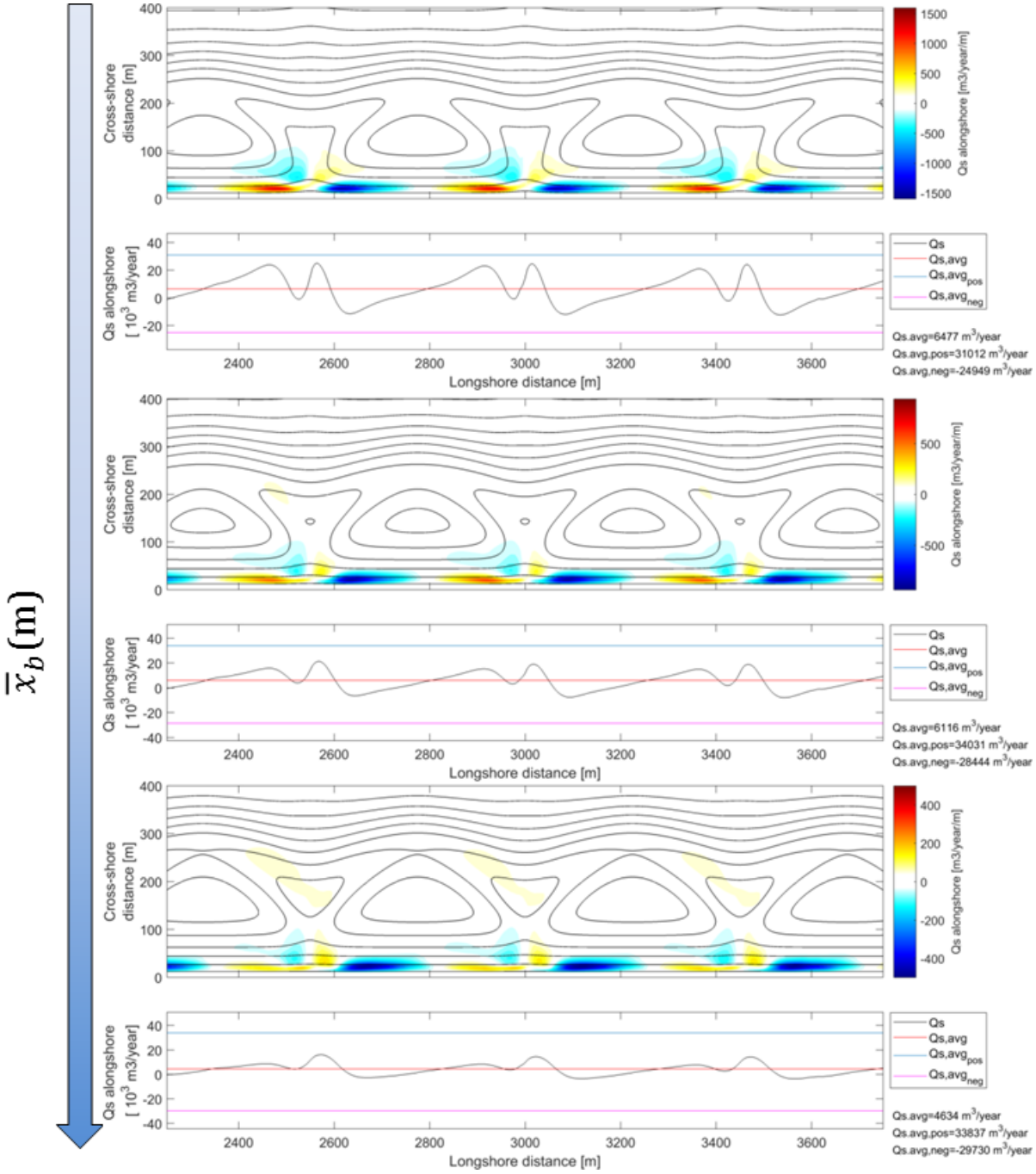

Figure C-5: Computed annual alongshore transport rates for s4,s5 and s6 scenarios. Upper panel: Spatial transport fields of the annual alongshore sediment transport component (positive directed to the South). Bottom panel: Cross-shore integrated alongshore transports $Q_S(x)$ (black line) and beach state averaged transport $Q_{S,AVG}$ (red line). Gross-positive (blue line) and gross-negative (purple line) beach state averaged transports are plotted as well.

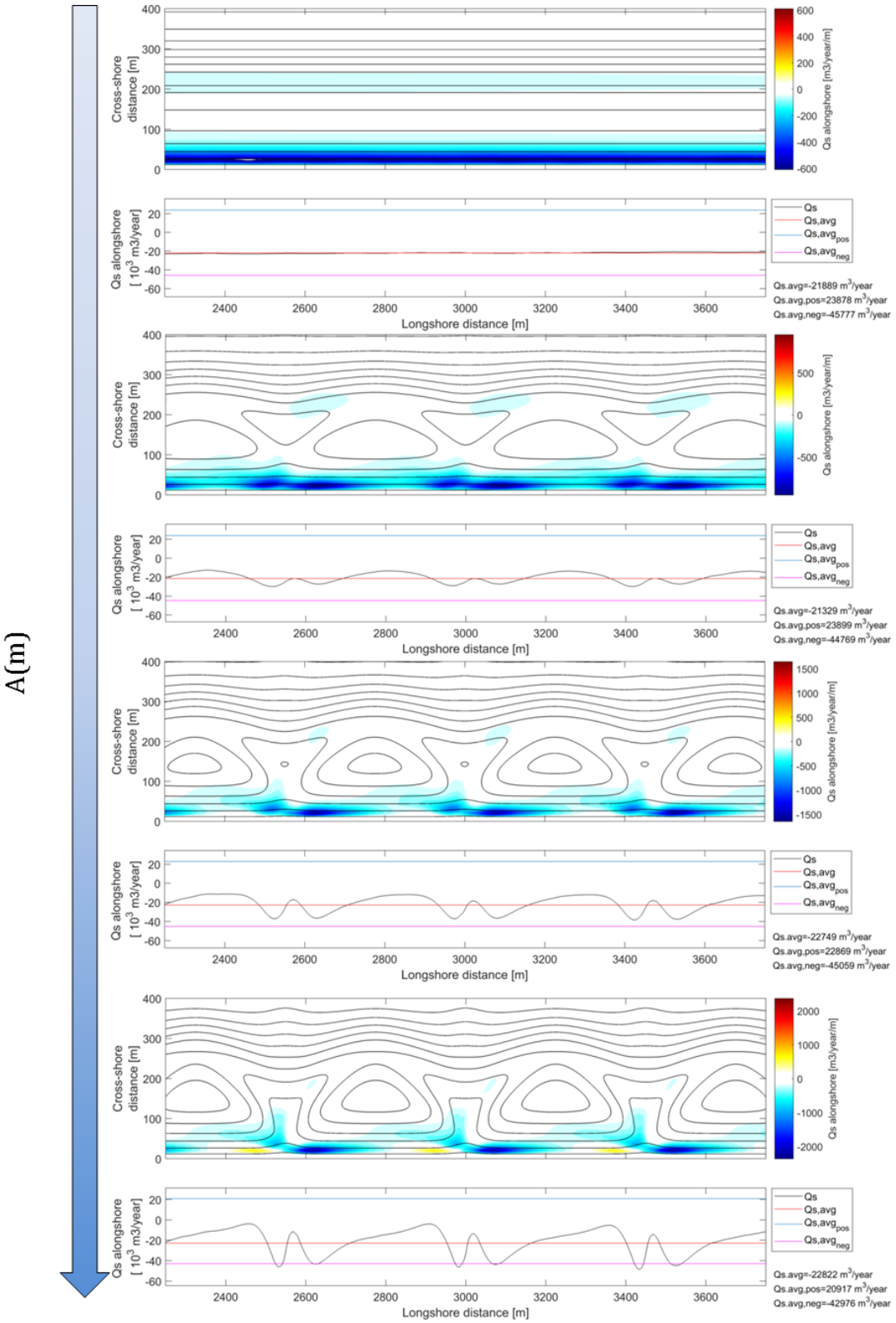

Figure C-6: Computed annual alongshore transport rates for s1,s2,s5 and s3 scenarios and the rotated WAM+6 degrees wave climate. Upper panel: Spatial transport fields of the annual alongshore sediment transport component (positive directed to the South). Bottom panel: Cross-shore integrated alongshore transports $Q_S(x)$ (black line) and beach state averaged transport $Q_{S,AVG}$ (red line). Gross-positive (blue line) and gross-negative (purple line) beach state averaged transports are plotted as well.

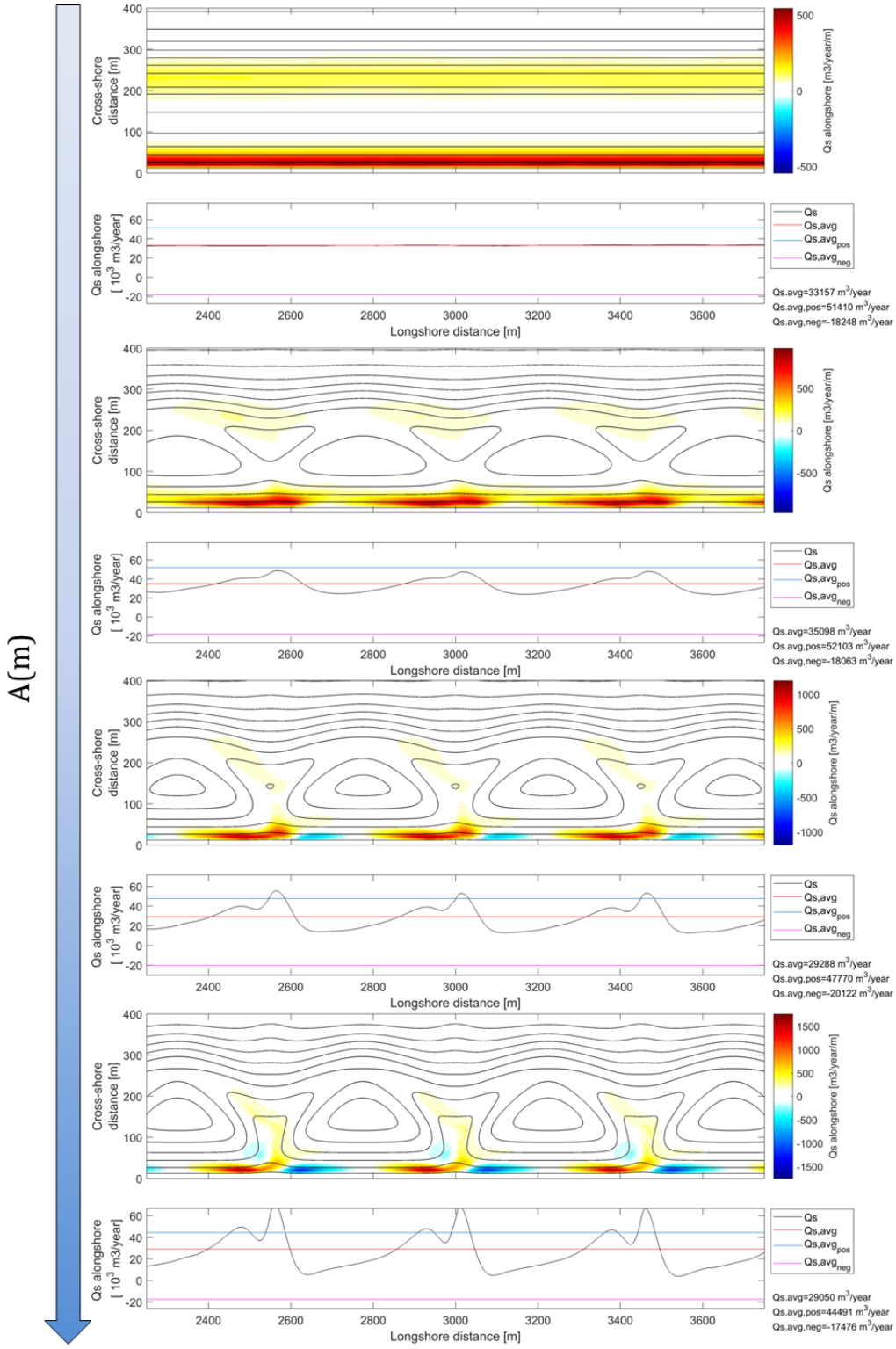

Figure C-7: Computed annual alongshore transport rates for s1,s2,s5 and s3 scenarios and the rotated WAM-6 degrees wave climate. Upper panel: Spatial transport fields of the annual alongshore sediment transport component (positive directed to the South). Bottom panel: Cross-shore integrated alongshore transports $Q_S(x)$ (black line) and beach state averaged transport $Q_{S,AVG}$ (red line). Gross-positive (blue line) and gross-negative (purple line) beach state averaged transports are plotted as well.

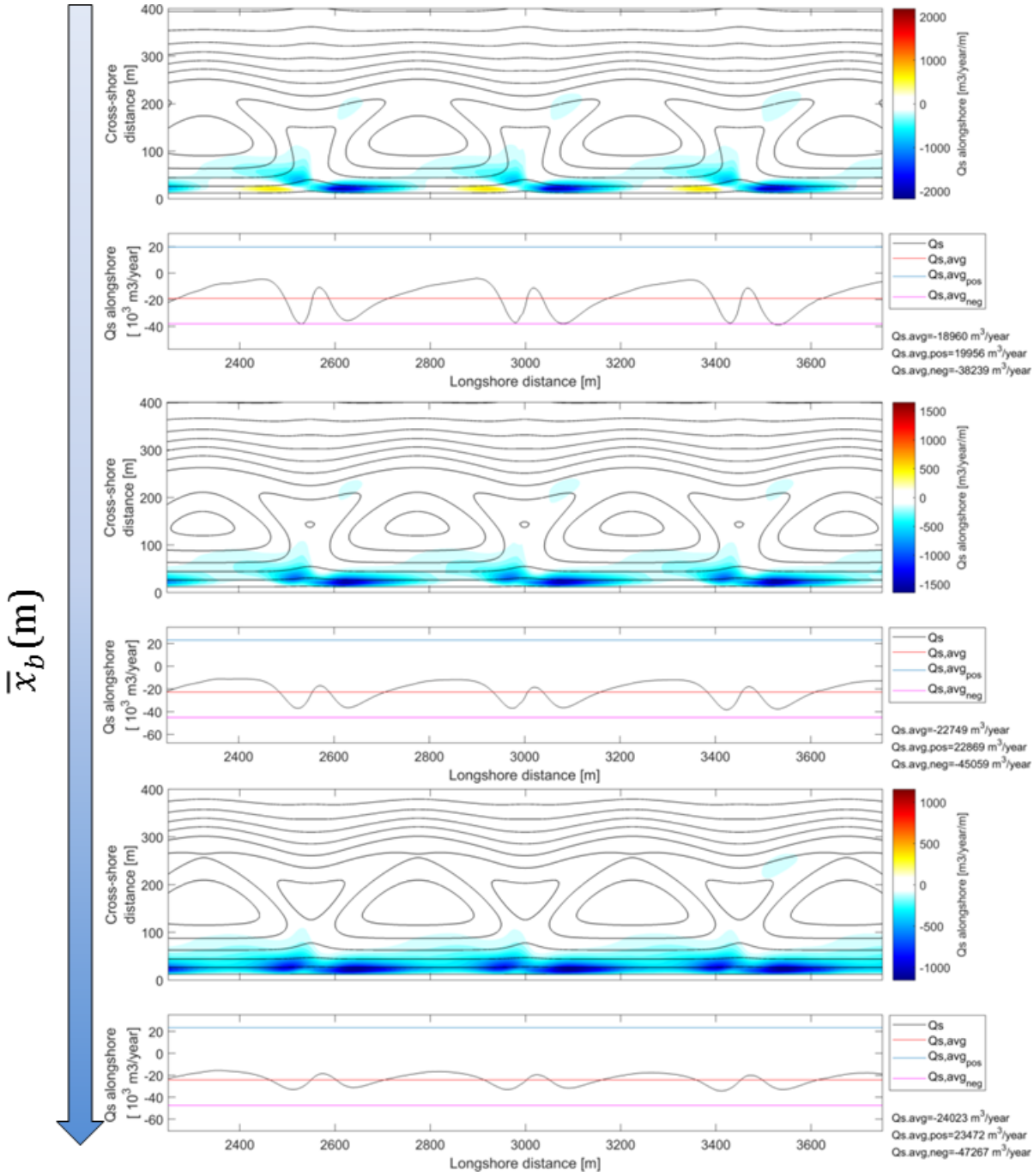

Figure C-8: Computed annual alongshore transport rates for s4,s5 and s6 scenarios and the rotated WAM+6 degrees wave climate. Upper panel: Spatial transport fields of the annual alongshore sediment transport component (positive directed to the South). Bottom panel: Cross-shore integrated alongshore transports $Q_S(x)$ (black line) and beach state averaged transport $Q_{S,AVG}$ (red line). Gross-positive (blue line) and gross-negative (purple line) beach state averaged transports are plotted as well.

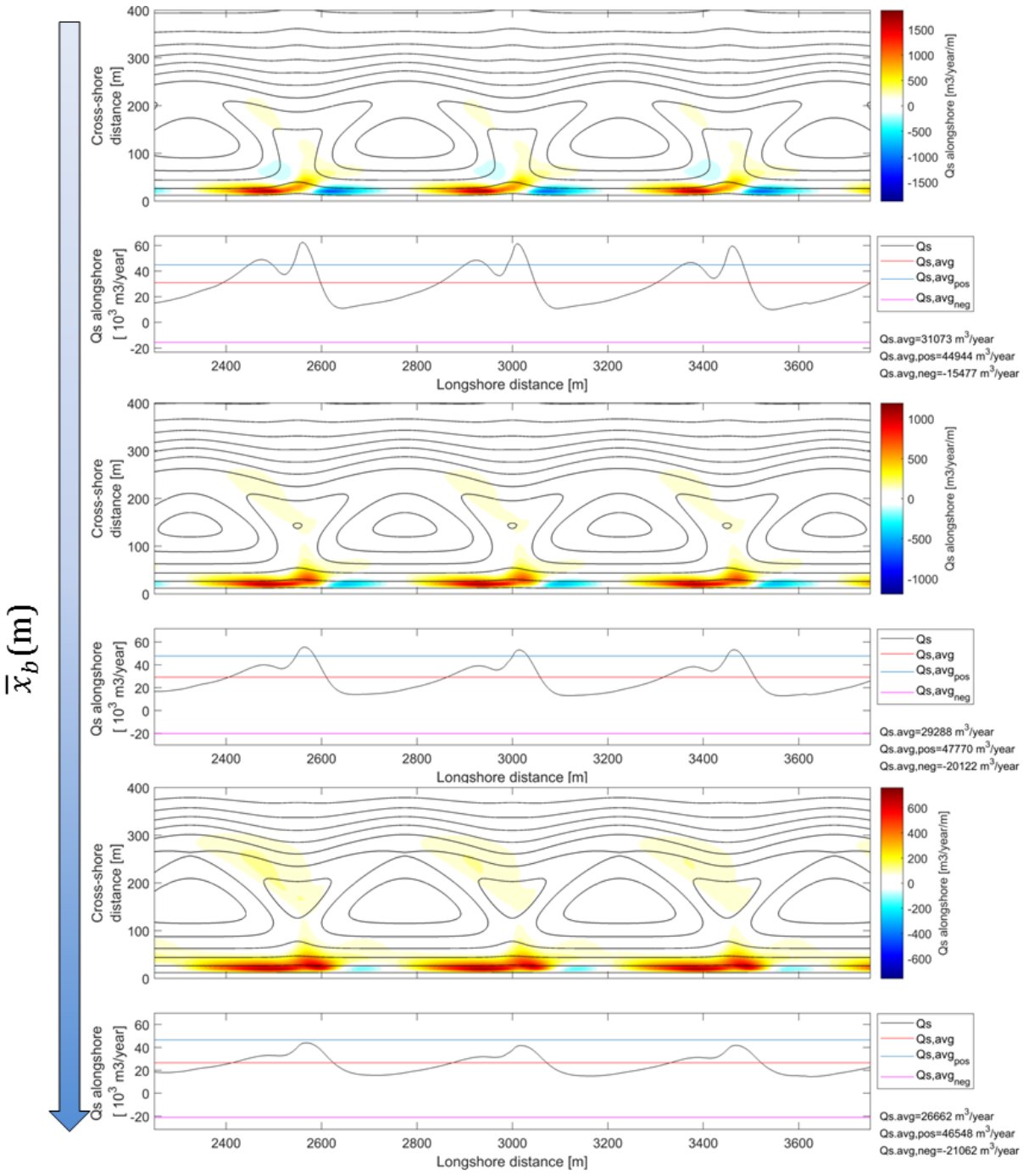

Figure C-9: Computed annual alongshore transport rates for s4,s5 and s6 scenarios and the rotated WAM-6 degrees wave climate. Upper panel: Spatial transport fields of the annual alongshore sediment transport component (positive directed to the South). Bottom panel: Cross-shore integrated alongshore transports $Q_S(x)$ (black line) and beach state averaged transport $Q_{S,AVG}$ (red line). Gross-positive (blue line) and gross-negative (purple line) beach state averaged transports are plotted as well.